Computational Studies of Complexes of Early Actinides with the Schiff-Base Polypyrrolic Ligand in Comparison to the U(VI) Analogues

By Gurpreet Kour

A Thesis Submitted to the Faculty of Graduate Studies of the University of Manitoba in Partial Fulfillment of the Requirements of the Degree of

Master of Science

Department of Chemistry

University of Manitoba

Winnipeg, Manitoba

Table of Contents

List of Figures

List of Tables

List of Abbreviations

An	Actinide
Th	Thorium
Pa	Protactinium
U	Uranium
Np	Neptunium
Pu	Plutonium
O.S.	Oxidation state
QTAIM	Quantum theory of atoms in molecules
CCI	Cation-Cation Interactions
DFT	Density Functional Theory
BO	Born Oppenheimer
HF	Hartree Fock
SCF	Self-Consistent Field
CI	Configuration Interaction
LDA	Local Density Approximation
GGA	Generalized Gradient Approximation
PBE	Perdew Burke Ernzerhof
XC	Exchange Correlation
AE	All Electron
RI	Resolution of Identity
STOs	Slater Type Orbitals
GTOs	Guassian Type Orbitals
ZORA	Zeroth-Order Relativistic Approximation
ADF	Amsterdam Density Functional
NBO	Natural Bonding Orbitals
CP	Critical Point

a.u.	Atomic units
BCPs	Bond Critical Points
M	Mononuclear
B	Butterfly
D	Diamond
Z	Zigzag
Tri	Triangle
THF	Tetrahydrofuran
BL	Bond Length
DI	Delocalisation Index
TM	Transition Metal

Abstract

A series of mononuclear and binuclear complexes of Th(IV), Pa(IV), Pa(V) and U(IV) with the octadentate tetraanionic Pacman ligand were investigated in comparison to their already known uranium (VI) analogues using relativistic density functional theory. The character of the bonding in these complexes was investigated using various quantum chemical parameters including bond lengths, bond orders and the topological analysis of the electron density using the quantum theory of atoms-in-molecules (QTAIM).

In another case, we investigated the bonding behavior of the actinyl in case of heterobinuclear complexes with the variation of the actinides (Th, Pa, U, Np and Pu), their oxidation states as well as with the 1variation of the transition metal in the lower pocket of the macrocycle. Optimized geometries, bond lengths, bond angles, atomic charges, natural bond order analysis and QTAIM analysis of the bonding interactions in these complexes were studied. All these complexes exhibit cation-cation interactions.

Acknowledgments

First and foremost, I am highly thankful to **Almighty** from the core of my heart who blessed me to successfully complete this work.

Words are not enough to express my inner sense of gratitude and indebtedness towards my supervisor Dr. Georg Schreckenbach, for his constant encouragement, unflagging keenness, sharp interest, inspiring criticism and highly creative supervision throughout the course of this work. I would also like to thank my advisory committee Dr. Peter Budzelaar, Dr. David Herbert and Dr. Chuang Deng for their help, advice, criticism and support during the work towards this thesis.

I would like to thank all my lab mates, Jeffery, Xiaobin and Saumya, for their constant help, inspiration and support. I also thank Dr. Grigory Shamova, our former member for the invaluable technical support. I would like to thank Dr. James Xidos for fruitful discussions. Friendly support from Pavan Mandapati is highly appreciated.

I wish to regard my deepest veneration towards my husband Dr. Gurpreet Singh, for rendering me love, encouragement and moral support during my research work.

Finally, my sweet little daughter Sehaj, without her cooperation, it would not have been possible for me to complete this work.

DEDICATED TO MY HUSBAND DR.

GURPREET SINGH KHALSA

Chapter 1

Introduction

1.1 Motivation

Over the past few decades, actinides have attracted significant attention not only because of their complex chemical nature, but also because of radioactive waste management, catalysis and number of other applications[1–3]. Among the most urgent technological and environment troubles to mankind worldwide are the problems created by nuclear reactors that are being used to produce electricity, nuclear weapons production, groundwater contamination due to the resulting nuclear waste, the treatment and storage of nuclear wastes and the cleanup of nuclear material sites[4–7]. The Hanford site in Washington state, USA, is a good example for the radioactive contamination which has evolved due to the nuclear weapons production for more than six decades[8]. All these problems are the sources of acute global concern and in all of them the actinide elements are closely involved. To deal with these problems, it is very important to understand the chemistry of these actinides. Indeed, both the science and technology of the actinides as we know them today owe much to the separation science[7].

There are number of important aspects of actinide chemistry which need to be understood, for instance, understanding of the bonding and electronic structure of the 5f electrons in their complexes and the bonding and chemical behavior of these actinides that may be released into the environment. An understanding of actinide chemistry represents challenges to both the synthetic chemist, where the toxicity, radioactivity, short lifetimes of various isotopes, scarcity etc. may hinder the experimental characterization, and also to the theoretical

chemist, where the relativistic and electron correlation effects (described in chapter 2) are quite expensive[1,9,10]. However, there have been tremendous developments in the field of computational chemistry for the study of actinide chemistry, and the theoretical chemists in collaboration with the experimentalists have been able to resolve various complexities of actinide chemistry. In some cases, the theoretical chemistry has been useful even in replacing the experimental work that requires harsh conditions.

Computational chemistry has been used to explore the structures of actinide complexes, bonding properties and their reactivity. The actinyl coordination chemistry of these actinides and most importantly the actinide oxo-group reactivity is very important as most of the heavier and radioactive fission products in nuclear waste form actinyl $[AnO_2]^{n+}$ ions[11]. The coordination chemistry of actinyl using different ligands has been a fascinating area of research to the inorganic chemists all over the world.

Certain macrocyclic ligands having aromatic π-electron systems are found to form stable complexes with the rare earths and help us understanding the physical and chemical properties of the actinides by giving access to novel electronic structures and covalent contributions to the metal-ligand bonding and hence they can act as a springboard to explore the coordination chemistry of these metal ions[12–14].

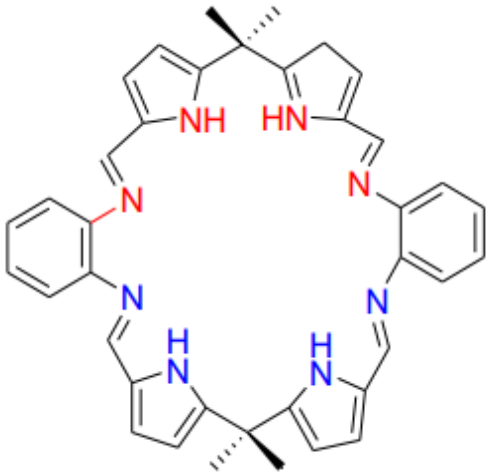

H_4L

Figure1.1: Structure of polypyrrolic macrocylic ligand (N atoms marked in red constitute one N4 donor site while those in blue ones constitute the other site).

Many mononuclear and binuclear complexes of Uranium, Neptunium and Plutonium with a binucleating Schiff base polypyrrolic macrocycle (Fig. 1.1) have been studied both computationally and experimentally[15–22]. Among early actinides, Thorium and Protactinium have not been as much studied as Uranium so far. Particularly, the inorganic chemistry of Thorium that includes the nature of bonding, structural and thermodynamic parameters as well as more applied research remain relatively unexplored[14] . Both homo- as well as hetero-bimetallic complexes of the early actinides was studied with emphasis on the bonding analysis. With the help of such studies, we are looking forward to adding to the existing knowledge of actinide complexes, in the hopes that the on-going research in this field will help in dealing with the nuclear fuel processing and waste storage problems in an effective way.

1.2 General introduction of actinides

The actinides (Fig. 1.2) or actinoids constitute the 15 elements with the atomic number varying from 89 to 103, corresponding to actinium to lawrencium respectively. They belong to the third group of the periodic table, and this series has been named after the first element of the series, actinium. Moving across the actinide series, the outermost shell being filled is the 5f shell, and accordingly they are also referred to as f-block elements. The only exception to this is lawrencium which behaves as a d-block element[23]. All the actinides are radioactive and usually unstable. They release large amounts of energy on undergoing spontaneous emission.

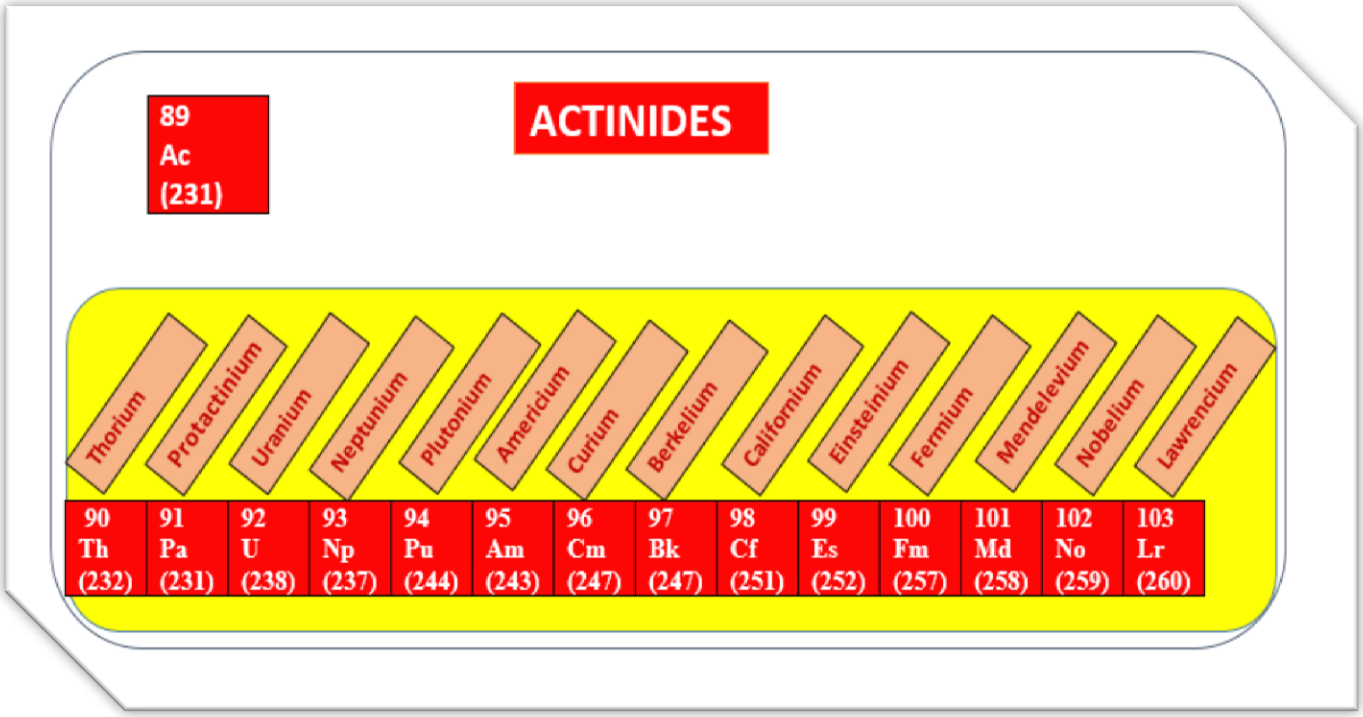

Figure1.2: The actinides series of the periodic table.

Among actinides, only thorium and uranium are found in considerable amounts in nature. The first actinides which were discovered are uranium by Klaproth in 1789 and thorium by Berzelius in 1829, but the rest of the actinides except Pa were man-made through various nuclear reactions of uranium and they are sometimes referred as transuranic elements. In terms of occurrence in

the earth crust, thorium is the most abundant with a total amount of 8.1 ppm whereas uranium is about 4 ppm. Thorium exists in many isotopes and one of its isotopes, Th-232, has a half-life of 14 billion years. The main source of thorium is from the thorium minerals like thorianite (ThO_2+UO_2), thorite ($ThSiO_4$) brabantite ($CaTh(PO_4)_2$) and monazite (a mixed rare-earth and thorium phosphate). Uranium exists in three major isotopes and is concentrated in many minerals like pitchblende, autunite, torbernite and carnotite. Large deposits of thorium are found in India and Australia whereas uranium deposits are found mainly in parts of Africa, Canada and the southwestern United States[24].

All the heavier actinide elements, the transuranic elements, as well as some isotopes of the lighter actinide elements, have been synthesized in the labs since 1940. Np and Pu are created from U in nuclear reactors on the commercial scale. The U-235 isotopes accept a neutron and get converted to an excited state of U-236, some of which undergoes fission, but some of them decay to the ground state of U-236 by emitting gamma rays. On further neutron capture U-237 is created which has a short half-life period and decays quickly to Pu-239. Many different isotopes of Np/Pu are created from the different isotopes of uranium using different combinations of neutron absorptions and radioactive decay. It has been found that rocks with high localized concentration of uranium can provide the right conditions for making small quantities of heavier elements naturally, but this occurs only in extremely rare cases. Moreover, traces of Np and Pu are also found in nature due to transmutation reactions in the uranium ores which is caused by the presence of neutrons[25].

Actinides have a wide range of applications in the energy production[26] through controlled nuclear fission, and production of nuclear weapons (plutonium) . They are used as smoke detectors (Am)[27], as well as coloring glasses and ceramics (UO_2)[28]. Depleted uranium is used in

making battle armors and projectiles. Nowadays it is also being used in the development of self-glowing actinide-doped materials with durable crystalline matrices as the addition of alpha-emitting radionuclides to some glasses and crystals may confer luminescence[26].

1.3 The electronic structures of the early actinides

The atomic and ionic radii of the actinides, like those of lanthanides, go down as we cross the series. This property arises due to the poor nuclear shielding of the f-electrons that increases the effective nuclear charge experienced by all the valence electrons, thus shrinking the system. This effect is referred to as actinide contraction.

In case of actinides, the inner shell electrons experience high nuclear charge so their velocities approaches speed of light and as a result 1s orbital undergo contraction. Electrons in other shells also tend to be stabilized owing to their orthogonality with 1s. In contrast, d and f orbitals remain expanded and therefore, destabilized and as a result, 5f, 6d and 7s orbitals become close in energy to one another. This effect is termed as relativistic effects. The early actinides (Th, Pa, U, Np, Pu) have extremely complex chemistry as they have several accessible oxidation states and readily undergo disproportionation in aqueous solution.[7,29,30] The electronic configurations of the actinides are as shown in Table 1.1.

The orbital energies of 5f, 6d and 7s electrons are close to one another due to the relative destabilization of the 5f orbitals which arises because of relativistic effects. As a result, the actinides can have a variety of oxidation states. Figure 1.3 shows the different oxidation states shown by the actinides; there is no simple trend across the period and a clear demarcation between the early and the late actinides. The stability of different oxidation states depends on the electronic configuration of the respective oxidized ion.

Actinide	Electronic configuration	Actinide	Electronic configuration
Actinium 89	[Rn]$6d^1$ $7s^2$	Berkelium 97	[Rn]$5f^9$ $7s^2$
Thorium 90	[Rn]$6d^2$ $7s^2$	Californium 98	[Rn] $5f^{10}$ $7s^2$
Protactinium 91	[Rn]$5f^2$ $6d^1$ $7s^2$	Einsteinium 99	[Rn] $5f^{11}$ $7s^2$
Uranium 92	[Rn]$5f^3$ $6d^1$ $7s^2$	Fermium 100	[Rn] $5f^{12}$ $7s^2$
Neptunium 93	[Rn]$5f^4$ $6d^1$ $7s^2$	Mendelevium 101	[Rn] $5f^{13}$ $7s^2$
Plutonium 94	[Rn]$6d^6$ $7s^2$	Nobelium 102	[Rn] $5f^{14}$ $7s^2$
Americium 95	[Rn]$6d^7$ $7s^2$	Lawrencium 103	[Rn]$5f^{14}$ $6d^1$ $7s^2$
Curium 96	[Rn]$5f^7$ $6d^1$ $7s^2$		

Table1.1: Actinides with the atomic number and electronic configuration. [Rn] is the noble gas core structure of Radon used for the electronic configuration.

Thorium predominantly occurs in the +4 state, as in its triply charged state, the stabilization of the 5f electrons is not sufficient to make the triply charged thorium a stable species. The chemistry of thorium in the +2 or +3 oxidation state (O.S.) is restricted to mostly iodides like ThI_2 and the cyclopentadienyl complex $Th(C_5H_5)_3$. Not much research was done on Protactinium as it exists only in small quantities and the most common O.S. shown by it is +5, whereas Uranium shows a rich redox chemistry as it can show oxidation states ranging from +3 to +6. Aqueous solutions of uranium in the +3, +4 and +6 oxidation states have brown-red, green and yellow colors, respectively. Among +4 and +6 oxidation state of uranium, U(VI) is more soluble in aqueous environment than U(IV) which commonly tends to form insoluble precipitates[31]. In the treatment of nuclear waste the U(VI) compounds are reduced to the +4 oxidation state as U(IV) compounds are less soluble in water and migrate more slowly than U(VI) complexes.[31] Both neptunium and plutonium exhibits O.S. from +3 to+7 and in case of Pu the +7 O.S. exists only under very alkaline conditions. All the tri-halides of Pu have pale pastel

colors like fluoride (violet-blue), chloride (blue-green), bromide (light-green) and iodide (bright-green). Most of the transplutonium actinides have fewer oxidation states and behave very similar to the trivalent lanthanides.

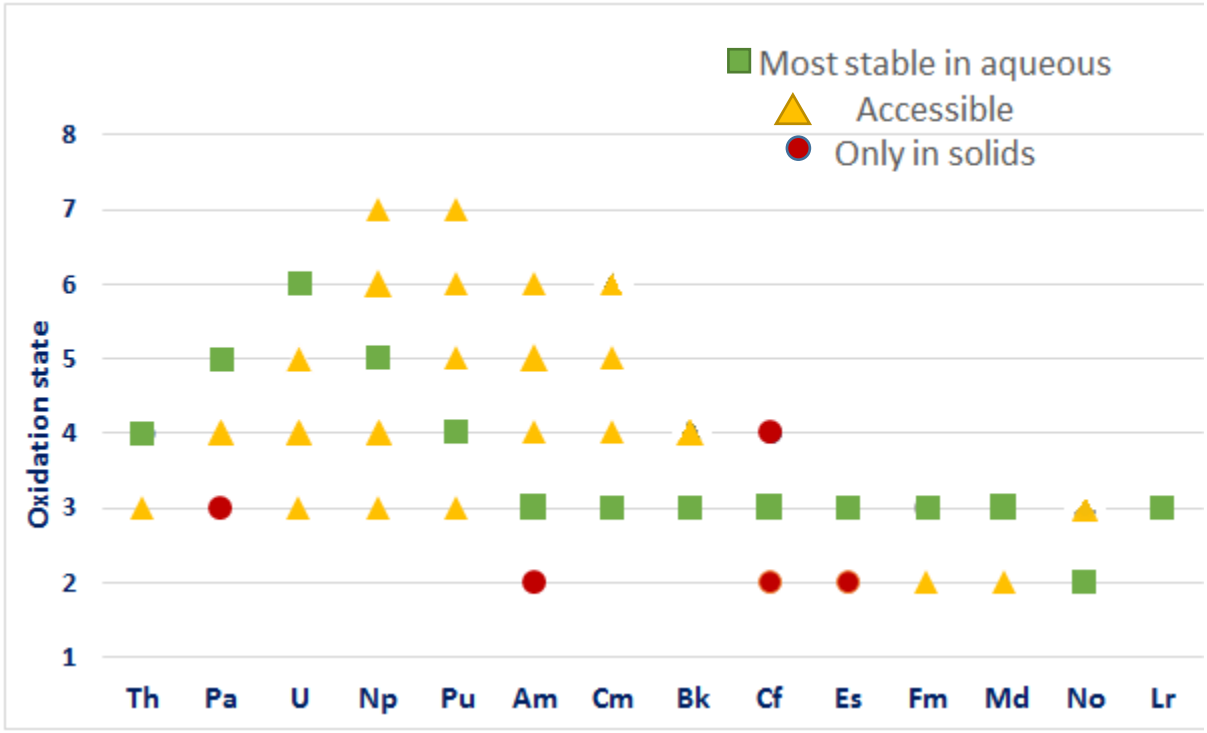

Figure1.3: The possible oxidation states for the actinides.

The variation in stable oxidation state across the actinide series arises due to the combination of both the orbital contraction as well as relativistic effects. Because of the relativistic effects the 6d and 5f orbitals become larger and more chemical accessible and, on the other hand, the orbital contraction in the later actinides make the 5f orbital more core-like[23]. There is a lot of variation in the radial extension of the 5f orbitals across the actinide series, it being closer to the other valence orbitals for Th to Pu and thus allowing the 5f orbitals to get involved in the chemical bonding, however for the later series the 5f orbital act like inert orbitals. Most of the actinide

complexes involve partially filled f-orbitals and these f-orbitals are very much diffuse and as a result can participate in bonding. Moreover, in these elements, the 6p atomic orbitals are also highly polarizable and diffuse[32] and have radial extension close to 6s and 5f. In case of actinides the 6p orbitals are often considered as the semi-core orbital which contrasts with the transition elements where the corresponding p orbitals are treated as core orbitals as they play no role in chemical bonding.

Most of the actinides in the high oxidation states are found in the form of actinyl AnO_2^{n+}, in which there are partial triple bonds between the actinide and the two oxygens, and this species is mostly present in a large variety of chemical environments.[33] Actinides being hard Lewis acids, they prefer to coordinate hard Lewis bases like F^-, Cl^-, O^{2-}, OH^-, SO_4^-, NO_3^-, CO_3^{2-}, neutral water, THF, and pyridine and other oxygen-containing electron donor ligands such as tributyl phosphates, ethers and ketones also form strong complexing agents. Coordination by 5 or 6 equatorial ligands around the actinyl moiety gives rise to pentagonal or hexagonal bipyramidal geometry.

For the singly charged anions, the complexing ability for the complexes containing the actinyl moiety follows the order $F^- > NO_3^- > Cl^- > ClO_4^-$ whereas for the doubly charger anions the order is $CO_3^{2-} > C_2O_4^{2-} > SO_4^{2-}$. Among tri-anions, PO_4^{3-} is a strong complexing agent[14].

1.4 Actinide macrocyclic complexes

The nuclear fuel waste that contains mainly a mixture of radioactive actinides poses a threat to the environment. For addressing this concern, there is a need that these radioactive elements must be separated and given treatment according to their recyclability and storage needs. Current approaches to manage the radioactive waste have been the segregation and storage for the short-lived waste, and deep burial for the high-level waste. The different bonding behavior between the

early and the later actinides can be used as a tool for their separation in the nuclear waste. Another separation technique generally involves adjusting the oxidation states of the actinide ion in aqueous solution and so their oxidation states can be adjusted to make their coordination chemistry different from the other species present. The ongoing quest for more efficient separations or isolation of radioactive elements encourages the exploration of f-element and radionuclide chemistry, and creates a need for the novel systems that can coordinate actinide cations with high specificity[11,34].

Computational chemistry has proved a powerful tool for the fundamental understanding of the actinide chemistry and also plays a significant role for the interpretation of the experimental data and also the prediction of chemical and physical behavior of actinides[1]. As previously mentioned actinides are in general hard acids and therefore have a strong affinity to hard donor ligands, so there are only few ligands which can compete with water itself. Among various ligands, the polypyrrolic macrocyclic ligands are being recognized as excellent cation complexation agents for the actinides as they can be tuned to provide the best fit for different cations and oxidation states by changing the size of the ligand cavity as well as flexibility etc. Macrocyclic systems such as calixarenes[35–39], crown ethers[40–43], pyrrole-based porphyrins[44–49], boron containing macrocycles[50] and phthalocyanines[14,51] are known to form stable complexes with various actinides. Several complexes of uranyl(VI) with the expanded porphyrins such as pentaphyrin[44], isoamethyrin[45], amethyrin[52], oxasapphyrin[53], and the Schiff base macrocycle, alaskaphyrin[53], have been reported experimentally. In addition to these, quite a few complexes of Neptunyl(V) and Plutonyl(V) with the expanded porphyrins are known[46,49]. Moreover, another class of expanded porphyrins has been reported in recent past that involves cyclo[6] pyrroles[54], cyclo[3]pyridine[3] pyrroles[47], cyclo[2]pyridine[4]pyrroles[47] and cyclo[1]furan[1]pyridine[4]

pyrrole.[48]

Quantum theory calculations on a number of complexes of actinides with various macrocyclic ligands[18,20,41,55–63] have been done by our research group and others[64–68] . Amongst them, there is a flexible Schiff-base pyrrole macrocyclic ligand H_4L (Fig.1.1), prepared by the Love[69] and Sessler[70] groups independently, which has been found to be a very good ligand for making very stable complexes with the actinides. This ligand[70] has two N_4 donor compartments, and the studies of Arnold and Love et al. have shown that this macrocyclic ligand can accommodate metal atoms like transition metal atoms, lanthanides as well as actinides in its two vacant sites[15,21,40,71–79]. The two aryl groups in this ligand act as hinges. This results in a relatively rigid molecular structure, sometimes referred as a Pacman structure[80–82].

Arnold, Love and co-workers used this ligand to synthesize the diuranium(VI) complex $K_2[(UO_2)_2(\mu\text{-}O_2)]$[78], the diuranium(V) complex $[\{(Me_3Si)OU(\mu\text{-}O)\}_2(L)]$[77], and diactinide(III) complexes $[(AnX)_2(L)]$ (An = U, X = I, BH_4; An = Np, X = I)[15], successfully. In addition to the synthetic part, quantum chemical calculations on many mononuclear and binuclear complexes of Uranium, Neptunium and Plutonium have also been done. Among earlier actinides, complexes of thorium and protactinium with these macrocyclic ligands have not been much studied either experimentally or theoretically. However, many comparative studies of various complexes of thorium and uranium with small ligands such as cyclopentadienyl[83], benzyne[84], metallocene[13], tetramethyltetraazaannulene[85] and corroles[19] have been reported in the recent past.

The studies of such complexes of actinides are helpful in gaining further knowledge about covalency as the covalency in the f-block elements has been the subject of much debate both experimentally as well as theoretically.[19,86,87] Till now the general idea is that there may be significant covalency in the bonding in early actinides as compared to the later actinides, which

are generally more ionic but these descriptions are constantly reassessed[88] as new complexes are made and characterized[12,87,89] and the nature of covalency has recently come under critical examination.[13,90]

1.5 Objectives

Understanding the nature of bonding within various complexes of actinides (Th, Pa and U) with the polypyrrolic macrocyclic ligand, and how these complexes differ from the already known U(VI) complexes are some of the main objectives of this work. In case of binuclear complexes, a comparison was made among Th(IV), Pa(IV) and U(IV) complexes and also Th(IV), Pa(V) and U(VI) complexes were studied. It is said that the chemical properties of actinides are governed by the number of f-electrons in them,[14] accordingly, we tried to analyze whether the bonding differences arise due to the change in actinide element or the oxidation state. Both binuclear and heterobinuclear analogues of U(VI) complexes were studied. In case of heterobinuclear complexes of actinides with the macrocyclic ligand, we looked for differences in the bonding behavior of various actinides ranging from thorium to plutonium as well as the transition elements. The nature of actinide-ligand bonding was investigated using density functional theory and quantum theory of atoms in molecules theory also known as QTAIM (discussed in chapter 2).

Another interesting feature of the actinide complexes considered in our study is the existence of cation-cation interactions (CCI). The complexation of AnO_2^+ and AnO_2^{2+} ions with some other cations is referred to as cation-cation interactions. These interactions were first observed in a study of the behavior of Np(V) in solutions of uranyl perchlorate[91]. These interactions occur only in 2% of the U(VI) compounds[92] and are much more common in Np(V) and U(V) compounds, both of which have been the focus of much attention[73,93–99]. These interactions provide novel

linkages within structural ligands and lead to the formation of dimers[100–104], oligomers,[105–107] one-dimensional chains[108–110] as well as multi-dimensional networks[93,105,109–116] that may occur without the support of ancillary ligands.

1.6 Organization of this thesis

The main objective of this work is to provide comparative studies on the bonding analysis for the polypyrrolic macrocyclic complexes of early actinides with the U(VI) complexes.

A brief introduction to the general actinide chemistry is contained in chapter 1. Chapter 2 describes the various quantum chemical details as well as the different software packages used to accomplish this work. Discussions on correlation effects as well as relativistic effects are included.

The first case study is presented in chapter 3, which involves the bonding analysis of the mononuclear as well as binuclear macrocyclic complexes of Th(IV), Pa(IV), Pa(V) and U(IV) in comparison to the U(VI) analogues. Both the DFT and QTAIM calculations were done for these complexes and the covalency trends along the series from Th to U were analyzed. Chapter 4 contains studies the heterobimetallic complexes containing both the actinide as well as a transition metal. We studied hetero-binuclear macrocyclic complexes of Th(IV), Pa(IV), Pa(V), U(IV), Np(VI), Pu(VI) and the transition metals considered in this study are Mn(II), Fe(II), Co(II) and Zn(II); all the transition metals are in high spin state.

In chapter 5, we present the conclusion and summarize our results along with outlook for future work.

Chapter 2

Computational Methods

Computational chemistry uses quantum mechanical based methods to calculate various chemical properties[117]. This area of chemical sciences is even more advantageous for probing and analyzing in the field of actinides[1] than in other areas of chemistry because of the radioactivity of most of these elements which may result in safety and security concerns particularly for the transuranic elements [6,118,119]. Some of the applications of computational chemistry involve the calculation of electron and charge distributions, molecular geometries or potential energy surfaces for different electronic states. To model actinide containing systems accurately, various methods to obtain an approximate wave function and density of that system are used. Inclusions of electron correlation effects which result from electron-electron interactions are very important in case of actinide containing systems. The actinide's inner shell orbitals also have high curvatures and thus kinetic energy giving rise to strong relativistic effects [120]. These effects are negligible for light elements but they are very prominent and important in heavy elements like actinides for modelling their behavior appropriately, as these core orbitals affect all other electronic behavior near the atom. In this chapter, computational information and some details required to model electronic structure used in this work are discussed.

2.1 Schrödinger Equation

The time-dependent Schrödinger [121] equation is a cornerstone of quantum mechanics and governs all phenomena of the microscopic world. It is a partial differential equation of the total energy operator, the Hamiltonian $\hat{H}$.

$$\text{í}\,\hbar\frac{\partial\Psi}{\partial t} = \hat{H}\,\Psi \qquad (2.1)$$

where í is the imaginary number, $\hbar = h/2\pi$, h is Planck's constant, $\partial/\partial t$ is a partial derivative with respect to time t, and Ψ is the wave function which provides the solution to the equation.

For a closed system, the conservation of energy makes a separation of time and spatial components possible. The time-independent Schrödinger wave function can be given by the equation 2.2

$$\hat{H}\,\Psi = E\,\Psi \qquad (2.2)$$

Where Ψ is some wave function and E is the energy of that state Ψ, and $\hat{H}$ is again the Hamiltonian operator. Atomic units, the system of units useful for atomic calculations, where mass of electron, electron charge, reduced Plank's constant, ħ, and Coulomb's constant ($k_e = \frac{1}{4\pi\varepsilon_0}$) are defined as unity, are used. The Hamiltonian for a molecular system contains five contributions which can be written (in atomic units) as

$$\hat{H} = -\sum_{i}\frac{1}{2}\nabla^2_i - \sum_{A}\frac{1}{2M_A}\nabla^2_A - \sum_{i,A}\frac{Z_A}{r_{iA}} + \frac{1}{2}\sum_{1<j}\frac{1}{r_{ij}} + \frac{1}{2}\sum_{A<B}\frac{Z_A Z_B}{R_{AB}} \qquad (2.3)$$

Where i, j stands for electrons and A, B for nuclei. M_A is the mass of nucleus, ∇^2 is the Laplacian operator, Z is the atomic number, R_{AB} is the distance between A and B. The first term in equation (2.3) is the kinetic energy operator for each electron in the system. The second term is the kinetic energy operator for each nucleus in the system. The third term is the total electron-nucleus Columbic attraction in the system. The fourth term is the potential energy from Columbic electron-electron repulsions. The fifth term is for potential energy of columbic nuclei-nuclei repulsions.

2.2 The Born-Oppenheimer approximation

This approximation,[122] also known as the adiabatic or "clamped nuclei" approximation, assumes that nuclei move at negligible speeds compared to the electrons. The nuclei are assumed to be stationary in comparison to the fast-moving electrons. This separation of the nuclear and electronic motion allows for an easier evaluation of the electron-nuclei, nuclei-nuclei interactions as well as the nuclear kinetic energies. The term in equation (2.3), describing the nuclear kinetic energy, can then be neglected, leading to the adiabatic approximation [123]. The electronic part of equation (2.3) including the nuclear repulsion can then be written (in atomic units) as

$$\hat{H} = -\sum_{i} \frac{1}{2} \nabla^2 i - \sum_{i,A} \frac{z_A}{r i A} + \frac{1}{2} \sum_{1<j} \frac{1}{r_{ij}} + \frac{1}{2} \sum_{A<B} \frac{z_A z_B}{R_{AB}} \qquad (2.4)$$

This approximation is well justified if the energy gap between ground and excited electronic states is large as compared to the energy scale of the nuclear motion. The Born Oppenheimer (BO) approximation breaks down for cases where the velocity of nuclei increases as for highly excited vibrational states, or when two or more potential energy surfaces approach or cross each other [124]. Moreover, Waschewsky et. al [125] proved that in the class of reactions known as Woodward-Hoffmann forbidden reactions, the BO approximation fails and can result in a marked reduction in the reaction rate. However, detailed discussion is beyond the scope of this work and we made use of this approximation throughout our studies.

2.3 The Hartree-Fock (HF) Approximation

Within the Hartree-Fock approximation, the many-electron wave function is assumed to be a simple product of one-electron wave functions. This approximation is equivalent to assuming that the motion of each electron is independent of the motion of all the other electrons.

Therefore, an electron senses only the average Coulomb repulsion energy associated with the electron-electron repulsion. The electrons are assumed to be uncorrelated because each one is unaware of the positions of the other electrons at any time and only their average position is felt.

However, the electrons obeying Fermi statistics imposes certain symmetry properties when the positions of two electrons are exchanged. This symmetry property is satisfied when the simple, independent particle product is generalized to a Slater determinant. The HF wave function, thus commonly represented as Slater determinant, is given by the equation (2.5).

This expression gives a wave function which is antisymmetric with respect to the electron exchange, obeying the Pauli Exclusion Principle. This property arises mathematically from the property of matrix determinants to change sign when any pair of rows or columns are exchanged, which in its use as a description of the wave function is equivalent to exchanging two electrons.

The Hartree-Fock wave function can be given by the Slater determinant

$$\Psi(1,2,.....N) = \frac{1}{\sqrt{(2N)!}} \begin{vmatrix} \psi_1\alpha(1) & \psi_1\beta(1) & ..... & \psi_N\alpha(1) & \psi_N\beta(1) \\ \psi_1\alpha(2) & \psi_1\beta(2) & ..... & \psi_N\alpha(2) & \psi_N\beta(2) \\ \vdots & \vdots & \ddots & \vdots & \vdots \\ \vdots & \vdots & . & . & \vdots \\ \psi_1\alpha(2N) & \psi_1\beta(2N) & \cdots & \psi_N\alpha(2N) & \psi_N\beta(2N) \end{vmatrix} \qquad (2.5)$$

The energy is given by

$$E_{ele} = \langle \psi^*(1,2,....,2N) \,|\, \hat{H} \,|\, \psi(1,2,...2N) \rangle \qquad (2.6)$$

This equation (2.6) can be written as

$$E_{ele} = 2\sum_{j=1}^{N} I_j + \sum_{i=1}^{N}\sum_{j=1}^{N}(2J_{ij} - K_{ij}) \qquad (2.7)$$

Where

$$I_j = \int dr_j \psi_j^*(r_j)(-\frac{1}{2}\nabla_j^2 - \sum_N^M \frac{Z_A}{r_{jA}})\psi_j(r_j)$$

$$J_{ij} = \int\int dr_1 dr_2 \psi_i^*(r_1)\psi_j^*(r_2)\frac{1}{r_{12}}\psi_i(r_1)\psi_j(r_2) \qquad (2.8)$$

$$K_{ij} = \int\int dr_1 dr_2 \psi_i^*(r_1)\psi_j^*(r_2)\frac{1}{r_{12}}\psi_i(r_2)\psi_j(r_1)$$

On applying the variational principle to equation (2.7), the spatial orbitals that minimize the energy satisfy the equations

$$\hat{F}(r_1)\psi_i(r_1) = \varepsilon_i\psi_i(r_1) \qquad i = 1,2,3,\ldots..,N \qquad (2.9)$$

Where $\hat{F}(r_1)$ is the Fock operator

$$\hat{F}(r_1) = \hat{f}(r_1) + \sum_{j=1}^{N}[2\hat{J}_j(r_1) - \hat{K}_j(r_1)] \qquad (2.10)$$

Where $\hat{f}(r_1) = -\frac{1}{2}\nabla_1^2 - \sum_A \frac{Z_A}{r_{1A}}$ (2.11)

$\hat{J}_j(r_1)$, the Coulomb operator,

$$\hat{J}_j(r_1)\psi_i(r_1) = \psi_i(r_1)\int dr_2 \psi_j^*(r_2)\frac{1}{r_{12}}\psi_j(r_2) \qquad (2.12)$$

$\hat{K}_j(r_1)$, the exchange operator

$$\hat{K}_j(r_1)\psi_i(r_1) = \psi_j(r_1)\int dr_2 \psi_j^*(r_2)\frac{1}{r_{12}}\psi_i(r_2) \qquad (2.13)$$

The energy for the i[th] molecular orbital can be obtained by multiplying equation (2.9) by $\psi_i^*(r_1)$ and integrating over r_1

$$\varepsilon_i = \int dr_1 \psi_i^*(r_1) \hat{F}(r_1) \psi_i(r_1) \qquad (2.14)$$

Using the Fock operator, equation (2.14) becomes

$$\varepsilon_i = I_j \sum_{j=1}^{N} (2J_{ij} - K_{ij}) \qquad (2.15)$$

Comparing this equation with equation (2.7), we can write

$$E = \sum_{i=1}^{N} (I_i + \varepsilon_i) \qquad (2.16)$$

Roothaan [126] represented the molecular orbitals as a linear combination of basis functions

$$\psi = \sum_{v=1}^{K} c_v \phi_v \qquad (2.17)$$

Thus, the Hartree-Fock-Roothaan equations are

$$\sum_v F_{\mu v} c_v = \varepsilon \sum_v S_{\mu v} c_v \qquad \mu=1,2,\ldots,K \qquad (2.18)$$

Where $F_{\mu v}$ are the Fock matrix elements

$$F_{\mu v} = \int dr_1 \phi_\mu^*(r_1) \hat{F}(r_1) \phi_v(r_1) \qquad (2.19)$$

And $S_{\mu v}$ are the overlap matrix elements

$$S_{\mu v} = \int dr_1 \phi_\mu^*(r_1) \phi_v(r_1) \qquad (2.20)$$

Equation (2.18) represents a set of algebraic equations for the c_v; they are known as Hartree-Fock-Roothaan equations. The Roothan equations [126] allow the orbitals to be expressed in terms of a set of linearly combined basis functions, the coefficients of which can then be adjusted to minimize the HF energy iteratively as a general optimization problem. Since the evaluation of the energy expressions at each iterative step involves the previously generated orbitals from the last step, this is commonly referred as self-consistent field or SCF [127] approach, and the energy value produced by it is known as SCF energy.

Although the HF method is known to obtain accurate geometries, the energies involving a change in the number of paired electrons are poorly calculated, due to only considering electron-electron repulsions as an interaction of each electron with a mean field. The contributions of electron correlation are relatively small (1%) as compared to the total energy. However, they induce large discrepancies in property calculations and reaction energies. Several approaches have been developed to correct for this by accounting for the missing electron correlation and thereby providing improved electronic energies. Among the popular techniques, which use the HF wave function as a starting point, are many-body perturbation theory, coupled-cluster theory, and configuration interaction (CI), and sometimes these are referred to as post Hartree-Fock approaches. Each of these methods yields more accurate results than the HF model alone, but they are computationally very much demanding, and this makes it very difficult to obtain results for moderately large molecules of chemical interest [127,128].

The significance of HF calculations is that due to the exact nature of the terms used and the lack of any approximate terms, the resulting energy serves as an upper bound to the true energy, and this property is known as the variational principle.

2.4 Density Functional Theory (DFT)

The DFT approach dramatically simplifies the computational demands by replacing the search for an accurate many-electron wave function, which is a function of the coordinates of all the electrons in the molecules (Eq. 2.2), with that for an accurate electronic density, which depends on the coordinates of just a single point in space. The DFT method thus provides a time saving advantage over the HF method and especially post Hartree-Fock methods. The two fundamental theorems in DFT are the Hohenberg-Kohn theorems [129], stating that the ground state electron density, ρ(r), uniquely determines the external potential V(r) and that the ground state energy can be obtained variationally, which means that the density that minimizes the total energy is the exact ground state density.

Equation (2.21), in theory, shows the expression for the energy in terms of that density alone, but it has been found that it is very tough to obtain accurate expressions for the electronic kinetic energy, exchange energy, and electron correlation energy, from the density alone.

$$\rho = \sum |\phi_i|^2 = \Psi^* . \Psi$$

$$E[\rho] = T[\rho] + V_{ne}[\rho] + J[\rho] + E_{xc}[\rho] \qquad (2.21)$$

The Kohn-Sham formulation instead expresses the density in terms of a Slater determinant for a system of non-interacting electrons.[130] The method used to obtain this result separates the terms of the Hamiltonian into two groups. The first group comprises the zero- and one-electron terms for the non-interacting electrons, the nucleus potential V_{nn} and the core Hamiltonian. The second group contains all interactions between electrons, through two terms: the Coulombic electron-electron repulsion $\hat{J}$ as in Hartree-Fock theory and a potential like term that in principle covers

exchange, any interaction correction to the kinetic energy, and non-classical correlation, E_{xc} which is also known as the exchange-correlation functional.

The exchange correlation term E_{xc} is a complex term, comprising two terms, one being the kinetic energy of a system of interacting electrons minus the kinetic energy of a system with non-interacting electrons with the same density, and another being the electron-electron interaction (total electron exchange and correlation) minus the classical Coulomb interaction. If the exact exchange-correlation term is known, a full solution to the Schrödinger equation will have been obtained. Despite the fact that a large number of approximate exchange-correlation functionals have been proposed and tested over the years,[130–135] still the exact nature of this functional remains unknown. Sometimes, this functional is split into the exchange functional and the correlation functional.

$$E_{xc} = E_x + E_c \qquad (2.22)$$

Exchange-Correlation Functional

There is a wide range of approximate functionals and the choice for use depends on the exact requirements of the calculations being performed. For instance, for ground state geometry optimizations, the simplest functional can provide us with accurate results but if we want to perform excitation energy calculations, the results can vary a lot between different functionals. Sometimes, selection of the functional also depends on factors like cost, availability of that functional in the codes that one is using, etc. The various functionals are often ranked in order of accuracy and computationally expense, into what has been termed a "Jacob's Ladder of density functional approximations" with the least accurate at the bottom and the ideal exact functional at the top [136]. The various approximations applied are as follows:

Localized Density Approximations (LDA) – The earliest known exchange-correlation functional is called the local density approximation (LDA), according to which at a given point in space, the exchange-correlation energy is equal to the exchange-correlation energy for a uniform gas of electrons which is characterized by the electron density, ρ. It tends to cause over binding in molecules as a result of overestimating correlation and underestimates the exchange energy by around 10% [137,138].

Generalized Gradient Approximations (GGAs) – The most common improvement to the LDA functional involves a correction to the rapidly changing electron densities found in molecular systems. In these functionals the gradient of the density is included in the formulations of the exchange-correlation functional. The PBE functional [139] is a non-empirical GGA functional and was widely used in the work done in this thesis.

Meta-GGAs- These functionals are dependent on the Laplacian of the electron density or the kinetic energy density in addition to density and gradient. TPSS [140] is one of the examples of a meta-GGA functional.

Hybrid Exchange-Correlation Functionals

Hybrid functionals, in many cases, provide an improvement on the performance of DFT. The rationale for the hybrid methods is that Hatree-Fock theory includes exchange naturally in the HF equations which is not the case with the Kohn-Sham equations. The exchange energy in DFT, using the adiabatic connection model, can be written as a linear combination of HF exchange and some DFT exchange and correlation functional. This technique improves the accuracy of DFT and is the basis of the hybrid functionals introduced by Becke. There are

several hybrid functionals available that have excellent performance for a wide range of elements and compounds.

The B3LYP exchange-correlation functional [141] is an example of a semi-empirical hybrid functional containing exact exchange, LDA and GGA exchange plus LDA and GGA correlation. No doubt, this method tends to result in better energies for delocalized systems, but the Hartree-Fock exchange term is computationally very expensive and may not be applied for larger systems like those considered in this work.

2.5 Basis sets

A basis set is a set of functions, usually called basis functions, that is used to represent the electronic wave function. A quantum chemical calculation requires a description of the molecular orbitals of the system using basis functions. For a molecular calculation, molecular orbitals are constructed using linear combinations of basis set functions (2.23). The coefficients, C_i, represent the contribution of each atomic orbital (each basis function) to the molecular orbital.

$$\varphi = \sum_{i=1}^{N} C_i \phi_i \qquad (2.23)$$

There are two main classes of functions used to represent atomic spin-orbitals in computational chemistry [127]. These are Slater type orbitals (STOs) and Gaussian type orbitals (GTOs). These can be splitted into an angular and a radial component and only the radial component differs among the two functional forms as shown in the equations (2.24) and (2.25). In these equations, r is the scalar radius, θ and ϕ are the two angular coordinates, R is the radial component, Y is the angular component, ζ is the function determining the steepness of the function, A is the

normalization coefficient, n is the principle quantum number and l is the orbital angular momentum.

The Slater-type orbital function is based on a functional fit to the hydrogenic solution to the Schrödinger equation. STOs can describe systems with a high level of accuracy, exhibiting exponential decay at long range. The main advantage of this type of orbital is that it models the density quite accurately, especially near the nucleus where it has the predicted cusp behavior, so relatively less functions are required to obtain a good fit. There are however computational challenges to calculate the integrals of an exponential decay function. In most cases, numerical solutions to the integrals of these functions are needed.

$$\varphi(r,\theta,\phi) = R(r)Y(\theta,\phi) \qquad (2.24)$$

$$R_{STO}(r) = Ar^{n-1}e^{-\zeta r} \qquad (2.25)$$

$$R_{GTO}(r) = Ar^{2n-1}e^{-\zeta r^2} \qquad (2.26)$$

On the other hand, less computationally intensive, GTOs decay very quickly due to the dependence on the e^{-r^2} instead of e^{-r} as shown in the above equation (2.26) (Figure 2.1) and often result in reduced accuracy compared to STOs when used for short- and long-range behavior of electrons. The curvature of these functions, especially near the nuclear center, does not model the orbital behavior very accurately, but because they are computationally inexpensive to perform multicenter integrals for, a collection of Gaussian functions can be used to approximate a Slater-type basis function. There are certain drawbacks of GTOs like wrong cusp shape and the overall poor long-range behavior because of quick decay of the function. To

overcome these drawbacks, usually several GTOs are used to present the basis function as shown in the equation (2.27)

$$C_1 e^{-b_1 r^2} + C_2 e^{-b_2 r^2} + C_3 e^{-b_3 r^2} \qquad (2.27)$$

Where C_i are the coefficients used to ensure agreement with the radial electronic distribution of the hydrogen atom

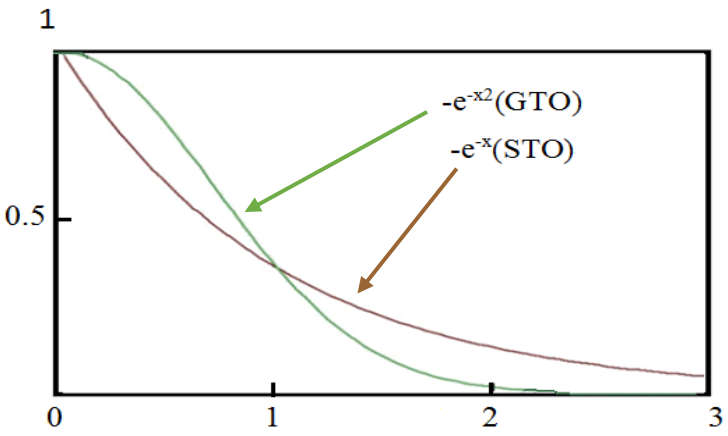

Figure2.1: A Slater-type basis function (brown) and Gaussian-type function (green).

For a molecular calculation, enough basis functions are required to describe all the electrons in an atom. For instance, for a hydrogen atom, a basis set for a hydrogen atom must contain at least one 1s function. The smallest basis set contains no additional functions. A double- ζ basis set contains two sets of functions. A triple- ζ contains three sets of functions whereas quadruple ζ contains four, and so on.

For a better description of the electron correlation and anionic systems or excited electronic states, polarization functions as well as diffuse functions are added. The electron density of an atom in a molecule is affected by the presence of other nuclei, so a high level of flexibility in the

spatial symmetry of the orbitals is beneficial. They allow a realistic description of bonding interactions as we know that, during a bonding interaction, the electron density is distorted in an asymmetrical manner. S-orbitals are polarized by adding p functions, p-orbitals by addition of d functions, and so on. Diffuse functions are generally useful for describing anionic systems and radial correlation. Diffuse functions are designed to provide an approximate representation of the part of the orbitals which is far away from the nucleus.

Sometimes the basis set is separated into a core and valence part as the core electron are chemically inert and do not take part in the bond formation or the ionization processes.

2.6 Relativistic Effects

Relativity is an important factor in calculations involving the lanthanides and actinides. Relativity has a significant effect on the electronic levels and on calculated energies and bond lengths for elements beyond krypton (Z>36) [120,128]. In case of molecules containing heavy elements, the speed of the core electrons is comparable to the speed of light. Because of the high speed attained by the 1s electrons of the heavy nuclei, these electrons have a greater effective mass according to the relativistic mass equation (2.28). This leads to the contraction of the 1s orbitals (by the same factor by which the mass increases), which in turn implies a contraction of the higher s orbitals due to orthogonality. The nucleus of the atom is more effectively shielded by contracted s orbitals, and so an additional effect of relativity is that the higher orbitals expand. The net effect of this on the p orbitals is negligible, but d and f are certainly more diffuse than they would be in the fictitious nonrelativistic case, particularly in the actinides [120,142,143].

$$m = m_0 \Big/ \sqrt{1 - \frac{v^2}{c^2}} \qquad (2.28)$$

Relativity is not accounted for by the Schrödinger equation, and so some additional description of the wave function of the heavy atom is required to perform the quantum mechanics calculations. The Dirac equation, which is shown by equation (2.29), was put forward in 1929 to describe the one-electron energies of relativistic systems [144].

$$(c.\alpha.p + \beta mc^2 + V)\psi = E\psi \qquad (2.29)$$

Where c is the speed of light, m is the mass of the electron, α is a vector of matrices constructed from the Pauli spin matrices $\sigma_{x,y,z}$ as shown in (2.30) and (2.31), β is given by equation (2.32) where I is the identity matrix, p is the momentum operator and V is the external potential, and the wave function is a four component column spinor, eq. (2.33), containing the large component, ψ_L, and the small component, ψ_S. The small component solution corresponds to the positrons whereas the large component solution corresponds to the electrons.

$$\alpha = \begin{pmatrix} 0 & \sigma_{x,y,z} \\ \sigma_{x,y,z} & 0 \end{pmatrix} \qquad (2.30)$$

$$\sigma_x = \begin{pmatrix} 0 & 1 \\ 1 & 0 \end{pmatrix}$$
$$\sigma_y = \begin{pmatrix} 0 & -i \\ i & 0 \end{pmatrix} \qquad (2.31)$$
$$\sigma_z = \begin{pmatrix} 1 & 0 \\ 0 & -1 \end{pmatrix}$$

$$\beta = \begin{pmatrix} I & 0 \\ 0 & -I \end{pmatrix} \qquad (2.32)$$

$$\psi = \begin{pmatrix} \psi_L \\ \psi_S \end{pmatrix} = \begin{pmatrix} \psi_L \uparrow \\ \psi_L \uparrow \\ \psi_S \downarrow \\ \psi_S \downarrow \end{pmatrix} \qquad (2.33)$$

The four components in the wave function produced by the Dirac equation make calculations more complex to do and the Dirac equation also has technical problems like variational collapse. Moreover, spin-orbit coupling effects make analysis even more complicated. To overcome these challenges, certain approximations to the Hamiltonian have been introduced. One of the common approximations is the zeroth-order relativistic approximation (ZORA) [145,146]. This approach approximates the Dirac equation in a way that reduces the four-component form to a two-component form, the two components being the alpha and beta spin orbitals in the scalar form. This approximation helps to reduce the complexity of the calculation [147].

I have used the Priroda code for my calculations, and this code uses a method whereby starting from the full Dirac equation it applies a relativistic scalar four-component process in which all the spin-orbit terms are separated from their scalar terms[148,149] and neglected[148,150–152] whereas the ADF code uses ZORA method to account for the relativistic effects, which I used to calculate natural bonding orbital analysis.

Spin-orbit effects are negligible for finding the geometry optimization and bonding energies of closed-shell molecules or in cases where the number of unpaired electrons remains constant, and under these situations the scalar relativistic calculations generally provide reasonable results. Spin-orbit effects are in general important to account for in excited states calculations or in chemical reactions involving complexes containing actinides but again scalar results are reasonable if the number of unpaired electrons stays the same throughout the reaction.

But for most of the open-shell complexes of actinides, it is necessary to incorporate the spin-orbit coupling. For all our polypyrrolic macrocyclic complexes, for unrestricted spin states, spin-orbit coupling effects are found to be appropriate to include.

2.7 Geometry Optimization and Vibrational Frequency Calculations

I have carried out geometry optimization using Cartesian coordinates; an initial geometry is input, an SCF calculation is carried out and then the first derivatives of the energy with respect to nuclear displacements are calculated. These gradients are used to identify stationary points on the potential energy surface as well as to find the optimized geometry. The vibrational frequencies are calculated by computing the second derivatives of the energy with respect to nuclear displacements along all the three Cartesian axes.

The vibrational frequencies were calculated to test the nature of stationary points for the optimized geometries.

2.8 Computational Analysis Techniques

A wide range of tools is available to analyze the bonding patterns of a simulated molecule. To gain insight into the chemical environment of the molecules, some of the molecular properties such as bond lengths, bond angles, atomic charges, bond orders and atomic charges are addressed in this work. We have used these parameters to comment on the relative covalency in the complexes of early actinides. Calculations of bond lengths, bond angles, bond orders, and atomic charges are usually built into a variety of computational software packages available, including the ones we are using for our work. Mayer bond order [153,154], NBOs [155] and Hirshfeld atomic charges [156] have been used and all of these are discussed in the following.

2.8.1 Mayer bond order analysis

There are various ways to analyze the nature of the bond between two atoms. One useful way is to use bond orders, which convert the output of quantum mechanical calculations into the concept of fractional, single, double, triple or even higher bonds. Bond orders can also be used to comment on the covalency or ionicity of a bond. The Mayer bond order [153,154] has proven useful in inorganic chemistry and is frequently used throughout this thesis. The Mayer bond order [154] between atoms A and B is given by

$$I_{AB} = I^{\alpha}{}_{AB} + I^{\beta}{}_{AB} = 2\sum_{a\in A}\sum_{b\in B}[(P^{\alpha}S)_{ba}(P^{\alpha}S)_{ab} + (P^{\beta}S)_{ab} + (P^{\beta}S)_{ba}] \qquad (2.34)$$

Where P^{α} and P^{β} are the alpha and beta density matrix respectively, and S is the overlap matrix. This equation can be rewritten using the total density matrix $P = P^{\alpha} + P^{\beta}$ and the spin density matrix $P^{S} = P^{\alpha} - P^{\beta}$

$$I_{AB} = \sum_{a\in A}\sum_{b\in B}\ [(PS)_{ba}(PS)_{ab} + (P^{S}S)_{ba}(P^{S}S)_{ab}] \qquad (2.35)$$

For the restricted close-shell case, since the spin density is zero, the formula can be simplified to

$$I_{AB} = \sum_{a\in A}\sum_{b\in B}(PS)_{ab}(PS)_{ba} \qquad (2.36)$$

Where the product PS is the Mulliken population and so the Mayer bond order is related strongly to Mulliken populations,[157] and is calculated from the former along with the density matrix containing all the orbital coefficients. The Mayer bond order provides us with a method of summing all the electron density contribution to the bond. However, due to the Mayer bond order being closely related to the Mulliken formulation of atomic charges there is basis set

dependence of the bond orders. Comparisons between different sets of calculations can thus only be done if the same basis sets have been used.

2.8.2 Hirshfeld Atomic Charges[127]

Further the Hirshfeld scheme partitions the total density into atomic contributions. It uses a weighing factor, w_A, to assign different amounts of density to the atoms in the molecule. w_A is based on how large the atomic density contribution, $\rho_{atomicdensity}$, to the total density of the system is if the total density is defined as the sum of all atomic densities (eq.2.37 and 2.38). This density is called the $\rho_{promolecule}$ while the real density is called $\rho_{molecule}$.

$$\rho_{promolecule}(r) = \sum_{A}^{M_{Atoms}} \rho_A^{atomicdensity}(r) \qquad (2.37)$$

$$w_A = \frac{\rho_A^{atomicdensity}(r)}{\rho_{promolecule}(r)} \qquad (2.38)$$

The Hirshfeld charge of an atom is then calculated by taking the difference between the nuclear charge and the electron density, assigned using the total density multiplied by w_A, integrated over all space.

$$Q_A = Z_A - \int w_A(r)\rho_{molecule}(r)d(r) \qquad (2.39)$$

2.8.3 Quantum Theory of Atoms in Molecules (QTAIM)

QTAIM, also referred as AIM, is a technique developed by Richard F. W. Bader [153]. It is a useful quantitative analysis technique based on the topology of the electron density in a molecular system and is used to analyze various molecular properties. Molecules can be divided into atomic basins, containing atomic nuclei. The basins are connected by surfaces where the scalar product of the gradient of the electron density with a vector perpendicular to the surface is

equal to zero. All gradient vector field lines in one basin merge to the atomic nucleus, defining the basin as region of space surrounding the nucleus. In topological analysis, the points at which the gradient norm of a function is zero (except at infinity) are known as critical points (CPs). Further, these CPs can be categorized depending upon how many eigenvalues of the Hessian matrix of the real space function are negative (Table 2.1).

Type	Notation	Represents
Nuclear	(3, -3)	An atomic centre
Bond	(3, -1)	Min. ρ on bond path
Ring	(3, +1)	Min. ρ within a ring of bonds
Cage	(3, +3)	Min. ρ at the centre of a cage of bonds

Table2.1: Types of critical points where ρ is the molecular density

A bond path, as defined by QTAIM, is a line of locally maximum electron density connecting two bonded atoms. The properties at a bond critical point are representative of the properties of the density along a bond path, which in turn are related to the properties of the bond between two atoms. Thus, the information about the bonding between atoms has been inferred from critical points that are local maxima in two directions and local minima in the third, called the bond critical points (BCPs)

The main goal here is to give a brief description of the parameters in QTAIM, which has been used in this thesis for the bonding analysis.

The values of electron density ρ, Laplacian of the density $\nabla^2\rho$, energy density H, and ellipticity at the BCPs are used to comment on the ionicity or the covalency of the bonds of interest. The value of the Laplacian of the density at a given point may be positive or negative representing charge depletion or charge accumulation respectively. The negative values of the Laplacian are correlated with the covalency of the bond. The energy density is a little more complex, as it can be considered as the sum of T, the local kinetic energy (positive), and V, the local potential energy density (negative). It shows to what extend the attractive forces on the electrons are balanced by the dispersive forces. There would be an overall negative value of the energy density for a point where the attractive forces exceed the repulsive ones and thus the negative values of H at the bond critical point are therefore considered as associated with the covalent character. The ellipticity ε is another parameter of interest that gives insight into the nature of bond. It describes how much cylindrical a bond is; its value is expected to be zero for single and triple bonds, while it should be nonzero for double bonds.

The QTAIM, that mainly focuses on the properties of the electron density, has been used to probe the bonding of a number of actinide complexes such as actinide dimetallocenes An_2Cp_2 [158], Bis(triazinyl)pyridine [159], actinocene $AnCOT_2$ [160] polyazine MX_3L[161] (M^{+3} = Ce, Nd, Eu, U, Am, and Cm; X = RCp^- or NO_3^-; L = N-donor ligand), uranyl complexes with the expanded porphyrin isoamethyrin and bis-triazinyl- pyridine [162] organoactinide complexes[68] of the form $[LAnX]^{n+}$, L=trans-calix[2]benzene[2]pyrrolide, actinide helium complexes [163] $AcHe_n^{3+}$ where n=1-17. These studies have proved QTAIM to be a good method for the bonding analysis in case of heavy element chemistry.

The Multiwfn code [164] has been used throughout this thesis to carry out the bonding analysis based on the QTAIM on molecular systems.

2.8.4 Natural bonding Orbital (NBO) analysis

The natural bond orbital methods encompass a suite of algorithms that helps us to obtain important fundamental bonding information from Hartree-Fock, DFT and post-Hartree-Fock calculations. The natural bond orbital analysis refers to a set of mathematical algorithms for analyzing electronic wave functions in terms of Lewis-like chemical bonds [155]. The NBO method [165] has been designed to represent a quantitative interpretation of the electronic structure of a molecule in terms of Lewis structure. More precisely, they are an orthonormal set of localized maximum occupancy orbitals whose leading N/2 members (or N in the open-shell case) represent the most exact possible Lewis-like description of the total N-electron density [155]. As the Lewis structures are popular bonding models in chemistry, the NBO method is commonly used for the interpretation of the bonding situation. One of the advantages of the NBO analysis is that the results are not basis set dependent.

I used ADF 16 [39] to calculate NBO bond orders for all the polypyrrolic complexes of the early actinides.

Chapter 3

A Relativistic DFT Study and QTAIM Analysis of Mono- and Complexes of Th(IV), Pa(IV), Pa(V) and U(IV) with an Extended Polypyrrolic Ligand in Comparison with Their U(VI) Analogues

3.1 Introduction

Our understanding for the actinide bonds is not as wide as that for the rest of the elements in the periodic table and understanding actinyl chemistry is essential for the development of the actinide chemistry both from the fundamental as well as from the technological viewpoint[14]. Complexes of actinides with aromatic π-electron systems are interesting as they help with the understanding of the physical and chemical properties of the actinides by providing insight into novel electronic structures and covalent contributions to the metal-ligand bonding. [12,14,166] Such covalent metal-ligand bonding interactions with soft ligands provide important evidence for the involvement of the 5f and other valence orbital in actinide bonding. In case of actinides, covalency is found to depend on the nature of the hard-soft interactions between the metal and the ligand, oxidation state of the actinide ion and also the accidental energy match of the ligand and metal valence orbitals[167]. It has been found that as we go from thorium to uranium, 5f orbitals gets stabilized and becomes approximately degenerate with the highest occupied orbitals of the ligand leading to an unusual situation where the valence molecular orbital has significant contributions from both the actinide and the ligand.[166] As a result, uranium forms marginally

more covalent bonds as compared to rest of the actinides. A lot of research is being done on the covalency in actinide complexes as well as on finding trends in covalency across the actinide series both experimentally and computationally[12,168–172].

Computational work[173,174] has been done to probe the bonding properties of the uranyl ion UO_2^{2+}, particularly the short U-O bond length, and, moreover, a number of interpretations have been proposed for the linearity of the uranyl dication. For instance, Wadt[175] ascribed it to U(5fπ)-O(2pπ) interactions and he found that the U(6p) orbitals do not play any significant role. Tatumi and Hoffman[176], in contrast to Wadt, found that there is cooperativity between the U(6p) and U(5f) orbitals and concluded that this determines the linear structure. According to one of the proposals, strong U(5f)-O(2p) bonding interactions hindered by U(6p)-O(2S) repulsive interactions are responsible for the shortness of the U-O bond.[173]

Our research group and many others have performed various quantum theory calculations on a number of complexes of actinides with the various macrocyclic ligand.[18,20,41,55–63] Amongst them, there is a flexible Schiff-base pyrrole macrocyclic ligand H_4L (Fig 3.1), prepared by the Love[69] and Sessler[70] groups independently, which has been found to be a very good ligand for making very stable complexes with the actinides. This ligand[70] has two N_4 donor compartments and the studies of Arnold and Love et al. have shown that this macrocyclic ligand can accommodate metal atoms like transition metals, lanthanides as well as actinides in its two vacant sites[15,21,40,71–79]. The two aryl groups in this ligand acts as hinges that results in a relatively rigid molecular structure, sometimes referred to as a Pacman structure[80–82]. The bite angle, in these type of complexes, between the two N_4 donor plane show a lot of variations, exhibiting its excellent flexibility.[16,22,74,77,79,177–179]

Arnold, Love and co-workers used this ligand to successfully synthesize the diuranium(VI) complex $K_2[(UO_2)_2(\mu\text{-}O_2)]$[78], the diuranium(V) complex $[\{(Me_3Si)OU(\mu\text{-}O)\}_2(L)]$[77], and diactinide(III) complexes $[(AnX)_2(L)]$ (An = U, X = I, BH_4; An = Np, X = I)[15], amongst others. In addition to the synthetic part, quantum chemical calculations on many mononuclear and binuclear complexes of Uranium, Neptunium and Plutonium have also been done. Among earlier actinides, complexes of thorium with these macrocyclic ligands have not been much studied either experimentally or theoretically. However, many comparative studies of various complexes of thorium and uranium with small ligands such as cyclopentadienyl[83], benzyne[84], metallocene[83] have been reported in the recent past.

All the binuclear complexes exhibit cation-cation interactions (CCI). These interactions occur through the coordination of one actinide metal center by the oxo atom of a second actinyl unit and these can lead to the formation of dimers[100–104] , oligomers,[105–107] one-dimensional chains[108–110] as well as multi-dimensional networks[93,105,109–116] that may occur without the support of ancillary ligands.

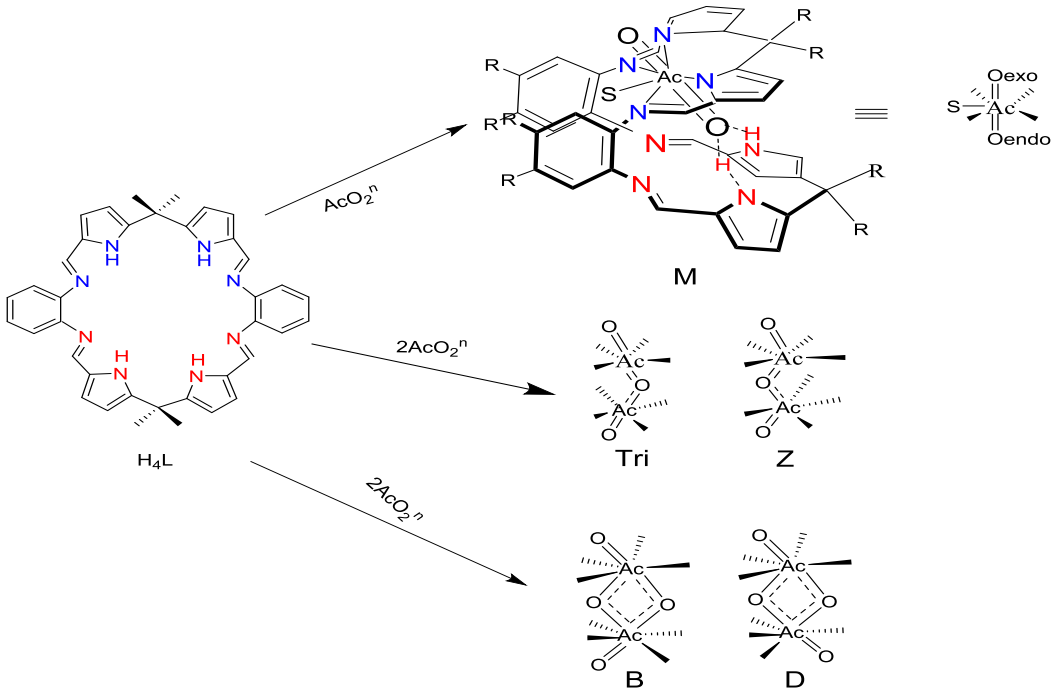

Figure3.1: Skelton structures of various theoretically predicted mononuclear and binuclear complexes of early actinides. The simplified structures represent the coordination sphere of the actinides sitting in the cavity.

Complexes	Abbreviations	Ref.
M $[(Th^{IV}O2)(H_2L)(THF)]^{-2}$	Th(IV)-M	This chapter
M $[(Pa^{IV}O2)(H_2L)(THF)]^{-2}$	Pa(IV)-M	This chapter
M $[(Pa^{V}O2)(H_2L)(THF)]^{-1}$	Pa(V)-M	This chapter
M $[(U^{IV}O2)(H_2L)(THF)]^{-2}$	U(IV)-M	This chapter
M $[(U^{VI}O2)(H_2L)(THF)]$	U(VI)-M	Ref. [88]
B-shaped $[(Th^{IV}O_2)_2(L)]^{-4}$	Th(IV)-B	This chapter
Protonated-B$[(Th^{IV}O_2)_2(H)(L)]^{-3}$	Th(IV)-BH	This chapter
$[(Th^{IV}O_2)_2(2H)(L)]^{-2}$	Th(IV)-B2H	This chapter
B-shaped$[(Pa^{IV}O_2)_2(L)]^{-4}$	Pa(IV)-B	This chapter
Protonated-B$[(Pa^{IV}O_2)_2(H)(L)]^{-3}$	Pa(IV)-BH	This chapter
$[(Pa^{IV}O_2)_2(2H)(L)]^{-2}$	Pa(IV)-B2H	This chapter
B-shaped$[(Pa^{V}O_2)_2(L)]^{-2}$	Pa(V)-B	This chapter
Protonated-B$[(Pa^{V}O_2)_2(H)(L)]^{-1}$	Pa(V)-BH	This chapter
$[(Pa^{V}O_2)_2(2H)(L)]$	Pa(V)-B2H	This chapter
B-shaped$[(U^{IV}O_2)_2(L)]^{-4}$	U(IV)-B	This chapter
Protonated-B$[(U^{IV}O_2)_2(H)(L)]^{-3}$	U(IV)-BH	This chapter
$[(U^{IV}O_2)_2(2H)(L)]^{-2}$	U(IV)-B2H	This chapter
B-shaped $[(U^{VI}O_2)_2(L)]$	U(VI)-B	Ref.[88]
Protonated-B$[(U^{VI}O_2)_2(H)(L)]^{+1}$	U(VI)-BH	Ref.[88]
$[(U^{VI}O_2)_2(2H)(L)]^{+2}$	U(VI)-B2H	Ref.[88]
D-shaped $[(Th^{IV}O_2)_2(L)]^{-4}$	Th(IV)-D	This chapter
D-shaped $[(Pa^{IV}O_2)_2(L)]^{-4}$	Pa(IV)-D	This chapter
D-shaped $[(Pa^{V}O_2)_2(L)]^{-2}$	Pa(V)-D	This chapter
Z-shaped $[(Th^{IV}{}_2O_3)(L)]^{-2}$	Th(IV)-Z	This chapter
Z-shaped $[(Pa^{IV}{}_2O_3)(L)]^{-2}$	Pa(IV)-Z	This chapter
Z-shaped $[(Pa^{V}{}_2O_3)(L)]$	Pa(V)-Z	This chapter
Tri-shaped$[(Pa^{V}{}_2O_3)(L)]$	Pa(V)-Tri	This chapter
Tri-shaped $[(U^{IV}{}_2O_3)(L)]^{-2}$	U(IV)-Tri	This chapter
Tri-shaped $[(U^{VI}{}_2O_3)(L)]^{-2}$	U(VI)-Tri	Ref.[88]

Table3.1: The calculated complexes with their abbreviations and references. M-mononuclear, B-butterfly, D-diamond, Z-zigzag and Tri-triangle

In this chapter, we present the mononuclear and binuclear complexes (Table 3.1) of ThO_2 (IV), PaO_2 (IV, V) and UO_2 (IV, VI) with the macrocyclic ligand H_4L using a density functional (DFT) approach. All these cation-cation complexes show unusual geometries. This study includes the optimized geometries, bond lengths, bond angles, atomic charges, natural bond order analysis as well as QTAIM analysis of the bonding.

In this study, we investigated the bonding patterns in these complexes and compared how the complexes of ThO_2 and PaO_2 differ from the already known uranyl (UO_2) complexes. Thus, we explored the changes in geometries and electronic structure of the complexes as a function of the actinide and we also probe the effect of changing the oxidation state of the actinide.

3.2 Computational Details

Both the relativistic and correlation effects are required to precisely model the actinides. In actinides, the 5f, 6d and 7s orbitals are close in energy which induces various low-lying metastable states around the ground state of actinides and thereby causing severe convergence problems especially for the open shell actinide complexes.

To determine the electronic structure of all the actinyl complexes of the polypyrrolic ligand in the ground state, calculations were performed in the gas phase using the Priroda code[150,180–183]. Priroda utilizes a fast resolution-of-identity (RI) method for evaluating both Coulomb and exchange-correlation integrals using auxiliary optimized fitted Gaussian basis sets and thereby improving the computational efficiency of the code. A scalar relativistic four-component all electron (AE) approach, based on the full Dirac equation, was used to account for the relativistic effects for the heavy elements[180]. In the Dirac equation, all the spin-orbit coupling

terms are separated from the scalar terms and neglected[149]. All the calculations were done with a spin restricted approach except for Pa(IV) and U(IV) complexes, for which a spin unrestricted formalism was applied. We used the Perdew-Burke-Ernzerhof (PBE) functional[139] of the generalized gradient approximation (GGA). All electron correlation-consistent Gaussian basis sets of double zeta polarized quality (B-I) were used[181]. The natures of the stationary points on the potential energy surface were confirmed further by carrying out frequency calculations, and then the thermodynamic data was obtained thereafter.

On the basis of these PBE calculations, both the population based Mayer bond orders[184] and atomic charges as developed by Hirshfield[185] were calculated. Both bond orders and atomic charges have been found quite helpful in explaining the chemical surroundings of a variety of actinide and actinyl complexes[41,55,186–189] although these are not quantum mechanical observables. Furthermore, single point ADF calculations on the Priroda geometries were performed which were then used to carry out the natural bond orbital (NBO) analyses using the NBO package[165] included in the ADF code[190] The scalar relativistic ZORA method[191–193] along with the Slater type ZORA-TZP basis sets comparable to those used in Priroda were employed in the ADF calculations.

The topology of the (3, -1) bond critical points in the gradient field of the electron density were analyzed using the quantum theory of atoms in molecules (QTAIM).[194] This was done with the Multiwfn[164] code.

3.3 Results and Discussion

Based on the uranyl complexes with the binucleating Schiff-Base polypyrrolic macrocyclic ligand (H_4L) (Fig 3.1) that resemble a Pacman structure, computational studies have

been performed on thorium (IV), protactinium (IV, V) as well as uranium(IV) in comparison to the uranium(VI) analogues. As shown in Figure 3.1, the macrocyclic ligand reacting with one equivalent of AcO_2^n produces mononuclear complexes whereas with two moles of AcO_2^n gives binuclear complexes viz. B, D, Z, and Tri -shaped structures.

Our primary aim is to investigate the nature of bonding in these complexes which will enhance our knowledge about the organometallic complexes of actinides. In this chapter, comparative studies of ThO_2 (IV), PaO_2(V) as well as UO_2(VI) complexes are presented, all of which contain a f^0 electronic configuration. In addition to this, we carried out the bonding analysis of the complexes of the first three actinides in the +4 oxidation state also.

3.3.1 Geometrical parameters

(a) Mononuclear complexes: All the Mononuclear complexes, **M** $[(AcO_2)(H_2L)(THF)]^{-2}$ [where Ac is Th(IV), Pa(IV, V) and U(IV)] with the Pacman ligand are examined with relativistic density functional theory using PBE functional. The nature of these structures as local minima was further confirmed by carrying out frequency calculations. In these complexes, only one actinyl ion is placed in one of the cavities while the other cavity is kept vacant. In the equatorial plane, the actinyl group is coordinated to N_4 of one compartment of the polypyrrolic ligand and the fifth equatorial position has been occupied by the solvent molecule tetrahydrofuran.

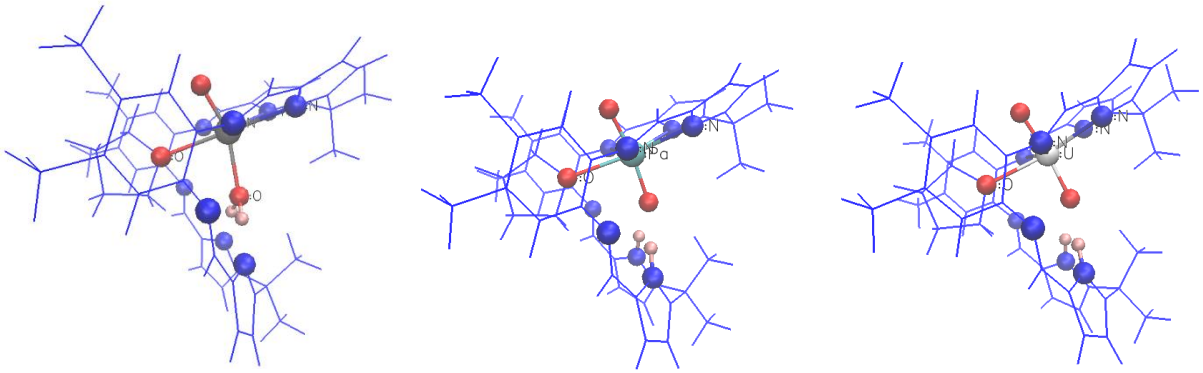

(a) Th(IV))-M **(b) Pa(IV)-M** **(c) U(IV)-M**

Figure3.2: The optimized gas phase geometries of mononuclear complexes, (a) $[(Th^{IV}O2)(H_2L)(THF)]^{-2}$, (b) $[(Pa^{IV}O2)(H_2L)(THF)]^{-2}$ and $[(U^{IV}O2)(H_2L)(THF)]^{-2}$ (Where Silver, Th; Cyan, Pa; White, U; Blue, Nitrogen; Red, Oxygen; White, Hydrogen)

The optimized geometries for the mononuclear complexes of Th(IV), Pa(IV) and U(IV) are shown in the Figure 3.2 with their geometrical parameters in the Table 3.2, calculated in their high spin ground state. As expected from the actinide contraction and increasing effective positive charge of the Ac ions, it is evident from the Table 3.2 that the calculated Ac-O as well as Ac-N bond distances decreases gradually as we go from thorium to uranium; a similar effect is observed upon oxidation of the actinide. In almost all the cases, the Ac-O_{endo} bond distance is longer than the Ac-O_{exo} (Fig. 3.3) which indicates that the actinide forms stronger bond with the O_{exo} than with the O_{endo}. The elongation of Ac-O_{endo} bond arises from the interaction of the O_{endo} with the two N-H of the lower cavity as depicted in Figure 3.2. Similar trends have been found in the experimentally reported mononuclear U(VI)-M[21] and various theoretically studied mononuclear complexes.[59] The Ac-O bonds in case of reduced actinyl complexes like Pa(IV) and U(IV) as compared to their oxidised counterparts, Pa(V) and U(VI) respectively, are elongated by about 0.01-0.03Å (Table 3.2). This increase of the Ac-O bond upon reduction is consistent

with previously reported theoretical[30,174,187,188,195] and experimental findings.[73,108,196–198]Similar effects have been found in case of Ac-N bond distances. All these findings indicate that U(VI) forms strongest bond whereas Th(IV) forms the weakest bond to the oxygen and this may be due to the accidental energy match of the 5f orbitals of the actinide and that of the ligand orbital.

Furthermore, in case of mononuclear structure of thorium, the Th-O_{endo} bond is large enough to abstract the two protons form the nitrogens of the lower cavity and thus in case of Th(IV)-M there is strong interactions between the O_{endo} and the hydrogens, the bond distance being 1.05 Å (see Table 3.1) so it is just acting like H_2O molecule which has weak interactions with the thorium ion, while on the other hand in case of both Protactinium and Uranium, there is only a weak interaction of the O_{endo} with the hydrogens. Moreover, in case of Th(IV)-M, the O_{exo}-Th-O_{endo} bond angle is quite bent (158.14º) as compared to the ones found in case of Pa (IV, V) (171.17º) as well as U (IV, VI) (173.33º) complexes.

BLs [BO]	Th(IV)-M	Pa(IV)-M	Pa(V)-M	U(IV)-M	U(VI)-M
Ac_1-O_{exo}	1.94 [2.34, *1.44*] [a]	1.87 [2.40, *1.85*]	1.86 [2.41, *1.87*]	1.84 [2.40, *1.96*]	1.80 [2.42, *2.10*]
Ac_1-O_{endo}	2.45 [0.65, *0.36*]	1.94 [2.02, *1.48*]	1.93 [1.92, *1.56*]	1.89 [2.10, *1.73*]	1.83 [2.20, *1.91*]
Ac_1-O_{eq}	2.63 [0.30, *0.19*]	2.57 [0.31, *0.23*]	2.60 [0.30, *0.24*]	2.57 [0.30, *0.25*]	2.48 [0.41, *0.38*]
Ac1-N	2.79/2.63 [0.19/0.26, *0.21/0.27*]	2.74/2.58 [0.20/0.29, *0.25/0.34*]	2.73/2.56 [0.21/0.30, 0.31/0.40]	2.71/2.55 [0.22/0.31, *0.29/0.39*]	2.60/2.46 [0.32/0.42, *0.43/0.53*]
O_{endo}-H	1.05 [0.77, *0.54*]	1.94 [0.10, *0.04*]	1.78 [0.15, *0.06*]	2.03 [0.07, *0.05*]	2.09 [0.05, *0.02*]
Bond angles					
O_{exo}-Ac-O_{endo}	158.14	171.17	171.16	173.34	175.19
Spin densities (Charges)[b]					

Ac	0.00 (0.50)	0.003 (0.47)	0.00 (0.48)	0.92 (0.43)	0.00 (0.55)
O_{exo}	0.00 (-0.50)	0.00 (-0.42)	0.00 (-0.40)	0.002 (-0.37)	0.00 (-0.29)
O_{endo}	0.00 (-0.24)	0.00 (-0.37)	0.00 (-0.36)	0.03 (-0.34)	0.00 (-0.30)

Table3.2: Optimized gas phase Bond lengths (BLs) and Bond orders [Mayer, NBO] for the complexes, Th(IV)-M, Pa(IV)-M, Pa(V)-M, U(IV)-M and U(VI)-M (BLs in Å and angles in degrees). [a]Calculated bond orders [Mayer, NBO] are indicated in parentheses. [b]Charges are given in parentheses.

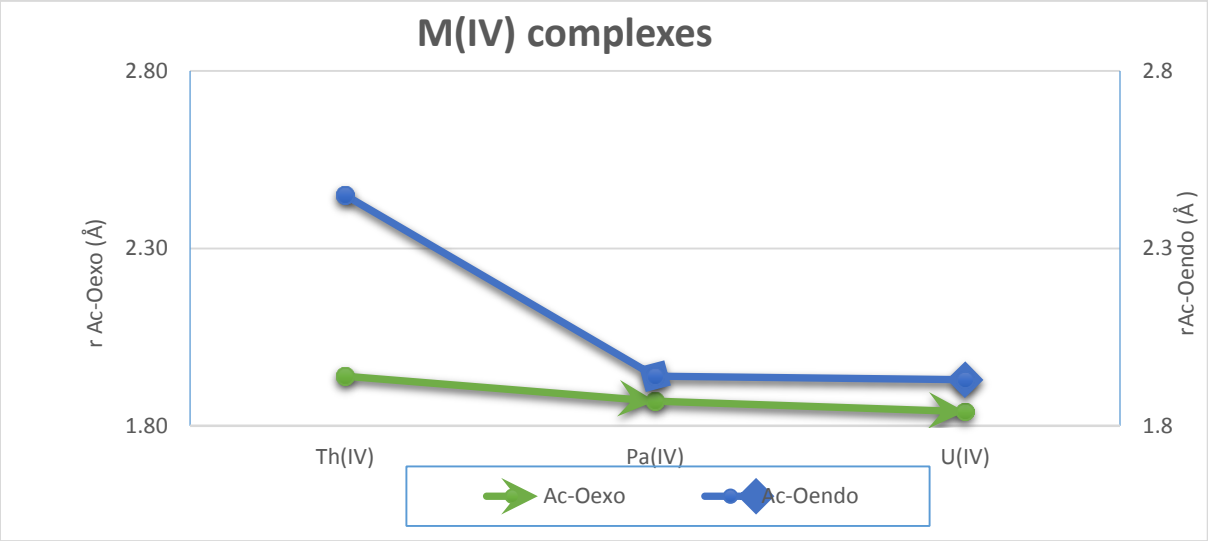

Figure3.3: Variation of bond length r (Ac-O_{exo}) as well as r (Ac-O_{endo}) for Ac(IV)-M complexes where Ac=Th, Pa and U.

The Ac=O_{exo} bond order increases from 2.34 to 2.42 as we move from Th(IV)-M to U(VI)-M, whereas in case of the Ac=O_{endo} bond, it varies from 0.65 to 2.20. In both cases, there is an abrupt change in the bond order in going from Th→Pa. In case of Th(IV)-M, the Th-O_{endo} bond order is 0.65 whereas it is 0.77 for the O_{endo} to H…N bond, indicating both as single bonds. Bond orders based on NBO analysis, as shown in Table 3.2 in *Italics,* follow the same trend as that of

the Mayer bond orders but are much smaller than their corresponding Mayer bond orders. Among these two bond orders, the Mayer bond order seems to be more reliable in case of actinides.[199,200]Bond order analysis also indicates more covalency in uranium complexes than the thorium and protactinium complexes.

Spin densities and charges of the atoms of interest in all the M complexes are also listed in Table 3.2. The charge on O_{endo} in case of Th(IV)-M is -0.24 which is less as compared to that on O_{endo} in U(VI)-M which is -0.30 implying that O_{endo} is somewhat more basic in the latter case than the former.

(b) Binuclear complexes A total of 24 binuclear complexes of the first three actinides in various oxidation states were studied. These structures were optimized followed by frequency calculations to confirm the nature of stationary points on the potential energy surface. Most of these complexes show very unusual coordination modes of the actinyl group. Corresponding to the well-known butterfly (B) structure of U(VI) Pacman complexes,[57] B structures in cases of ThIV), Pa (IV, V) and U(IV) were studied. In addition to this, their protonated forms B-H, B-2H where one of the O_{endo} gets protonated first singly and then doubly are also studied. As seen in our previous studies[57], the protonation changes the structures of the original complexes greatly. In case of Th(IV)-B, protonation of one of the O_{endo} lengthens the Ac-O_{endo} bond from 2.21 Å to 2.49 Å in the B-H structure while it goes to 3.08 Å in B-2H structures. Accordingly, their respective bond orders vary from 1.14 to 0.60 in case of single protonation whereas it reduces to 0.15 in case of the double protonation. Similar trends are observed in all other cases of Pa and U (Table S1 in the appendix). In the doubly protonated B structure, the water can easily be removed by dehydration giving rise to the Z structure in case of Th(IV) and Pa(IV) while it forms Tri

shaped complexes in Pa(V), U(IV) and U(VI). All these names are based on the shape of the skeleton containing the actinide and the oxygen atoms, Figure 3.1.

Butterfly B and **Diamond D structures** $[(AcO_2)_2(L)]^n$, n=0, -2, -4 where Ac=U(VI), n=0; Ac=Pa(V), n=-2; Ac=Th(IV), Pa(IV) or U(IV), n=-4: The optimized geometries for the butterfly and diamond structures are depicted in Figure 3.4. All the B complexes show very similar geometries. In case of D structures, the two Ac-O_{exo} bonds are pointing in opposite directions and, moreover, the actinide in the lower cavity is not in the plane formed by four nitrogen which contrasts with the case of the B complexes. Table 3.3 contains calculated bond lengths and bond angles for the B structures. The effect of the actinide contraction is also seen in cases of B and D structures as we move from Th→Pa→U (Table 3.3). There is a sharp decline of 0.13 Å in the Ac-O_{exo} bond length in going from Th(IV)-B to Pa(IV)-B and then it goes down gradually thereafter with a total decrease of 0.21 Å. The Ac-N bonds also show the effect of the actinide contraction as there is a total reduction of 0.32 Å as we move along the actinide series from the thorium complex to the corresponding uranium complex. As found in case of the mononuclear complexes, here also the Ac-O_{endo} bond is longer than the Ac-O_{exo} bond and moreover the reduced complexes have again longer Ac-O bonds in comparison to their oxidized complexes. In case of B structures, the two actinides have very similar chemical environments as the bond lengths (Table 3.3) and bond angles involving the two actinides are very much the same. However, in case of D structures, each of the two actinides has slightly different bonding parameters, and the bond angles O_{exo}-Ac2-O_{endo} are quite bent as compared to the O_{exo}-Ac1-O_{endo}. Among B and D geometries, B structures are much lower in energy than their corresponding D isomers. In case of Thorium, the B structure is -10.69 kcal/mol lower in energy than the D isomer, whereas the B complexes of Protactinium(IV) and Protactinium(V) are

stabilized by -13.02 kcal/mol and -21.48 kcal/mol respectively compared to their D geometries. The bite angle (α) between the two N_4 donor planes of the polypyrrolic ligand in case of binuclear complexes was calculated, and it varies from 87.99° in case of Th(IV)-B to 72.22° in U(VI)-B (Table S2). The decrease in the bite angle as we proceed from Th to U might be due to the decreasing size of the actinide because of actinide contraction. The flexibility of the Pacman ligand can be seen from the variation of the bite angle in going from the mononuclear to the corresponding binuclear complexes as it changes from 69^0 to 88^0 in case of Th(IV) complexes.

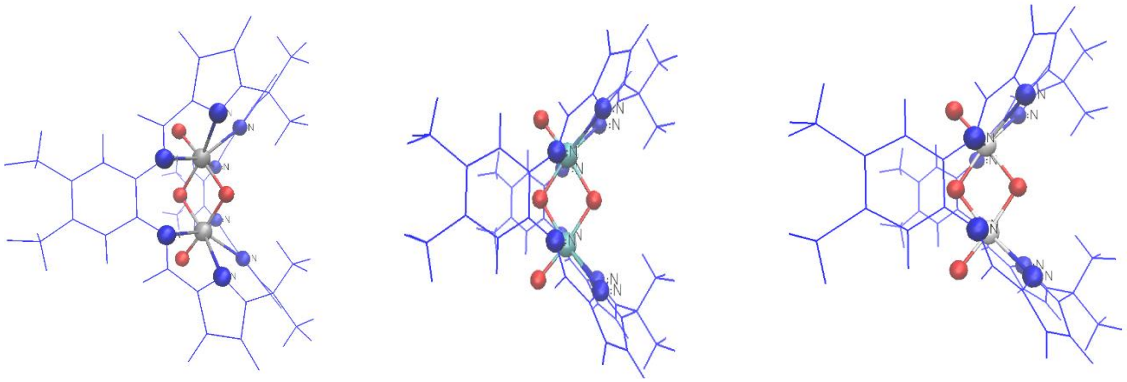

(a) (b) (c)

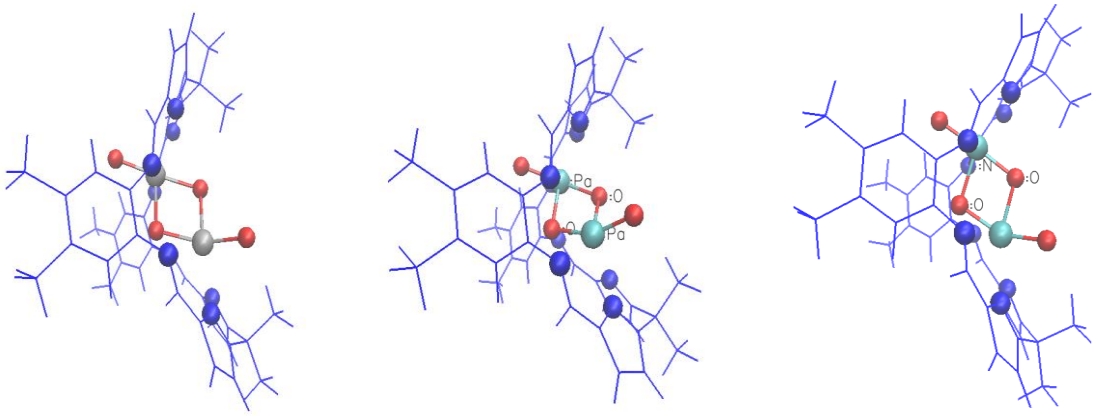

(d) (e) (f)

Figure3.4: Optimized geometries for the butterfly structures (a) Th(IV)-B (b) Pa(IV)-B and (c) U(IV)-B and the diamond structures (d) Th(IV)-D (e) Pa(IV)-D and (f) Pa(V)-D

Bond orders, both Mayer and NBO, and Mulliken Charges for the B and D structures are contained in Table S3 and Table S4 respectively in the appendix. Like the mononuclear complexes, here also in case of B and D structures, the Ac-O bonds become stronger as we go from Th→Pa→U indicating marginally more covalency in case of uranium complexes. Among B and D geometries, the Ac-O bond order is greater in B structures than their diamond isomers. In addition to this, the two Ac-O_{endo} bond in D structures are not the same as is the case for the B isomers. Moreover, the actinide ions in case of D structures have higher charges than those of the B structures. Like the M complexes, in case of B and D structures also, the NBO bond orders are less than their corresponding Mayer bond orders. The charge on the actinide in case of the B structures is half that of the actinides in case of M and Z or Tri complexes.

The protonated versions of these B structures in case of thorium, protactinium as well as uranium were also studied in which one of the two O_{endo} of the B complexes was protonated first singly and then doubly (Figure S1). On examining the geometrical parameters for the B, B-H and B-2H, we found that on protonation, there is a slight decrease in the Ac-O_{exo} bond length and Ac-O_{endo} bond but on the contrary, there is a large increase in the Ac-O_{endo} (protonated O_{endo}) bond in each case. The double protonation of the O_{endo} lengthens the Ac-O_{endo} bond to such an extent that the endo oxygen in each case is weakly bonded to the actinide (e.g. the Ac-O_{endo} bond order gets reduced to 0.15 on double protonation in case of Th(IV)-B). Thus, it acts just like a water molecule which upon removal gave rise to certain other geometries that are discussed in the next section.

Zigzag, Z, and Triangle, Tri, structures: After the removal of the water molecule which has formed due to double protonation of the B, certain other geometries like Z and Tri-shaped have been found which also fall in the category of binuclear complexes. The optimized geometries for the Z and Tri shaped complexes are depicted is figure S2 (appendix). Table S5 shows the geometrical parameters for these structures. These Z and Tri structures are equivalent to their corresponding doubly-protonated butterfly structures. There is a reduction of 0.15Å in the bond length across the series of the first three actinides. With the decrease of bond length due to the increase in the density of the nuclear charge across the An series, one might have expected that a stronger bond would have formed but in fact there is weakening of the bond occurring because of the actinide contraction of the valence 5f orbitals.[201]

BL's	Th(IV)-B	Th(IV)-D	Pa(IV)-B	Pa(IV)-D	Pa(V)-B	Pa(V)-D	U(IV)-B	U(VI)-B
Ac1-O_{exo}	2.02	2.01	1.89	1.87	1.88	1.87	1.86	1.81
Ac1-O_{endo}	2.21 2.24	2.21 2.25	2.14	1.99 2.38	2.14	2.00 2.32	2.12	2.09 2.11
Ac1-N	2.78 2.89	2.77 2.88	2.62 2.70	2.62 2.65 2.84 3.86	2.60 2.67	2.63 2.58 2.58 2.68	2.59 2.65	2.46 2.48
Ac2-O_{exo}	2.02	2.01	1.89	1.88	1.88	1.86	1.86	1.81
Ac2-O_{endo}	2.21 2.24	2.20 2.23	2.14	1.98 2.36	2.13	2.00 2.26	2.12	2.07 2.11
Ac2-N	2.78 2.89	2.74 2.82 3.00 3.76	2.62 2.70	2.60 2.67 2.76 4.19	2.60 2.67	2.62 2.64 2.76 3.16	2.59 2.65	2.46 2.52
Ac1-Ac2	3.54	3.52	3.45	3.47	3.43	3.45	3.39	3.37
BA's								
O_{exo}-Ac1-O_{endo}	177.77 103.42	176.03 108.26	173.42 100.35	159.17 94.48	175.20 101.72	176.74 104.61	174.75 101.00	176.07 102.96
O_{exo}-Ac2-O_{endo}	177.83 103.36	156.33 95.48	173.43 100.34	155.64 92.01	175.16 101.67	153.06 84.78	174.74 101.00	176.05 102.94

Table3.3: Optimized gas phase bond lengths (BL's in Å) and bond angles (BA's in degrees) for the complexes, Th(IV)-B, Th(IV)-D, Pa(IV)-B, Pa(IV)-D, Pa(V)-B, Pa(V)-D, U(IV)-B and U(VI)-B.

All the Z and Tri shaped complexes have two shorter Ac-O_{exo} bonds (1.80-1.95 Å) and two long Ac-O_{endo} bonds (2.16-2.06 Å). The Tri-shaped geometry bears resemblance to the experimentally reported binuclear V-O-V[202] and Fe-O-Fe[203] polypyrrolic complexes. The Z structure differs from the Tri shaped complex in the sense that O_{exo}-Ac_1-O_{endo} bond angle (Table S5) in the Z structure is strongly bent (110° -117°) as compared to the Tri shaped (152°-164°) complex. Th(IV) and Pa(IV) show only the Z shape whereas Pa(V) shows both the Z as well as the Tri shape, and in contrast to the early two actinides, U in both oxidation states considered prefers only the Tri- shape. Among the Z and Tri-structures of Pa(V), the Tri-isomer is found to be 48.54 kcal/mol more stable than its Z- counterpart. In all these complexes, the Ac-O_{endo} (2.16

Å – 2.06Å) is longer than the Ac-O_{exo} bond (1.95 Å -1.80 Å); their bond orders vary from 2.34 to 2.47 for the Ac-O_{exo} and is half about that for the Ac-O_{endo} bond (1.14-1.17). The inner bond becomes weaker due to the coordination from the oxygen atom of one actinyl to the other actinyl present in the other pocket, indicating the presence the cation-cation interactions.

3.3.2 Topology analysis of electron density using QTAIM approach: To gain further knowledge about the electronic structure of these complexes, the quantum theory of atoms in molecules (QTAIM) approach was applied. This approach focuses on the properties of the molecular electron density and not on the orbital structure. QTAIM has been known to well interpret the extend of covalency in multiconfigurational systems[13,204,205]and it has been previously applied to a number of actinide-ligand and other metal-ligand bonds[204–211]and thus it would help to develop the selective separation of the minor actinides[13,204,205,212,213]. Form the results so far, it has been concluded that, while actinide bonding is predominantly ionic, we can nevertheless differentiate the differences in the degree of covalency across the 5f series.

According to the QTAIM approach, there is one bond critical point (BCP) between each pair of atoms that are bonded to one another, and the chemical bonding interactions may be defined and categorized based on the properties of the electron density ρ, its laplacian $\nabla^2\rho$, and the energy density H (which is the sum of the kinetic and potential energy densities) at these BCP's.[214]

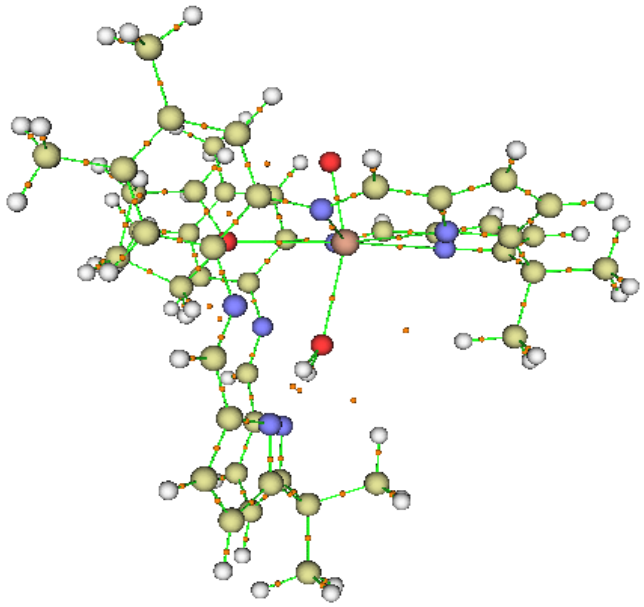

Figure3.5: QTAIM calculated molecular graph of the Th(IV)-M complex. Bond critical points (BCPs) are shown as red dots [Brown Th, Blue N, Red O, Green C and White H]. Picture created using Multiwfn.

After analysis of different systems, Bader proposed a general rule in which he suggested that ρ_{BCP} is greater than $0.2e^{-}/bohr^{3}$ for covalent bonds and is lower than $0.1e^{-}/bohr^{3}$ for closed-shell interactions. However, these limits are not strict but result from the studies across many molecular systems. The sign of $\nabla^{2}\rho$ at the BCP is also considered as a criterion for differentiating the bond types[215]. Covalent bonds are supposed to have a negative sign (accumulation of charge in the bonding region) while the closed-shell interactions have a positive sign. However, in case of strongly polar bonds there is significant accumulation of electron density between the nuclei, but the laplacian can be of either sign. In case of significant sharing of electrons between the bonding pairs, the energy density H is negative and its value demonstrates the extent of covalency.[216]

Other parameters of interest are the bond ellipticity ε and delocalisation index DI. The bond ellipticity, ε measures the shape of the electron density distribution in a plane through the bond critical point and perpendicular to the bond (cylindrical symmetry of a bond). The ellipticity of the bond tells us how cylindrical a given bond is; it is expected to be zero for single and triple bonds, while it is nonzero for a double bond. If two atoms are connected by an atomic interaction line the DI can be taken as a measure of bond order. The magnitude of the exchange of the electrons in the basins of one atom with those in the basin of another atom is termed as DI between them. It integrates the electron density in the bonding region of the bonded atoms and it is important to note that the computed values of the DI are always smaller than the values expected from the Lewis structures.[194]

These QTAIM parameters have been found very useful in predicting the nature of the bonding interactions but sometimes only taking the BCPs into consideration does not serve the purpose, or in other words, it is not sufficient to comment on the nature of the bond of interest. Improper position of the BCP as well as neglect of the surrounding environment of the BCP tend to result in erroneous conclusions.[215]Moreover, in case of actinide complexes especially for the metal-metal bonds, Kaltsoyannis et al.[213,217] has pointed out that these metal-metal bond has a topological behavior of their own, possessing neither ionic nor covalent features.

(a) Mononuclear complexes: Table 3.4 shows the calculated QTAIM metrics at the bond critical points for the Ac-O_{exo}, Ac-O_{endo} and the Ac-N bonds for the mononuclear complexes of the first three actinides in different oxidation states.

Ac-O bond: From Table 3.4, the electron density at the BCP for all the Ac-O_{exo} bonds is around 0.2 a.u. and there is a total variation of 0.08 a.u in going from Th(IV)-M to U(VI)-M for the Ac-

O_{exo} bond. As we go along the series, ρ_{BCP} increases, indicating more covalency in case of U (IV)-M than its thorium counterpart which is in accordance with the geometrical parameters findings. Moreover, on shifting from Pa (IV) to Pa (V) as well as from U (IV) to U(IV), the value of ρ_{BCP} shows an increase. For each of the complexes, the value of ρ_{BCP} for the Ac-O_{endo} bond is less than their respective Ac-O_{exo} bonds (Fig. S3), indicating that the Actinide is bonded more strongly to the O_{exo} than to the O_{endo} which is also supported by the bond length and bond order data in Table 3.2. In case of Th(IV)-M, the O_{endo}-H bonds as discussed earlier is a kind of covalent bond, and this is further supported by the QTAIM parameters (Table 3.4).

Although the ρ_{BCP} is larger than 0.2 a.u., the laplacian $\nabla^2\rho$ is positive for the Ac-O bonds in all the mononuclear complexes, indicating that the charge density is concentrated in the separated atomic basins instead of the internuclear region, which is thus locally depleted of electronic charge. The laplacian $\nabla^2\rho$ is usually positive for strongly polar bonding.[214] Such an interaction is usually considered as an intermediate between shared and closed shell interactions.[218,219]

The values for the energy density H at the BCP are negative, implying that there is shared shell interactions in these bonds. The magnitude of H becomes more negative for the uranium complex, indicating that there is more covalency as compared to the thorium and protactinium complexes. The values of the ellipticity for the all the Ac-O bonds is zero, which indicates the presence of a triple bond, also supported by the DI values which are close to three.

Parameters	Th(IV)-M	Pa(IV)-M	Pa(V)-M	U(IV)-M	U(VI)-M
ρ Ac-O_{exo}	0.20	0.23	0.24	0.24	0.28
ρ Ac-O_{endo}	0.06	0.20	0.19	0.22	0.25
ρ O_{endo}-H	0.26				
ρ Ac-N4,15	0.034	0.037	0.037	0.038	0.050
ρ Ac-N6,14	0.048	0.052	0.054	0.054	0.068
∇^2ρ Ac-O_{exo}	0.40	0.41	0.41	0.43	0.44
∇^2ρ Ac-O_{endo}	0.18	0.39	0.38	0.43	0.45
∇^2ρ O_{endo}-H	-0.12				
∇^2ρ Ac-N4,15	0.093	0.100	0.101	0.111	0.121
∇^2ρ Ac-N6,14	0.120	0.134	0.135	0.154	0.157
H Ac-O_{exo}	-0.11	-0.15	-0.16	-0.16	-0.20
H Ac-O_{endo}	-0.007	-0.11	-0.10	-0.13	-0.17
H O_{endo}-H	-0.38				
H Ac-N4,15	-0.001	-0.002	-0.002	-0.002	-0.006
H Ac-N6,14	-0.005	-0.007	-0.007	-0.007	-0.012
ε Ac-O_{exo}	0	0	0	0	0
ε Ac-O_{endo}	0.14	0	0	0	0
ε O_{endo}-H	0.01				
ε Ac-N4,15	0.15	0.19	0.20	0.13	0.23
ε Ac-N6,14	0.19	0.22	0.22	0.06	0.27
DI Ac-O_{exo}	2.68	2.81	2.81	2.84	2.89
DI Ac-O_{endo}	1.18	2.51	2.51	2.72	2.76
DI O_{endo}-H	0.60				
DI Ac-N4,15	0.80	0.81	0.81	0.92	0.95
DI Ac-N6,14	0.95	0.98	0.99	1.10	1.12

Table3.4: Topological analysis of calculate electron densities at the Ac-O_{exo}/Ac-O_{endo} BCPs for

the Mononuclear complexes. ρ = magnitude of electron density at BCPs, $\nabla^2\rho$= laplacian of ρ at BCPs, H = energy density at the BCPs, ε= ellipticity of the bond. All the values are given in a.u. The Nitrogens at positions 4 and 15, as well as those at 6 and 14 have the same values of the parameters.

In case of Th(IV)-M, the O_{endo} is abstracting two protons from the two N of the lower pocket and is forming bonds; this is also evidenced by the QTAIM parameters for these bonds. The electron density, laplacian as well as the energy density values all are indicative of a covalent bond. The ellipticity values for the Th-O_{endo} bond is 0.14 whereas it is almost zero for the O_{endo}-H bond.

Ac-N bond: The values of ρ, $\nabla^2\rho$, H, ε as well as DI are also contained in Table 3.4. Although for the Ac-N bond the ρ values are larger than the values for the Ac-O bond, the laplacian, H and DI values are all very small, indicating that the Actinide forms weaker bonds with Nitrogen than to the oxygen. The ε values also deviate from zero, meaning that the bonds are in between single and triple bond.

(b) Binuclear complexes: Table S6 gives the QTAIM parameters for the butterfly complexes and Table S7 summarizes the values for the Zigzag and triangle shaped complexes for both the Ac-O and Ac-N bonds. In case of binuclear complexes, we have two cavities each containing an actinide and we found that the environment of each of the two actinides is very similar; owing to this we have reported the QTAIM parameters of only one of them.

All the parameters for the Ac-O bond in case of butterfly, zigzag and triangle shaped complexes follow the same trend as in case of mononuclear complexes. Here also, we can see that there is more covalency in case of uranium complexes than in case of earlier two actinides

and more covalent character in uranium complexes has been established by various other works[13,204,205].

In addition to this, the Ac-O bond is stronger than the Ac-N bond and this is also supported by the DI index of these two bonds in various complexes and from the data on the respective bond lengths. The Ac-O_{exo} bond in the binuclear complexes is not as strong as it is in case of the Mononuclear, Zigzag and Triangle complexes. This statement is further supported by the ρ_{BCP} data (Fig. S4 and Fig. S5); this may be due to the presence of two O_{endo} in case of the former making it slightly weaker than in the latter case where there is only one O_{endo} present. Among the Z and Tri complexes as shown by Pa(V), the Tri-isomer based on the topology analysis is more stable, which agrees with the conclusion drawn based on the geometrical parameter analysis.

3.4 Conclusions

Many mononuclear as well as the binuclear complexes with the Pacman ligand of the first three actinides in various oxidations states in comparison with their analogues Pacman complexes of Uranium (VI) were studied using the relativistic density functional theory. All the structures were optimized followed by frequency calculations to confirm the nature of the stationary points.

The effect of actinide contraction is seen in these complexes as they all show a reduction of the bond lengths along the series Th-Pa-U. There is a total reduction of 0.14 Å (in the bond length) in going from Th(IV)-M to U(VI)-M for the Ac-O_{exo} bond where as in case of binuclear complexes, it shows a total decrease of 0.21 Å in the corresponding bond length. Likewise, the Ac-N bond in all the complexes has also shown the effect of actinide contraction along the series

(up to uranium). On the basis of the geometrical parameters, bond order as well as the QTAIM analysis, we found that uranium complexes exhibits more covalent character as compared to the other counterparts in accordance with various studies.[13,171,204,205]

All the binuclear complexes exhibit cation-cation interactions as in most of these complexes, the Ac-O_{endo} bond is quite long as compared to the Ac-O_{exo} bond. In case of Th (IV)-M this bond is long enough to even abstract the two protons from the lower cavity. In all the complexes, we found that the U (VI) forms stronger bonds with the axial oxygen than the other considered complexes.

In addition to the B structures shown by all the actinide considered in this work, certain others unusual and novel geometries were encountered such as D and Z structures. Both D and B structures have the same formula and are exhibited by Th (IV), Pa (IV), and Pa (V) complexes. Among the B and D isomers, B structure is symmetrical as compared to the D structure and thus B structure in each case is found to be more stable than their corresponding D structures. In addition to these B and D structures, we also studied the various protonated forms of these structures which in turn gave rise to certain other geometries namely Tri and Zigzag structures. Th(IV) and Pa(IV) showed only Z geometries but Pa(V) exhibited both Tri and Z geometries. In case of Pa(V) complexes, Tri-isomer is found to be more stable than the Z-counterpart. The reason that why Pa(V) prefers the Tri geometry over the Z is not clear, especially given that on the other hand Pa(IV) adopts only the Z-geometry.

QTAIM analysis was also carried out on these complexes and the data further supports the conclusions drawn based on geometrical analysis. QTAIM bond critical point data suggest that both U−O and Pa−O are more covalent than the Th analogues and the Ac-O_{exo} bond is stronger than the Ac-O_{endo} bond.

Information in the appendix

Addition information on the protonated structures of the B, butterfly structures. Table containing charges, Mayer bond order and NBO for the B and D structures are available. Geometrical parameters for the Z and Tri structures are also listed. Tables containing topological parameters on the M, B, Z and Tri structures are given. Moreover, plots showing the variation of the electron density as well as the DI at the BCPs in Ac-O_{exo} bond with the actinides are given.

Chapter 4

A Computational Density Functional Study of Heterobinuclear Polypyrrolic Macrocyclic Complexes of Actinides

4.1 Introduction

Macrocycles play a very significant role in the study of the coordination chemistry of the actinyl cations, particularly uranyl[22,220] and neptunyl[221] cations. Among various macrocyclic ligands, a class of binucleating Schiff-base polypyrrolic macrocycles have been extensively used to study the complexation behavior of the actinyls, and these macrocycles upon complexation with the metals adopt Pacman shaped cleft structures[72]. One of these macrocycles is shown in the Figure 3.1 (Chapter 3), denoted by H_4L^1. Apart from this, other, related macrocycles L^2 and L^3 are also known[18]. The two N4 donor compartments are connected with phenyl, napthalenyl and anthracenyl linkers in L^1, L^2 and L^3 respectively. The theoretical calculations were also done in 2012 by our group to see the effects of hinge size in these Pacman like uranium complexes[18] (L^1, L^2 and L^3) on their structures.

Arnold and Love et al. have extensively explored the reduction and functionalization of the uranyl dication using these macrocycles. They have used these binucleating ligand to synthesize a wide range of main group, transition metal, lanthanide and. actinide complexes[222]. Many low valent actinide complexes such as $[(U^{IV})(L^1)]$, $[(An^{III}X)_2(L^1)]$ (An=U, X=I, BH_4; An = Np, X= I), $[Li(THF)_4].[U^{III}BH_4)_2(\mu\text{-}BH_4)(L^1)]$ and $[Na(THF)_4].[(THF)_2(U^{III}BH_4)_2(\mu\text{-}BH_4)(L^2)]$[15,179,223], were synthesized using this octadentate polypyrrolic ligand. All these complexes adopts the Pacman shape except $[Li(THF)_4].[U^{III}BH_4)_2(\mu\text{-}BH_4)(L^1]$ which adopts a

bowl shape[179]. In addition to these, highly valence diversified diuranium complexes of the Schiff-base polypyrrolic macrocycle were also studied computationally[60].

Furthermore isostructural heterobimetallic complexes were studied both experimentally as well as theoretically[56]. The most interesting feature of these complexes were the interactions of the uranyl endo oxygen with the 3d transition metal[56]. Such type of structures in which there is an interaction between the Lewis basic oxo-group of one cation with another metal cation are known as cation-cation complexes. Actinyl cation-cation interactions play a significant role in spent nuclear fuel processing as well as environmental waste management[30].

The current study explores the differences in the bonding behavior of the actinyl in case of heterobinuclear complexes with the variation of the actinides (Th, Pa, U, Np and Pu) and their oxidation states as well as with the variation of the transition metal in the lower pocket of the macrocycle. In this work, we also analyzed the interactions of the actinyl endo oxygen with the dicationic transition metals (TM) viz. Mn^{II}, Fe^{II}, Co^{II} and Zn^{II} which adds to our existing knowledge of cation-cation interaction complexes. Here and in the following (TM) stands for the four transition metals namely Mn^{II}=(1), Fe^{II}=(2) Co^{II} =(3) and Zn^{II} =(4). Optimized geometries, bond lengths, bond angles, atomic charges, natural bond order analysis and QTAIM analysis of the bonding interactions in these complexes were studied. As found in our first case study of mononuclear as well as binuclear complexes of macrocyclic ligand, here also we found that the uranium-oxo bond is the shortest among all other actinyl-oxo bonds pointing more covalency in uranium complexes.

4.2 Computational Details

Approximate density functional theory (DFT) in the form of the Perdew-Burke-Ernzerhof (PBE) functional[139] was applied in our calculations. Gradient corrected calculations with the PBE[139] exchange correlation (XC) functional have been found to save time over the hybrid functional B3LYP[141,224,225] but on average provides less accurate Gibbs free energies[186] whereas the PBE functional often provides nearly accurate geometries and vibrational frequencies.

The gas phase geometry optimizations of all the hetrobinuclear complexes of the Pacman ligand were done using Priroda code. It employs a fast RI method for calculating both Coulomb and exchange-correlation (XC) integrals with the optimized fitted Gaussian basis sets. A scalar relativistic four-component all electron (AE) approach, based on the full Dirac equation, was used to account for the relativistic effects for the heavy elements[151]. In the Dirac equation, all the spin-orbit coupling terms are separated from the scalar terms and neglected[149]. All electron correlation-consistent Gaussian basis sets of double zeta polarized quality (B-I) were used[181]. The nature of the stationary points on the potential energy surface were confirmed further by carrying out frequency calculations, and then the thermodynamic data was obtained thereafter. Previously, a number of test calculations have been performed on different molecules such as actinyl cations, actinide fluorides, oxides, oxofluorides[186], dinitrogen tetraoxide adducts of uranyl nitrate[189], actinyl aquo complexes[55,187] and macrocyclic complexes of the actinides,[41,55] and in all cases the Priroda code was found to be a very reliable code as it was found to provide the same results as other relativistic methods. Also, additional time is saved with the inclusion of the resolution-of-identity (RI)[150] method for evaluating both Coulomb and exchange-correlation integrals using auxiliary optimized fitted Gaussian basis sets which also improves the computational efficiency of the Priroda code[150–152,181,182]

The unrestricted, open-shell Kohn-Sham approach was applied to the systems with unpaired electrons. Spin multiplicities (2S+1) were calculated with high spin states for the transition metals. On the basis of these PBE calculations, both the population based Mayer bond orders[184] and atomic charges as developed by Hirshfield[185] were calculated. Both bond orders and atomic charges have been found quite helpful in explaining the chemical surroundings of a variety of actinide and actinyl complexes[55,186–189,199] although these are not quantum mechanical observables. Furthermore, single point ADF calculations on the Priroda geometries were performed which were then used to carry out the natural bond orbital (NBO) analyses using the NBO package[165] included in the ADF code.[190] The scalar relativistic ZORA method[191–193] along with the Slater type ZORA-TZP basis sets comparable to those used in Priroda were employed in the ADF calculations.

The topologies of the (3, -1) bond critical points in the gradient field of the electron density were analyzed using the quantum theory of atoms in molecules (QTAIM).[194] This was done with the Multiwfn[164] code.

4.3 Results and Discussion

In addition to the various mononuclear and binuclear complexes of polypyrrolic Pacman complexes (studied in Chapter 3), certain heterobinuclear complexes were studied with the emphasis on the actinyl-oxo to 3d transition metal bonding. It is an extension of previous work in which a number of complexes with the $AnO_2^{n+}\ldots M^{p+}$ (where M is an alkali metal or transition metal) interactions were synthesized and structurally studied. Our main aim is to look for the periodic trends for Ac-O bond across the actinide series up to plutonium. We studied 32 complexes of the early actinides starting from Th to Pu in different oxidation states, each one containing a transition metal. The structural properties of hetero bimetallic complexes of Th(IV),

Pa(IV,V), U(IV,VI), Np(VI) and Pu(VI) were examined using Kohn-Sham density functional theory calculations with scalar relativistic effects. The structural parameters of the all these complexes were compared to the previously studied uranyl, neptunyl and plutonyl hetero bimetallic analogues and furthermore QTAIM studies were performed on these complexes using Multiwfn.

4.3.1 Structure

(a) Metal-coordination environment: In this work, we studied 32 heterobinuclear Pacman complexes with the actinide placed in one of the pockets, and the TM lying in the other. In the complexes considered in this case study, we have two types of coordination environment around the actinide. In most of the complexes, the actinide has nearly pentagonal bipyramidal geometry with the actinide in the center of the plane formed by the four nitrogens of the ring, and the two axial sites are occupied by the oxygen, whereas the seventh position is occupied by the oxygen of an equatorial coordinating THF solvent molecule. However, in some of the complexes like $^{B}Th^{IV}O_2(1\text{-}4)\ L]^{2-}$, (thorium complexes only), the coordination environment around the thorium is slightly different as the O_1-Th-O_2 is bent (of the order of 125º) and there is no room for the coordinating solvent THF, and so the thorium is only 6-coordinate.

Similarly, we found three different types of coordination environment around the TM. In case 1, shown by all the neptunium and plutonium complexes except $[Pu^{VI}O_2(4)\ L]$, the TM in the lower pocket is bonded to 3 of the 4 pyrrolic nitrogens, the actinyl oxygen, O_2, and O_4 from the THF, and so in these cases, the TM has 5-coordinate geometry. All the Th(IV), U(VI) complexes, $[Pu^{VI}O_2(4)\ L]$, $[Pa^{IV}O_2(3)\ L]^{2-}$ and $[U^{IV}O_2(3)\ L]^{2-}$exhibit case 2, where the TM is a 4-coordinate metal. In case of Th(IV), U(VI) and $[Pu^{VI}O_2(4)\ L]$ complexes, the TM has strong coordination to two of the four pyrrolic nitrogens of the ring whereas the other two positions of nearly

tetrahedral geometry are occupied by the two oxygens, O_4 oxygen of the THF molecule and the O_2, actinyl-endo oxygen, (Fig. 4.1(a) and Fig. 4.1(d)). However, in $[Pa^{IV}O_2(3)\ L]^{2-}$ and $[U^{IV}O_2(3)\ L]^{2-}$ complexes, the TM is coordinated to 3 pyrrolic nitrogens and O_2. The O_1-M-O_2 bond angle in these cases ranges from 113.6 to 144.4º compared to 109.5º for purely tetrahedral geometries.

In addition to these two cases, there exists case 3 which has no TM-THF bond and thus TM is coordinated to only 3 atoms (as shown in Fig. 4.1(b) and Fig. 4.1 (c)). This case is shown by $^{L}Th^{IV}O_2(1\text{-}4)\ L]^{2-}$, all protactinium complexes and U(IV) complexes except $[Pa^{IV}O_2(3)\ L]^{2-}$ and $[U^{IV}O_2(3)\ L]^{2-}$ complexes.

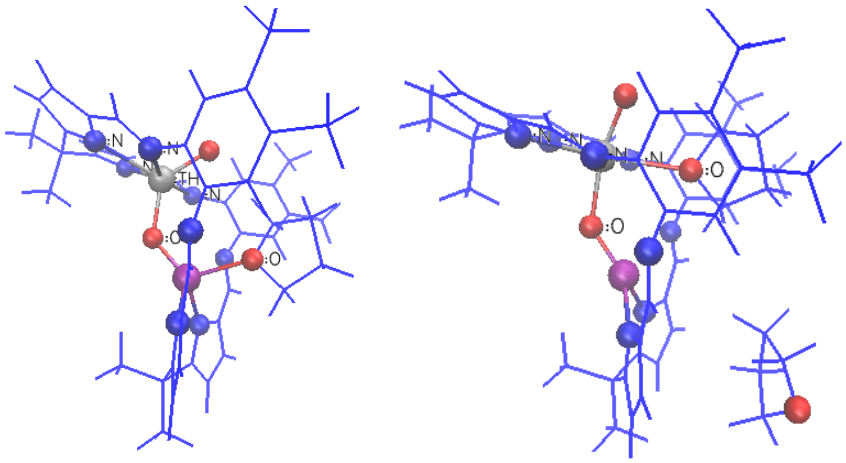

(a) (b)

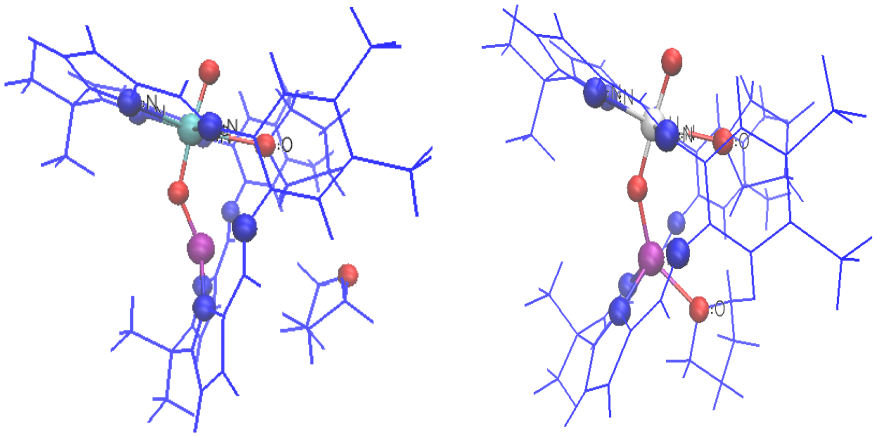

(c) (d)

Figure4.1: Optimized geometries of (a) $^{B}[Th^{IV}O_2(1)L]^{2-}$, where the TM is 4-coordinate, (b) $^{L}[Th^{IV}O_2(1)L]^{2-}$ where TM is 3-coordinate, (c) $[Pa^{V}O_2(1)L]^{-}$ where the TM is 3-coordinate, and (d) $[U^{VI}O_2(1)L]$ where the TM is 4-coordinate; the actinide is 7-coordinate except in (a) where it has only coordination number of 6 (cyan, Pa; white, U; purple, Mn; blue, nitrogen; red, oxygen). All other complexes have similar optimized geometries.

(b) Bond Lengths, Bond Angles, Bond Orders and Charges: Calculated structural parameters like bond lengths and bond angles, as well as bond orders for the complexes studied in this work are presented in Table 4.1, Table 4.2 and Table 4.3 respectively. Both Mayer and NBO bond orders have been calculated, and, as observed in the previous calculations (as in chapter 3) on the binuclear complexes, Mayer bond orders are more reliable for the actinide complexes as there values for various considered bonds are quite close to the literature values and moreover the bond orders from NBO calculations are very low as compared to the Mayer bond orders, so in our discussion we have considered only the Mayer bond orders for all the bonds.

There is reduction of about 0.16 Å in the bond length of Ac=O_1 and of about 1.48 Å in case of Ac=O_2 as we move from Th to Pu in these complexes with a sharp reduction of about 0.10 Å in case of Ac=O_1 and of about 0.13 Å for the Ac=O_2 as we substitute thorium with protactinium in the primary cavity. The decrease in the strength of the Ac=O bond together with the shorter Ac=O distance is observed across the actinide series with the increase in the atomic number of the actinide. The bond orders (Table 4.3) for Ac=O_1 and Ac=O_2 in the complexes vary from 2.26 to 2.42 and 0.96 to 1.97 respectively, which implies that for every complex, the Ac=O_1 is stronger and shorter than their respective Ac=O_2 bond. Similar trends were found in case of homonuclear complexes (studied in chapter 3). Moreover, the Hirshfeld charges (shown in Table 4.4) on the O_1 is more negative than that on the O_2, so the actinide forms a stronger bond to the O_{exo} (O_1) than to O_{endo} (O_2).

On comparing the bonding parameters of the mononuclear complexes (studied in chapter 3) with these heterobinuclear complexes, particularly for the actinyl moiety, we found that there is almost no change in the bond length of Ac=O_1 whereas the Ac=O_2 bond gets elongated on the substitution of TM in the secondary cavity except for the thorium complexes where there is a shrinking of the Ac=O_2 bond. These findings are further supported by the bond order data (Table 4.3) as it can be observed that the bond order does not change much for the Ac=O_1 on switching from the mononuclear complexes to the respective heterobimetallic complexes as well as on changing the TM in the lower cavity. On the other hand, the bond order for the Ac=O_2 decreases on the substitution of the TM in the respective complexes but in case of thorium, the bond order exhibits an increase from 0.65 to about 1.35. This elongation of the Ac=O_2 bond or the decrease in its bond order within these complexes can be interpreted as desymmertization of the linear actinyl moiety as otherwise the actinyl fragment is quite symmetrical, which in turn leads to the

weakening of the actinyl bond. Moreover, this elongation in the $Ac{=}O_2$ bond can be correlated to the significant $TM\text{-}O_2$ interactions as because of elongation of the $Ac{=}O_2$ bonds the endo oxygen becomes quite close to the TM in the lower pocket.

In the upper cavity, the actinide lies in the plane created by the four pyrrolic nitrogen of the ligand and binds slightly more strongly to two of the four pyrrolic nitrogens for all the complexes. Among actinides, thorium has weak bonding interactions to the pyrrolic nitrogen in the cavity whereas uranium shows the strongest bonding interactions. In case of the lower cavity, the TM lies slightly above the N_4 plane and it binds very strongly to the pyrrolic nitrogens N_7, and N_8 and weakly to the N_5 and N_6. Neptunium and plutonium complexes with the macrocyclic complexes having manganese and iron in the lower cavity show comparatively stronger interactions with the N_7 and N_8 with a bond order of the order of 0.65 compared to about 0.50 in all other cases. In most of the complexes, N_5 and N_6 are equidistant from the TM but in some of the complexes particularly $^{L}[Th^{IV}O_2(1)\ L]^{2-}$, one of these pyrrolic nitrogens is closer to the TM than the other by 1.35 Å. On analyzing the Hirshfeld charges on the pyrrolic nitrogen, we found that all they are all in the range of -0.10 ± 0.02 except for the $N_{7,8}$ pyrrolic nitrogens of $[Np^{VI}O_2(2)\ L]$ which have smaller absolute charges of -0.06 ± 0.02.

In all the complexes of case 1, THF is coordinated to both the actinide as well as the TM, and these are the part of first solvation shell. In all these structures, we found that $An\text{-}O_3$ range from 2.98 to 2.50 Å whereas the $TM\text{-}O_4$ distance varies from 2.31 to 2.18 Å. In every complex of case 2, we found that the bond length of $TM\text{-}O_4$ is always shorter than the $Ac\text{-}O_2$ and the bond orders for $TM\text{-}O_4$ is greater than that of $Ac\text{-}O_3$; this is consistent with the difference in size between the two metals.

Complexes	Ac=O_1	Ac=O_2	Ac-O_3	Ac-$N_{1,4}$	Ac-$N_{2,3}$	Ac-M	M-O_2	M-O_4	M-N_5	M-$N_{7,8}$	M-N_6
$^{B}[Th^{IV}O_2(1)L]^{2-}$	1.96	2.12	None	2.81	2.66	3.64	1.87	2.31	3.13	2.12	3.08
$^{L}[Th^{IV}O_2(1)L]^{2-}$	1.95	2.34	2.98	2.80	2.56	3.98	1.72	None	2.17	2.00	3.52
$[Pa^{IV}O_2(1)L]^{2-}$	1.86	1.98	2.62	2.65	2.52	3.70	1.91	None	3.13	2.07	3.09
$[Pa^{V}O_2(1)L]^{1-}$	1.85	1.99	2.63	2.65	2.51	3.68	1.90	None	3.05	2.07	3.06
$[U^{IV}O_2(1)L]^{2-}$	1.84	1.97	2.62	2.64	2.52	3.64	1.90	None	3.10	2.08	3.07
$[U^{VI}O_2(1)L]$	1.80	1.86	2.54	2.53	2.44	3.76	2.05	2.23	2.77	2.07	2.66
$[Np^{VI}O_2(1)L]$	1.81	1.97	2.60	2.59	2.45	3.76	1.84	2.29	3.29	1.96	2.13
$[Pu^{VI}O_2(1)L]$	1.80	1.96	2.59	2.58	2.47	3.74	1.83	2.28	3.29	1.96	2.13
$^{B}[Th^{IV}O_2(2)L]^{2-}$	1.95	2.16	None	2.82	2.66	3.53	1.81	2.27	3.00	2.06	3.21
$^{L}[Th^{IV}O_2(2)L]^{2-}$	1.95	2.26	2.75	2.76	2.61	3.65	1.70	None	3.09	1.86	3.09
$[Pa^{IV}O_2(2)L]^{2-}$	1.86	2.00	2.60	2.65	2.53	3.68	1.85	None	3.17	2.01	3.15
$[Pa^{V}O_2(2)L]^{1-}$	1.85	2.00	2.61	2.64	2.52	3.67	1.84	None	3.08	2.01	3.11
$[U^{IV}O_2(2)L]^{2-}$	1.84	2.00	2.60	2.64	2.52	3.62	184	None	3.14	2.02	3.14
$[U^{VI}O_2(2)L]$	1.80	1.89	2.55	2.55	2.44	3.69	1.96	2.20	2.79	2.01	2.71
$[Np^{VI}O_2(2)L]$	1.80	1.92	2.62	2.56	2.45	3.68	1.89	2.26	3.14	1.96	2.19
$[Pu^{VI}O_2(2)L]$	1.80	1.97	2.65	2.56	2.46	3.67	1.82	2.27	3.19	1.96	2.11
$^{B}[Th^{IV}O_2(3)L]^{2-}$	1.96	2.13	None	2.81	2.67	3.61	1.81	2.20	3.15	2.00	3.15
$^{L}[Th^{IV}O_2(3)L]^{2-}$	1.96	2.24	2.72	2.79	2.63	3.75	1.74	None	3.35	2.00	3.35
$[Pa^{IV}O_2(3)L]^{2-}$	1.86	1.98	2.66	2.65	2.54	3.64	1.88	None	3.56	2.00	2.43
$[Pa^{V}O_2(3)L]^{1-}$	1.85	1.99	2.62	2.65	2.52	3.67	1.85	None	3.06	1.96	3.08
$[U^{IV}O_2(3)L]^{2-}$	1.84	1.96	2.66	2.65	2.53	3.58	1.88	None	3.52	2.37	2.37
$[U^{VI}O_2(3)L]$	1.80	1.86	2.52	2.54	2.44	3.75	1.98	2.18	2.83	1.97	2.84
$[Np^{VI}O_2(3)L]$	1.79	1.85	2.55	2.55	2.43	3.72	1.99	2.23	3.11	1.99	2.34
$[Pu^{VI}O_2(3)L]$	1.79	1.87	2.65	2.56	2.46	3.66	1.94	2.24	3.10	1.97	2.22
$^{B}[Th^{IV}O_2(4)L]^{2-}$	1.96	2.11	None	2.83	2.67	3.68	1.84	2.29	3.20	2.03	3.19
$^{L}[Th^{IV}O_2(4)L]^{2-}$	1.97	2.17	2.76	2.80	2.63	3.77	1.79	None	3.30	2.02	3.27
$[Pa^{IV}O_2(4)L]^{2-}$	1.86	1.99	2.60	2.66	2.53	3.71	1.87	None	3.26	1.97	3.24
$[Pa^{V}O_2(4)L]^{1-}$	1.85	1.98	2.60	2.66	2.52	3.70	1.85	None	3.21	1.97	3.19
$[U^{IV}O_2(4)L]^{2-}$	1.84	1.97	2.58	2.65	2.52	3.65	1.86	None	3.24	1.98	3.22
$[U^{VI}O_2(4)L]$	1.80	1.85	2.50	2.54	2.44	3.80	2.00	2.27	2.90	1.96	2.94
$[Np^{VI}O_2(4)L]$	1.79	1.84	2.51	2.55	2.43	3.78	2.02	2.29	3.08	1.96	2.60
$[Pu^{VI}O_2(4)L]$	1.78	1.85	2.52	2.56	2.48	3.73	1.99	2.29	2.94	1.97	2.91

Table4.1: Gas-Phase bond lengths for the various heterobimetallic complexes $[Ac^{IV}O_2(TM)L]^{2-}$where Ac=Th, Pa, U; $[Pa^{V}O_2(TM)L]^{1-}$, Ac=$[Ac^{VI}O_2(TM)L]$ where Ac=U, Np and Pu; bond lengths are given in Å.

Complexes	O_1-Ac-O_2	N_1-Ac-O_3	$N_{1,3}$-Ac-$N_{2,4}$	N_2-Ac-N_3	Ac-O_2-M	O_2-M-O_4	O_2-M-$N_{7,8}$
$^{B}[Th^{IV}O_2(1)L]^{2-}$	125.9	None	63.5	68.0	131.3	116.9	125.9
$^{L}[Th^{IV}O_2(1)L]^{2-}$	157.0	71.3	84.8	70.18	157.3	None	136.4
$[Pa^{IV}O_2(1)L]^{2-}$	172.8	78.3	66.1	70.1	142.7	None	133.4
$[Pa^{V}O_2(1)L]^{1-}$	173.8	78.2	66.2	70.3	142.3	None	132.1
$[U^{IV}O_2(1)L]^{2-}$	176.6	78.3	66.0	70.1	139.0	None	132.7
$[U^{VI}O_2(1)L]$	176.5	76.6	67.9	71.4	146.8	144.4	116.4
$[Np^{VI}O_2(1)L]$	174.5	77.8	67.1	67.1	161.6	125.1	145.2
$[Pu^{VI}O_2(1)L]$	175.4	78.6	66.9	71.1	161.7	124.8	130.1
$^{B}[Th^{IV}O_2(2)L]^{2-}$	128.7	None	63.1	67.5	125.0	127.1	117.9
$^{L}[Th^{IV}O_2(2)L]^{2-}$	167.5	83.4	64.0	69.2	134.1	None	121.5
$[Pa^{IV}O_2(2)L]^{2-}$	173.1	78.7	65.9	69.8	145.4	None	132.0
$[Pa^{V}O_2(2)L]^{1-}$	174.1	78.2	66.0	70.2	144.8	None	131.1
$[U^{IV}O_2(2)L]^{2-}$	176.4	78.7	65.8	69.8	141.5	None	131.3
$[U^{VI}O_2(2)L]$	178.5	76.4	67.9	71.4	146.8	144.4	114.5
$[Np^{VI}O_2(2)L]$	176.2	76.7	68.1	71.9	149.2	140.4	125.3
$[Pu^{VI}O_2(2)L]$	176.9	77.7	67.6	71.2	150.7	136.9	118.5
$^{B}[Th^{IV}O_2(3)L]^{2-}$	127.5	None	63.1	67.7	132.1	118.6	121.7
$^{L}[Th^{IV}O_2(3)L]^{2-}$	167.5	83.9	63.6	68.9	140.6	None	133.8
$[Pa^{IV}O_2(3)L]^{2-}$	170.3	81.2	65.8	69.7	140.6	None	147.6
$[Pa^{V}O_2(3)L]^{1-}$	173.3	78.4	65.9	70.2	145.0	None	129.4
$[U^{IV}O_2(3)L]^{2-}$	174.4	79.9	65.3	69.9	137.7	None	144.0
$[U^{VI}O_2(3)L]$	175.2	75.4	67.7	70.9	154.7	135.4	115.0
$[Np^{VI}O_2(3)L]$	178.1	76.5	68.3	71.7	150.3	140.2	118.0
$[Pu^{VI}O_2(3)L]$	176.9	77.5	67.6	70.9	147.4	143.2	118.5
$^{B}[Th^{IV}O_2(4)L]^{2-}$	128.5	None	63.2	67.9	137.4	113.6	125.7
$^{L}[Th^{IV}O_2(4)L]^{2-}$	136.2	83.9	63.8	69.0	143.6	None	134.4
$[Pa^{IV}O_2(4)L]^{2-}$	172.5	78.8	65.8	69.8	148	None	131.2
$[Pa^{V}O_2(4)L]^{1-}$	173.2	78.6	65.9	70.1	148.6	None	131.5
$[U^{IV}O_2(4)L]^{2-}$	176.3	78.6	65.7	69.9	144.3	None	131.2
$[U^{VI}O_2(4)L]$	174.7	76.4	67.7	70.8	159.4	129.1	118.2
$[Np^{VI}O_2(4)L]$	178.7	75.9	68.2	72.0	156.2	134.2	122.3
$[Pu^{VI}O_2(4)L]$	178.7	77.2	66.8	70.0	153.5	131.9	118.2

Table4.2: Gas-Phase calculated bond angles (in degrees) for the complexes.

Moreover, in all the U(VI) complexes, the bond to the THF molecules are comparatively stronger than in all other complexes, being the strongest in case of $[U^{VI}O_2(3)L]$ and $[U^{VI}O_2(4)$ L complexes. The Hirshfeld atomic charges (as shown in Table 4.4) on the oxygen of both the THF solvent molecules are nearly the same in most of the complexes.

The bond angle O_1-Ac-O_2 (Table 4.2) in case of thorium complexes is quite bent as compared to all other complexes. Among various complexes studied, we found two optimized geometries for the thorium complexes, namely $^{B}[Th^{IV}O_2(TM)\ L]^{2-}$ and $^{L}[Th^{IV}O_2(TM)\ L]^{2-}$ with the bond angle O_{exo}-Th-O_{endo} in the range 125.9º-128.7º and 136.2º-167.5º respectively. The TM in the lower pocket in the former case is found to have a coordination number of 4 whereas in the latter, it is only 3-coordinate. Among these two different structures, the one with bent angle O_{exo}-Th-O_{endo} is more stable than the other by an amount of 24.88kcal/mol. Furthermore, in case of these heteronuclear complexes of thorium, the bending is more pronounced as compared to that in mononuclear complexes of thorium where the O_{exo}-Th-O_{endo} is 158.1^0 (Table 3.2).

The Hirshfeld charges on the actinyl moiety are listed in the Table (4.4) The formal charges on the actinyl in case of $Ac^{IV}O_2$, $Ac^{V}O_2$ and $Ac^{VI}O_2$ complexes are 0, 1 and 2 respectively, and we found that the charges on the actinyl moiety in case of Th(IV), Pa(IV) and U(IV) complexes are the highest among all, whereas in case of uranium it is the lowest. It can be noted that there is appreciable charge transfer from the ligand to the actinyl fragment in case of uranium complexes which may be one of the factors for the enhanced covalency in these complexes.

Complexes	Ac=O_1	Ac=O_2	Ac-O_3	Ac-$N_{1,4}$	Ac-$N_{2,3}$	Ac-M	M-O_2	M-O_4	M-N_5	M-$N_{7,8}$	M-N_6
$^{B}[Th^{IV}O_2(1)L]^{2-}$	2.30, *1.43*	1.34 *0.89*	None	0.26 *0.19*	0.41 *0.25*	0.14 *0.08*	0.91 *0.50*	0.26 *0.09*	0.10 *0.02*	0.47 *0.22*	0.12 *0.03*
$^{L}[Th^{IV}O_2(1)L]^{2-}$	2.28 *1.45*	1.17 *0.81*	0.25 *0.16*	0.26 *0.20*	0.40 *0.28*	0.15 *0.09*	1.07 *0.62*	None	0.09 *0.02*	0.50 *0.22*	0.12 *0.03*
$[Pa^{IV}O_2(1)L]^{2-}$	2.41 *1.91*	1.63 *1.34*	0.31 *0.24*	0.35 *0.30*	0.48 *0.39*	0.17 *0.09*	0.66 *0.35*	None	0.14 *0.03*	0.56 *0.27*	0.16 *0.03*
$[Pa^{V}O_2(1)L]^{1-}$	2.42 *1.93*	1.61 *1.34*	0.32 *0.24*	0.34 *0.30*	0.48 *0.40*	0.17 *0.09*	0.67 *0.36*	None	0.16 *0.04*	0.54 *0.26*	0.16 *0.04*
$[U^{IV}O_2(1)L]^{2-}$	2.42 *1.97*	1.61 *1.39*	0.30 *0.25*	0.34 *0.32*	0.47 *0.41*	0.19 *0.10*	0.67 *0.36*	None	0.15 *0.04*	0.55 *0.26*	0.17 *0.04*
$[U^{VI}O_2(1)L]$	2.41 *2.10*	1.97 *1.76*	0.36 *0.34*	0.44 *0.45*	0.56 *0.54*	0.19 *0.13*	0.35 *0.20*	0.30 *0.11*	0.24 *0.07*	0.51 *0.27*	0.28 *0.07*
$[Np^{VI}O_2(1)L]$	2.42 *2.10*	1.48 *1.31*	0.30 *0.25*	0.37 *0.34*	0.50 *0.45*	0.19 *0.12*	0.80 *0.56*	0.32 *0.14*	0.10 *0.02*	0.60 *0.48*	0.45 *0.32*
$[Pu^{VI}O_2(1)L]$	2.40 *2.10*	1.47 *1.28*	0.30 *0.23*	0.36 *0.32*	0.49 *0.42*	0.18 *0.11*	0.79 *0.56*	0.33 *0.15*	0.10 *0.02*	0.62 *0.49*	0.46 *0.32*
$^{B}[Th^{IV}O_2(2)L]^{2-}$	2.32 *1.44*	1.24 *0.82*	None	0.26 *0.19*	0.41 *0.26*	0.15 *0.10*	1.01 *0.62*	0.26 *0.09*	0.13 *0.03*	0.50 *0.25*	0.08 *0.02*
$^{L}[Th^{IV}O_2(2)L]^{2-}$	2.26 *1.44*	0.96 *0.70*	0.26 *0.16*	0.27 *0.21*	0.42 *0.28*	0.21 *0.11*	1.24 *0.81*	None	0.11 *0.03*	0.67 *0.34*	0.12 *0.03*
$[Pa^{IV}O_2(2)L]^{2-}$	2.42 *1.91*	1.56 *1.27*	0.32 *0.25*	0.35 *0.30*	0.48 *0.39*	0.18 *0.10*	0.73 *0.43*	None	0.12 *0.03*	0.59 *0.31*	0.12 *0.03*
$[Pa^{V}O_2(2)L]^{1-}$	2.42 *1.93*	1.54 *1.27*	0.32 *0.25*	0.35 *0.30*	0.48 *0.40*	0.18 *0.10*	0.74 *0.45*	None	0.13 *0.03*	0.57 *0.30*	0.13 *0.03*
$[U^{IV}O_2(2)L]^{2-}$	2.42 *1.96*	1.52 *1.29*	0.30 *0.25*	0.34 *0.31*	0.47 *0.41*	0.19 *0.11*	0.76 *0.47*	None	0.12 *0.03*	0.58 *0.30*	0.13 *0.03*
$[U^{VI}O_2(2)L]$	2.42 *2.10*	1.85 *1.64*	0.35 *0.32*	0.43 *0.42*	0.55 *0.53*	0.51 *0.43*	0.46 *0.28*	0.34 *0.14*	0.23 *0.08*	0.58 *0.33*	0.26 *0.08*
$[Np^{VI}O_2(2)L]$	2.41 *2.11*	1.67 *1.49*	0.30 *0.26*	0.39 *0.37*	0.53 *0.49*	0.36 *0.25*	0.62 *0.42*	0.32 *0.14*	0.11 *0.03*	0.60 *0.42*	0.41 *0.24*
$[Pu^{VI}O_2(2)L]$	2.39 *2.09*	1.44 *1.25*	0.28 *0.21*	0.37 *0.32*	0.49 *0.42*	0.18 *0.11*	0.81 *0.58*	0.33 *0.14*	0.10 *0.03*	0.65 *0.50*	0.46 *0.31*
$^{B}[Th^{IV}O_2(3)L]^{2-}$	2.30 *1.42*	1.30 *0.86*	None	0.26 *0.19*	0.41 *0.25*	0.14 *0.08*	0.96 *0.55*	0.28 *0.10*	0.07 *0.02*	0.53 *0.27*	0.08 *0.02*
$^{L}[Th^{IV}O_2(3)L]^{2-}$	2.28	1.02	0.26	0.26	0.41	0.18	1.22	None	0.01	0.53	0.01

	1.44	*0.69*	*0.17*	*0.20*	*0.28*	*0.12*	*0.79*		*0.01*	*0.27*	*0.01*
$[Pa^{IV}O_2(3)L]^{2-}$	2.41 *1.92*	1.63 *1.34*	0.29 *0.22*	0.34 *0.30*	0.47 *0.39*	0.16 *0.09*	0.67 *0.37*	None	0.38 *0.14*	0.64 *0.29*	0.00 *0.00*
$[Pa^{V}O_2(3)L]^{1-}$	2.42 *1.92*	1.60 *1.33*	0.32 *0.24*	0.34 *0.30*	0.48 *0.40*	0.17 *0.09*	0.69 *0.36*	None	0.13 *0.03*	0.61 *0.33*	0.13 *0.03*
$[U^{IV}O_2(3)L]^{2-}$	2.41 *1.96*	1.64 *1.42*	0.28 *0.23*	0.34 *0.32*	0.46 *0.41*	0.18 *0.10*	0.66 *0.36*	None	0.13 *0.12*	0.62 *0.33*	0.39 *0.28*
$[U^{VI}O_2(3)L]$	2.41 *2.08*	1.96 *1.60*	0.38 *0.31*	0.45 *0.40*	0.57 *0.51*	0.15 *0.11*	0.38 *0.30*	0.34 0.14	0.20 *0.07*	0.58 *0.35*	0.20 *0.09*
$[Np^{VI}O_2(3)L]$	2.42 *2.12*	1.93 *1.75*	0.35 *0.32*	0.42 *0.42*	0.55 *0.53*	0.23 *0.15*	0.40 *0.23*	0.32 0.13	0.12 *0.03*	0.58 *0.34*	0.35 *0.31*
$[Pu^{VI}O_2(3)L]$	2.38 *2.08*	1.80 *1.60*	0.29 *0.22*	0.38 *0.35*	0.49 *0.43*	0.28 *0.18*	0.50 *0.29*	0.31 0.12	0.13 *0.03*	0.60 *0.38*	0.39 *0.20*
$^{B}[Th^{IV}O_2(4)L]^{2-}$	2.32 *1.44*	1.39 *0.90*	None	0.25 *0.18*	0.40 *0.25*	0.11 *0.03*	0.85 *0.24*	0.25 0.04	0.05 *0.00*	0.50 *0.15*	0.05 *0.00*
$^{L}[Th^{IV}O_2(4)L]^{2-}$	2.27 *1.44*	1.24 *0.84*	0.24 *0.16*	0.25 *0.20*	0.40 *0.27*	0.14 *0.04*	0.98 *0.30*	None	0.01 *0.00*	0.53 *0.16*	0.01 *0.00*
$[Pa^{IV}O_2(4)L]^{2-}$	2.42 *1.96*	1.62 *1.34*	0.32 *0.26*	0.34 *0.28*	0.48 *0.39*	0.15 *0.04*	0.66 *0.21*	None	0.06 *0.00*	0.60 *0.19*	0.07 *0.00*
$[Pa^{V}O_2(4)L]^{1-}$	2.42 *1.96*	1.61 *1.34*	0.32 *0.26*	0.34 *0.28*	0.48 *0.39*	0.15 *0.04*	0.67 *0.21*	None	0.07 *0.00*	0.58 *0.18*	0.08 *0.00*
$[U^{IV}O_2(4)L]^{2-}$	2.42 *1.98*	1.61 *1.39*	0.30 *0.26*	0.33 *0.31*	0.47 *0.41*	0.16 *0.04*	0.67 *0.21*	None	0.07 *0.00*	0.59 *0.19*	0.08 *0.00*
$[U^{VI}O_2(4)L]$	2.42 *2.12*	1.97 *1.76*	0.39 *0.37*	0.45 *0.46*	0.57 *0.54*	0.10 *0.03*	0.36 *0.12*	0.29 0.06	0.14 *0.02*	0.55 *0.16*	0.14 *0.02*
$[Np^{VI}O_2(4)L]$	2.42 *2.14*	1.97 *1.79*	0.36 *0.33*	0.43 *0.43*	0.55 *0.52*	0.10 *0.03*	0.35 *0.12*	0.28 0.06	0.10 *0.01*	0.54 *0.15*	0.24 *0.16*
$[Pu^{VI}O_2(4)L]$	2.39 *2.11*	1.90 *1.70*	0.34 *0.27*	0.41 *0.37*	0.48 *0.42*	0.11 *0.03*	0.39 *0.12*	0.28 0.06	0.13 *0.02*	0.55 *0.15*	0.15 *0.03*

Table4.3: Calculated gas-phase bond orders [Mayer, *NBO*] for the various bonds in the complexes.

Complexes	Ac	O_1	O_2	AcO_2	O_3	$N_{1,4}$	$N_{2,3}$	M	O_4	N_5,N_6	$N_{7,8}$
$^{B}[Th^{IV}O_2(1)L]^{2-}$	0.46	-0.52	-0.40	-0.46	-0.05	-0.09	-0.13	0.21	-0.05	-0.10	-0.10
$^{L}[Th^{IV}O_2(1)L]^{2-}$	0.39	-0.50	-0.39	-0.50	-0.05	-0.09	-0.11	0.24	None	-0.10	-0.10
$[Pa^{IV}O_2(1)L]^{2-}$	0.51	-0.40	-0.34	-0.23	-0.06	-0.10	-0.12	0.31	None	-0.12	-0.12
$[Pa^{V}O_2(1)L]^{1-}$	0.52	-0.39	-0.33	-0.20	-0.06	-0.10	-0.12	0.31	None	-0.12	-0.11
$[U^{IV}O_2(1)L]^{2-}$	0.42	-0.38	-0.32	-0.28	-0.05	-0.10	-0.11	0.31	None	-0.12	-0.12
$[U^{VI}O_2(1)L]$	0.56	-0.29	-0.25	+0.02	-0.05	-0.10	-0.11	0.27	-0.06	-0.11	-0.10
$[Np^{VI}O_2(1)L]$	0.43	-0.30	-0.27	-0.14	-0.06	-0.10	-0.11	0.32	-0.06	-0.11	-0.08
$[Pu^{VI}O_2(1)L]$	0.38	-0.27	-0.26	-0.15	-0.06	-0.10	-0.11	0.32	-0.06	-0.11	-0.08
$^{B}[Th^{IV}O_2(2)L]^{2-}$	0.47	-0.51	-0.38	-0.42	-0.05	-0.09	-0.13	0.17	-0.05	-0.10	-0.10
$^{L}[Th^{IV}O_2(2)L]^{2-}$	0.44	-0.49	-0.31	-0.36	-0.05	-0.09	-0.12	0.05	None	-0.12	-0.10
$[Pa^{IV}O_2(2)L]^{2-}$	0.52	-0.40	-0.32	-0.20	-0.06	-0.10	-0.12	0.24	None	-0.12	-0.11
$[Pa^{V}O_2(2)L]^{1-}$	0.53	-0.39	-0.32	-0.18	-0.06	-0.10	-0.12	0.24	None	-0.10	-0.10
$[U^{IV}O_2(2)L]^{2-}$	0.42	-0.38	-0.31	-0.27	-0.05	-0.10	-0.11	0.24	None	-0.12	-0.11
$[U^{VI}O_2(2)L]$	0.54	-0.29	-0.26	-0.01	-0.05	-0.10	-0.11	0.27	-0.05	-0.10	-0.10
$[Np^{VI}O_2(2)L]$	0.45	-0.28	-0.25	-0.08	-0.06	-0.10	-0.11	0.24	-0.06	-0.06	-0.08
$[Pu^{VI}O_2(2)L]$	0.38	-0.26	-0.24	-0.12	-0.06	-0.10	-0.10	0.24	-0.06	-0.10	-0.07
$^{B}[Th^{IV}O_2(3)L]^{2-}$	0.47	-0.52	-0.38	-0.43	-0.05	-0.09	-0.13	0.14	-0.04	-0.10	-0.09
$^{L}[Th^{IV}O_2(3)L]^{2-}$	0.42	-0.50	-0.34	-0.42	-0.05	-0.09	-0.10	0.12	None	-0.10	-0.09
$[Pa^{IV}O_2(3)L]^{2-}$	0.51	-0.40	-0.32	-0.21	-0.06	-0.10	-0.12	0.19	None	-0.11	-0.09
$[Pa^{V}O_2(3)L]^{1-}$	0.52	-0.39	-0.32	-0.19	-0.06	-0.10	-0.11	0.22	None	-0.10	-0.09
$[U^{IV}O_2(3)L]^{2-}$	0.42	-0.37	-0.30	-0.25	-0.06	-0.10	-0.10	0.19	None	-0.11	-0.09
$[U^{VI}O_2(3)L]$	0.56	-0.28	-0.24	+0.04	-0.05	-0.09	-0.11	0.21	-0.05	-0.10	-0.09
$[Np^{VI}O_2(3)L]$	0.47	-0.26	-0.23	-0.02	-0.05	-0.09	-0.10	0.21	-0.06	-0.10	-0.11
$[Pu^{VI}O_2(3)L]$	0.39	-0.25	-0.23	-0.09	-0.06	-0.09	-0.10	0.21	-0.06	-0.10	-0.07
$^{B}[Th^{IV}O_2(4)L]^{2-}$	0.44	-0.53	-0.43	-0.52	-0.07	-0.09	-0.13	0.32	-0.07	-0.10	0.11
$^{L}[Th^{IV}O_2(4)L]^{2-}$	0.37	-0.51	-0.42	-0.56	-0.05	-0.09	-0.11	0.33	None	-0.10	-0.11
$[Pa^{IV}O_2(4)L]^{2-}$	0.51	-0.40	-0.35	-0.27	-0.06	-0.09	-0.12	0.39	None	-0.13	-0.12
$[Pa^{V}O_2(4)L]^{1-}$	0.51	-0.39	-0.35	-0.23	-0.06	-0.10	-0.12	0.40	None	-0.11	-0.11
$[U^{IV}O_2(4)L]^{2-}$	0.42	-0.37	-0.33	-0.28	-0.05	-0.09	-0.11	0.39	None	-0.11	-0.12
$[U^{VI}O_2(4)L]$	0.56	-0.28	-0.26	+0.02	-0.05	-0.09	-0.11	0.38	-0.08	-0.12	-0.11
$[Np^{VI}O_2(4)L]$	0.47	-0.26	-0.25	-0.04	-0.05	-0.09	-0.10	0.38	-0.08	-0.12	-0.11
$[Pu^{VI}O_2(4)L]$	0.40	-0.24	-0.24	-0.08	-0.05	-0.08	-0.10	0.38	-0.08	-0.11	-0.11

Table4.4: Hirshfeld atomic charges on various atoms of interest in the heterobimetallic complexes of actinides

Complexes	Bite angle(^{0})	d(**Å)**	Complexes	Bite angle(^{0})	d(**Å)**
$^{B}[Th^{IV}O_2(1)L]^{2-}$	84.30	0.50	$[Th^{IV}O_2(3)L]^{2-}$	88.95	0.42
$^{L}[Th^{IV}O_2(1)L]^{2-}$	87.61	0.82	$^{a}[Th^{IV}O_2(3)L]^{2-}$	84.33	0.88
$[Pa^{IV}O_2(1)L]^{2-}$	81.62	0.73	$[Pa^{IV}O_2(3)L]^{2-}$	79.17	0.72
$[Pa^{V}O_2(1)L]^{1-}$	80.03	0.72	$[Pa^{V}O_2(3)L]^{1-}$	77.49	0.69
$[U^{IV}O_2(1)L]^{2-}$	80.45	0.75	$U^{IV}O_2(3)L]^{2-}$	78.33	0.73
$[U^{VI}O_2(1)L]$	66.18	0.15	$[U^{VI}O_2(3)L]$	63.41	0.18
$[Np^{VI}O_2(1)L]$	54.42	0.27	$[Np^{VI}O_2(3)L]$	60.53	0.21
$[Pu^{VI}O_2(1)L]$	55.60	0.26	$[Pu^{VI}O_2(3)L]$	60.39	0.23
$^{B}[Th^{IV}O_2(2)L]^{2-}$	88.29	0.50	$[Th^{IV}O_2(4)L]^{2-}$	88.95	0.42
$^{L}[Th^{IV}O_2(2)L]^{2-}$	76.72	0.45	$^{a}[Th^{IV}O_2(4)L]^{2-}$	85.62	0.82
$[Pa^{IV}O_2(2)L]^{2-}$	79.17	0.72	$[Pa^{IV}O_2(4)L]^{2-}$	78.21	0.73
$[Pa^{V}O_2(2)L]^{1-}$	77.49	0.69	$[Pa^{V}O_2(4)L]^{1-}$	76.61	0.73
$U^{IV}O_2(2)L]^{2-}$	78.33	0.73	$U^{IV}O_2(4)L]^{2-}$	77.23	0.75
$[U^{VI}O_2(2)L]$	63.41	0.18	$[U^{VI}O_2(4)L]$	63.71	0.15
$[Np^{VI}O_2(2)L]$	60.53	0.21	$[Np^{VI}O_2(4)L]$	62.58	0.18
$[Pu^{VI}O_2(2)L]$	60.40	0.23	$[Pu^{VI}O_2(4)L]$	65.85	0.18

Table4.5: Bite angle and d(Å), the distance of the TM from the pyrrolic nitrogen plane in the lower cavity.

Table 4.5 provides the bite angle between the two pyrrolic nitrogen planes and the distance, d, of the TM from the lower cavity plane. The flexibility of the Pacman ligand can be seen from the variation of the bite angle among the various complexes. The bite angles for the complexes $Ac^{IV}O_2$ and $Ac^{V}O_2$ range from 76.61º to 88.95º whereas it is much lower (54.42 º to 66.18 º) for the $Ac^{VI}O_2$ complexes. The effect of the actinide contraction and the higher oxidation state makes the Ac(VI) smaller than those in the IV and V oxidation states, and thus the angle between the two planes in the former case becomes much smaller. The two pyrrolic planes are found to be far apart in case of Th(IV) complexes and they are close for the $[Np^{VI}O_2(1)\ L]$ and $[Pu^{VI}O_2(1)\ L]$ complexes.

For the case 3 complexes, where there is no TM-THF bond, the TM sits above the center of the aryl ring and this is quantified by the distance d. This distance measures the extent to which the metal is offset from the center and it is found to be the highest in case of Th(IV), Pa(IV), Pa(V) and U(IV) complexes. On the other side, the Ac(VI) complexes, TM sits almost in the cavity plane formed by the pyrrolic nitrogens in the bottom pocket.

All the 32 heterobimetallic macrocyclic complexes studied in this work are found to have appreciable interactions of the transition metal sitting in the lower cavity with the actinyl endo oxygen, O_2. The variation of the bond length of the M-O_2 bond among various actinide complexes having one transition metal are shown in Figure 4.2. In this figure, there is a dip at $^{L}[Th^{IV}O_2(1\text{-}4)\ L]^{2-}$, indicating the smallest M-O_2 bond length compared to the various other complexes. In case of $^{B}[Th^{IV}O_2(1\text{-}4)\ L]^{2-}$ complexes, the M-O_2 bond is also strong but not as much as it is in the case of $^{L}[Th^{IV}O_2(1\text{-}4)\ L]^{2-}$ complexes. We observed this earlier also that, in these complexes, the TM is pulled out of the plane towards O_2 and that is why they form strong M-O_2 bonds in these complexes. However, in $Pa^{IV}O_2$, $Pa^{V}O_2$ and $U^{IV}O_2$ complexes, there is not much variation in the bond length of M-O_2 and the bond order of M-O_2 is in the range of 0.66 to 0.69 with iron complexes have comparatively shorter bond length with a bond order of about 0.75. Among $Ac^{VI}O_2$ complexes, $U^{VI}O_2$ together with $[Np^{VI}O_2(4)\ L]$ and $[Pu^{VI}O_2(4)\ L]$ complexes exhibit quite weak bonding of the TM to the actinyl endo oxygen with the bond order in the range of 0.35 to 0.46. Among transition metals, iron forms the strongest interactions with the endo oxygen whereas manganese and zinc forms weak interactions with the O_2. $Np^{VI}O_2$ and $Pu^{VI}O_2$ complexes, however, shows a quite variation in the bond order across the transition metals with Mn and Fe forming the strongest bond with the O_2. These kinds of interactions of the actinyl oxygen with the other cation within the same isostructural binuclear complexes form the basis of cation-cation interactions (CCI).

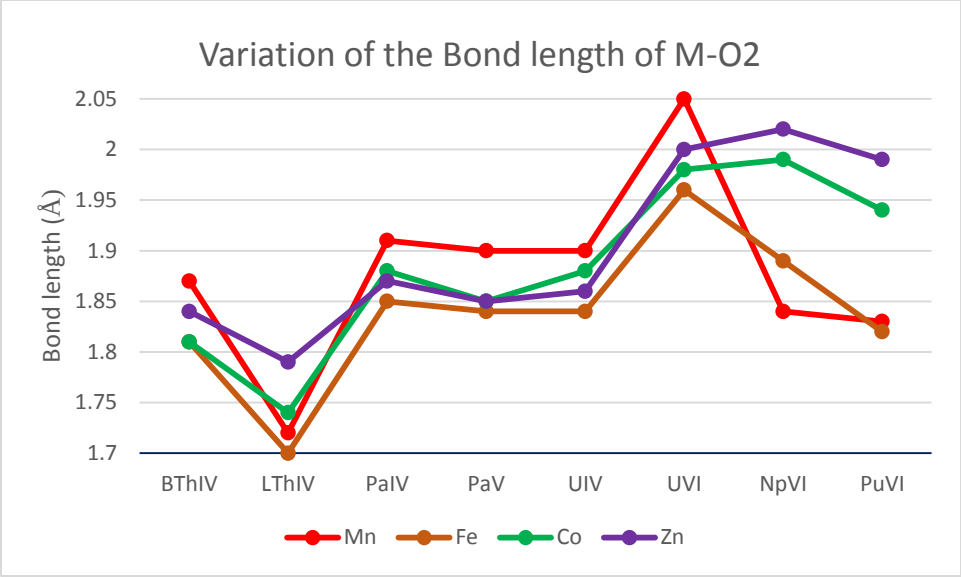

Figure4.2: Plot showing the variation of the M-O2 bond across the actinide series as well as with the variation of TM.

4.3.2 QTAIM analysis

Like the previous case study of the mononuclear and binuclear Pacman complexes of the polypyrrolic macrocyclic ligand studied in chapter 3, here we also applied the quantum theory of atoms in molecules (QTAIM) approach to analyze the electronic structure of the complexes. The details about all these QTAIM parameters have been discussed in chapter 3. We calculated the electron density ρ, its laplacian $\nabla^2\rho$, energy density H (which is the sum of the kinetic and potential energy densities) and DI at the metal-oxygen and metal nitrogen BCPs in the various complexes.

Parameters	$^{B}[Th^{IV}O_2(1)L]^{2-}$	$^{L}[Th^{IV}O_2(1)L]^{2-}$	$[Pa^{IV}O_2(1)L]^{2-}$	$[Pa^{V}O_2(1)L]^{1-}$	$[U^{IV}O_2(1)L]^{2-}$	$[U^{VI}O_2(1)L]$	$[Np^{VI}O_2(1)L]$	$[Pu^{VI}O_2(1)L]$
ρ Ac-O_1	0.18	0.18	0.237	0.241	0.245	0.274	0.261	0.260
ρ Ac-O_2	0.12	0.10	0.170	0.169	0.173	0.234	0.167	0.169
ρ Ac-O_3	None	0.026	0.038	0.037	0.036	0.045	0.039	0.038
ρ M-O_2	0.11	0.13	0.098	0.101	0.100	0.066	0.120	0.121
ρ Ac-N	0.03/0.04	0.03/0.04	0.045/0.059	0.045/0.060	0.043/0.057	0.058/0.071	0.051/0.066	0.051/0.061
ρ M-N	0.01/0.07	0.01/0.07	0.078	0.079	0.077	0.080	0.104	0.069/0.101
ρ M-O_4	0.03	None	None	None	None	0.039	0.040	0.041
∇^2ρ Ac-O_1	0.39	0.38	0.400	0.397	0.417	0.434	0.448	0.483
∇^2ρ Ac-O_2	0.34	0.29	0.397	0.398	0.408	0.472	0.458	0.482
∇^2ρ Ac-O_3	None	0.10	0.146	0.143	0.149	0.171	0.153	0.157
∇^2ρ M-O_2	0.60	0.69	0.529	0.549	0.537	0.347	0.626	0.638
∇^2ρ Ac-N	0.08/0.11	0.03/0.04	0.114/0.144	0.115/0.146	0.123/0.148	0.138/0.165	0.142/0.169	0.143/0.170
∇^2ρ M-N	0.290	0.290	0.318	0.320	0.313	0.315	0.239/0.359	0.242/0.357
∇^2ρ M-O_4	0.17	None	None	None	None	0.180	0.175	0.181
H Ac-O_1	-0.10	-0.09	-0.157	-0.163	-0.162	-0.201	-0.178	-0.174
H Ac-O_2	-0.04	-0.03	-0.0170	-0.080	-0.081	-0.147	-0.071	-0.071
H Ac-O_3	None	0	0	0	0	-0.002	0	0
H M-O_2	-0.02	-0.03	-0.015	-0.016	-0.015	-0.005	-0.022	-0.022
H Ac-N	0/0	0	-0.004/0.009	0	-0.004/0.008	-0.009/-	-0.005/-0.011	-0.006/-0.009
H M-N	0/0	-0.01	-0.013	-0.01	-0.013	0.014	-0.009/-0.020	-0.009/-0.020
H M-O_4	0	None	None	None	None	-0.001	-0.002	-0.002
ε Ac-O_1	0.002	0	0.004	0.005	0.003	0.003	0.007	0.007
ε Ac-O_2	0.012	0.03	0.038	0.039	0.046	0.033	0.038	0.020
ε Ac-O_3	None	0.05	0.004	0.008	0.191	0.011	0.060	0.163
ε M-O_2	0.007	0	0.011	0.013	0.010	0.023	0.029	0.033
ε Ac-N	0.114/0.22	0.15/0.21	0.195/0.236	0.200/0.240	0.333/0.179	0.243/0.285	0.243/0.271	0.244/0.133
ε M-N	0.29/0.08	0.67/0.08	0.094	0.096	0.094	0.098	0.064/0.104	0.467/0.105
ε M-O_4	0.08	None	None	None	None	0.076	0.105	0.106
DI Ac-O_1	2.624	2.606	2.814	2.828	2.839	2.897	2.895	2.894
DI Ac-O_2	1.852	1.673	2.151	2.139	2.148	2.491	2.057	2.060
DI Ac-O_3	None	0.716	0.869	0.865	0.854	0.957	0.878	0.886
DI M-O_2	1.326	1.515	1.122	1.141	1.132	0.789	1.277	1.278
DI Ac-N	0.751/0.919	0.777/0.942	0.893/1.037	0.891/1.041	0.894/1.030	1.019/1.133	0.941/1.088	0.940/1.065
DI M-N	0.212/0.971	0.195/0.994	0.247/1.053	0.279/1.014	0.262/1.040	0.414/1.017	0.936/1.163	0.942/1.171
DI M-O_4	0.691	None	None	None	None	0.737	0.739	0.750

Table4.6: QTAIM topological analysis showing the calculated electron density ρ, $\nabla^2\rho$, H, ε, and DI at The BCPs of various bonds of interest in Mn containing actinide complexes $[AcO_2(Mn)\ L]^n$ where n=0,-1,-2. All the values are in a.u. $^{B}[Th^{IV}O_2(1)\ L]^{2-}$ has O_1-Th-O_2 is bent with no Ac-O_3 bond whereas the other $^{L}[Th^{IV}O_2(1)\ L]^{2-}$ has no M-O_4 bond.

Table 4.6 depicts the QTAIM parameters for the Pacman complexes of the actinide complexes (Th-Pu) containing manganese, Mn, as a heteroatom. The trends in Ac-O as a function of the actinide is possibly the most informative and is very much like the ones observed in case of mononuclear as well as binuclear complexes of actinides (chapter 3). For the Ac-O_1 bond, the electron density at the BCPs (Table 4.6) is more than 0.2 a.u. except for the thorium complexes. The electron density goes on increasing across the series till uranium and then it becomes either constant or decreases for the Np and Pu complexes. Like the mononuclear as well as binuclear complexes of actinides (studied in chapter 3) the electron density is maximum in case of uranium complexes for the Ac-O_1 bond indicating shared shell interactions in uranium complexes as compared to all other complexes studied in this work. Among Pa(IV), Pa(V), U(IV) and U(VI) complexes, ρ at the BCPs of the Ac-O_1 bond in case of the respective oxidized actinide complexes is more than their reduced counterparts, implying more covalent character of the Ac-O1 bond in case of Pa(V) and U(VI) complexes. In all these complexes, the actinides are found to form stronger bonds to the exo oxygen, O_1 than the endo oxygen, O_2 as ρ at the BCPs of the Ac-O_2 is very small as compared to the that of Ac-O_1 bond except for the $[U^{VI}O_2(1)\ L]$ complex where U(VI) binds strongly to both uranyl oxygens.

The actinides in all these complexes bind comparatively stronger to N_2 and N_3 than to N_1 and N_4, and this can be observed from the DI values at the BCPs of the Ac-N bonds. The DI value at the BCP basically measures the bond order of that bond. From its value for M-N bond, it can be inferred that the transition metal has only strong interactions with two of the four nitrogens. However, in case of $[Np^{VI}O_2(1)L]$ and $[Pu^{VI}O_2(1)L]$, the transition metal is binding to three of the four nitrogens instead of two as seen in earlier cases.

The large negative values for the energy density at the BCP of the U-O_1 bond also supports our observation of its high covalency as compared to all other Ac-O_1/Ac-O_2 bonds. Furthermore, its delocalization index value (DI) in Table 4.6 is the highest among all other bonds that are considered in our study. Although the electron density values, ρ, for all the Ac-O_1 bonds, except for the Th-O_1 bond, are more than 0.2 a.u, $\nabla^2\rho$ values are all positive which is very common in case of strongly polar bonds[214]. The ellipticity of the bonds, ε, are almost zero for every case except for the Ac-N/M-N bonds.

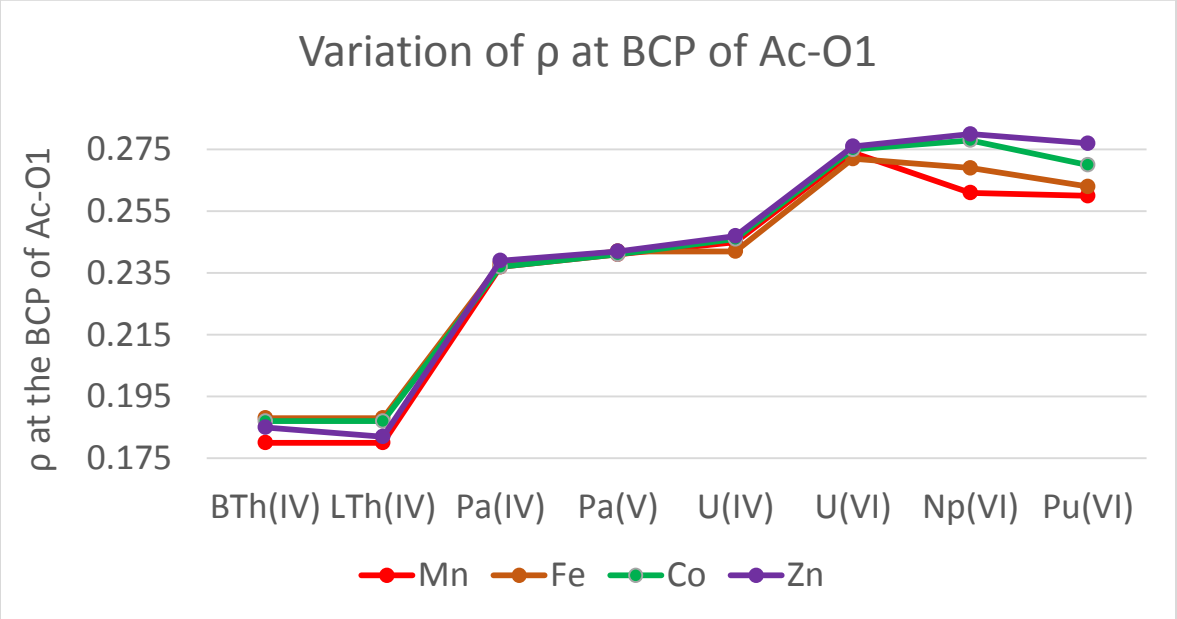

Figure4.3: Plot showing the variation of the electron density at the BCPs of the Ac-O_1 for the heterobinuclear complexes.

The electron density values and laplacian at the BCP of the M-O_2 bond indicates an ionic interaction between the transition metal and the endo oxygen. The ellipticity values for the M-O_2 bond is about zero, inferring it as a single bond and moreover DI values at the BCP of the M-O_2 range from 0.789-1.515. The Mn-O_2 bond in case of [$U^{VI}O_2$(1) L] has the lowest DI value of 0.789 and it can be correlated with the shortness of the U-O_2 bond.

Table 4.7, Table 4.8 and Table 4.9 represent the QTAIM parameters for the various bonds in the Fe, Co and Zn containing actinide Pacman complexes respectively. From the analysis of the QTAIM metrics for these complexes, we observed that there is not much variation in the bonding behavior of the actinyl moiety among different transition metal complexes. As found in case of [AnO_2(1) L]$^{-n}$ complexes, where n=0,1,2 in case of [AnO_2(2) L]$^{-n}$, [AnO_2(3) L]$^{-n}$ and [AnO_2(4) L]$^{-n}$ complexes, respective U-O_1/U-O_2 bonds are the strongest indicating that uranium binds more closely to the actinyl oxygen than any other actinide (Th, Pa, Np, Pu) irrespective of the transition metal. This behavior is also supported by the bond length and bond order data as seen in the previous section.

Parameters	$^{B}[Th^{IV}O_2(2)L]^{2-}$	$^{L}[Th^{IV}O_2(2)L]^{2-}$	$[Pa^{IV}O_2(2)L]^{2-}$	$[Pa^{V}O_2(2)L]^{1-}$	$[U^{IV}O_2(2)L]^{2-}$	$[U^{VI}O_2(2)L]$	$[Np^{VI}O_2(2)L]$	$[Pu^{VI}O_2(2)L]$
ρ Ac-O_1	0.188	0.188	0.238	0.242	0.242	0.272	0.269	0.263
ρ Ac-O_2	0.114	0.086	0.162	0.162	0.162	0.216	0.193	0.166
ρ Ac-O_3	None	0.028	0.039	0.039	0.039	0.044	0.037	0.033
ρ M-O_2	0.128	0.172	0.113	0.116	0.116	0.084	0.100	0.123
ρ Ac-N	0.030/0.043	0.035/0.048	0.045/0.059	0.045/0.060	0.046/0.060	0.057/0.071	0.054/0.067	0.052/0.062
ρ M-N	0.075	0.118	0.090	0.090	0.090	0.090	0.106	0.106
ρ M-O_4	0.040	None	None	None	None	0.047	0.041	0.041
∇^2ρ Ac-O_1	0.398	0.401	0.403	0.399	0.399	0.428	0.457	0.495
∇^2ρ Ac-O_2	0.318	0.272	0.391	0.392	0.392	0.460	0.466	0.454
∇^2ρ Ac-O_3	None	0.111	0.150	0.149	0.149	0.168	0.147	0.136
∇^2ρ M-O_2	0.672	0.878	0.602	0.623	0.623	0.436	0.518	0.639
∇^2ρ Ac-N	0.088/0.115	0.096/0.124	0.115/0.142	0.115/0.144	0.116/0.144	0.137/0.163	0.141/0.171	0.141/0.171
∇^2ρ M-N	0.030/0.346	0.567	0.348	0.355	0.355	0.372	0.390/0.446	0.418/0.465
∇^2ρ M-O_4	0.188	None	None	None	None	0.222	0.181	0.179
H Ac-O_1	-0.104	-0.103	-0.159	-0.164	-0.164	-0.199	-0.189	-0.174
H Ac-O_2	-0.037	-0.019	-0.073	-0.073	-0.073	-0.125	0.193	-0.068
H Ac-O_3	None	0.001	0	0	0	0	0	0
H M-O_2	-0.029	-0.051	-0.021	-0.021	-0.022	-0.011	-0.016	-0.024
H Ac-N	-0.001/-0.004	-0.001/-0.005	-0.004/-0.009	-0.004/-0.009	-0.004/-0.009	-0.008/-0.013	-0.007/-0.012	-0.006/-0.010
H M-N	-0.013	0.344	-0.018	-0.018	-0.018	-0.018	-0.019/-0.023	-0.023/-0.027
H M-O_4	-0.001	None	None	None	None	-0.003	-0.002	-0.041
ε Ac-O_1	0.006	0.005	0.004	0.005	0.005	0.003	0.007	0.007
ε Ac-O_2	0.014	0.022	0.033	0.030	0.030	0.056	0.040	0.037
ε Ac-O_3	None	0.042	0.012	0.012	0.012	0.041	0.119	0.149
ε M-O_2	0.047	0.011	0.093	0.080	0.080	0.032	0.020	0.051
ε Ac-N	0.117/0.230	0.143/0.188	0.192/0.228	0.200/0.230	0.200/0.238	0.264/0.269	0.268/0.244	0.273/0.132
ε M-N	0.125,0.234	0.796	0.09	0.075	0.075	0.143	0.299/0.220	0.288/0.209
ε M-O_4	0.247	None	None	None	None	-0.003	0.129	0.160
DI Ac-O_1	2.642	2.598	2.820	2.833	2.840	2.885	2.891	2.888
DI Ac-O_2	1.754	1.450	2.095	2.084	2.068	2.388	2.239	2.029
DI Ac-O_3	None	0.740	0.885	0.887	0.871	0941	0.862	0.825
DI M-O_2	1.389	1.701	1.179	1.196	1.211	0.886	1.048	1.253
DI Ac-N	0.770/0.919	0.798/0.950	0.896/1.034	0.894/1.042	0.892/1.027	0.999/1.125	0.967/1.088	0.954/1.071
DI M-N	0.145/0.958	0.211/1.230	0.196/1.067	0.225/1.056	0.209/1.054	0.359/1.053	0.801/1.108	0.896/1.143
DI M-O_4	0.665	None	None	None	None	0.761	0.697	0.695

Table4.7: QTAIM Topological analysis showing the calculated electron density ρ, ∇^2ρ, H, ε, and DI at the BCPs Of various bonds of interest in the iron, Fe containing actinide complexes $[AcO_2(Fe)\ L]^n$ where n=0,-1,-2 All the values are in a.u.

Parameters	$^{B}[Th^{IV}O_2(3)L]^{2-}$	$^{L}[Th^{IV}O_2(3)L]^{2-}$	$[Pa^{IV}O_2(3)L]^{2-}$	$[Pa^{V}O_2(3)L]^{1-}$	$[U^{IV}O_2(3)L]^{2-}$	$[U^{VI}O_2(3)L]$	$[Np^{VI}O_2(3)L]$	$[Pu^{VI}O_2(3)L]$
ρ Ac-O_1	0.187	0.187	0.237	0.241	0.246	0.275	0.278	0.270
ρ Ac-O_2	0.119	0.094	0.171	0.168	0.178	0.232	0.232	0.213
ρ Ac-O_3	None	0.030	0.034	0.038	0.033	0.048	0.043	0.034
ρ M-O_2	0.123	0.153	0.101	0.108	0.101	0.073	0.073	0.086
ρ Ac-N	0.031/0.043	0.033/0.047	0.047/0.058	0.045/0.059	0.047/0.058	0.058/0.071	0.055/0.070	0.053/0.063
ρ M-N	0.085	0.088	0.103	0.098	0.102	0.095	0.090	0.054/0.095/0.105
ρ M-O_4	0.044	0.007	None	None	None	0.048	0.043	0.042
∇^2ρ Ac-O_1	0.398	0.391	0.404	0.399	0.420	0.434	0.457	0.493
∇^2ρ Ac-O_2	0.335	0.274	0.397	0.404	0.411	0.493	0.501	0.512
∇^2ρ Ac-O_3	None	0.119	0.134	0.145	0.136	0.180	0.172	0.139
∇^2ρ M-O_2	0.650	0.841	0.101	0.599	0.551	0.414	0.393	0.449
∇^2ρ Ac-N	0.088/0.116	0.093/0.121	0.118/0.141	0.116/0.059	0.288/0.147	0.137/0.163	0.140/0.166	0.143/0.173
∇^2ρ M-N	0.399	0.367	0.294/0.455	0.420	0.448	0.416	0.435	0.193/0.390/0.451
∇^2ρ M-O_4	0.233	None	None	None	None	0.236	0.043	0.191
H Ac-O_1	-0.102	-0.103	-0.158	-0.163	-0.163	-0.203	-0.203	-0.185
H Ac-O_2	-0.040	-0.024	-0.082	-0.078	-0.017	-0.145	-0.141	-0.115
H Ac-O_3	None	-0.001	0	0	0	-0.002	-0.001	0
H M-O_2	-0.027	-0.042	0.101	-0.020	-0.017	-0.008	-0.008	-0.012
H Ac-N	0/-0.004	-0.001/-0.005	-0.004/-0.008	-0.004/-0.009	-0.004/-0.008	-0.009/-0.013	-0.008/-0.012	-0.006/-0.010
H M-N	-0.0158	-0.017	-0.012/-0.161	-0.021	-0.023	-0.020	-0.021	-0.008/-0.020/-0.024
H M-O_4	-0.002	0	None	None	None	-0.003	-0.003	-0.002
ε Ac-O_1	0.004	0.005	0.003	0.007	0.004	0.002	0.005	0.006
ε Ac-O_2	0.040	0.013	0.033	0.003	0.044	0.049	0.047	0.060
ε Ac-O_3	None	0.050	0.004	0.01	0.158	0.023	0.100	0.137
ε M-O_2	0.030	0.048	0.070	0.190	0.042	0.493	0.186	0.192
ε Ac-N	0.110/0.220	0.157/0.196	0.178/0.237	0.199/0.240	0.197/0.288	0.238/0.277	0.313/0.226	0.270/0.128
ε M-N	0.270	0.145	0.215	0.280	0.282	0.144	0.121	0.024/0.478
ε M-O_4	0.220	None	None	None	None	0.050	0.451	0.453
DI Ac-O_1	2.629	2.617	2.811	2.827	2.832	2.887	2.890	2.880
DI Ac-O_2	1.834	1.551	2.186	2.157	2.200	2.516	2.499	2.385
DI Ac-O_3	None	0.769	0.829	0.872	0.817	0.986	0.946	0.835
DI M-O_2	1.301	1.617	1.043	1.090	1.037	0.769	0.769	0.870
DI Ac-N	0.751/0.914	0.778/0.936	0.899/1.022	0.888/1.037	0.919/1.024	1.020/1.136	1.018/1.131	0.974/1.071
DI M-N	0.137/0.984	0.102/0.993	0.617/1.085	0.197/1.078	0.658/1.070	0.305/1.044	0.609/1.039	0.717/1.061
DI M-O_4	0.674	None	None	None	None	0.732	0.451	0.660

Table4.8: QTAIM Topological analysis showing the calculated electron density ρ, ∇^2ρ, H, ε, and DI at the BCPs of various bonds of interest in the cobalt containing actinide complexes $[AcO_2(Co)L]^n$ Where n=0,-1,-2 All the values are in a.u.

Parameters	$^{B}[Th^{IV}O_2(4)L]^{2-}$	$^{L}[Th^{IV}O_2(4)L]^{2-}$	$[Pa^{IV}O_2(4)L]^{2-}$	$[Pa^{V}O_2(4)L]^{1-}$	$[U^{IV}O_2(4)L]^{2-}$	$[U^{VI}O_2(4)L]$	$[Np^{VI}O_2(4)L]$	$[Pu^{VI}O_2(4)L]$
ρ Ac-O_1	0.185	0.182	0.239	0.242	0.247	0.276	0.280	0.277
ρ Ac-O_2	0.125	0.108	0.168	0.167	0.172	0.431	0.238	0.229
ρ Ac-O_3	None	0.027	0.041	0.040	0.039	0.050	0.047	0.044
ρ M-O_2	0.112	0.123	0.101	0.104	0.101	0.070	0.067	0.073
ρ Ac-N	0.029/0.043	0.031/0.046	0.044/0.058	0.044/0.059	0.042/0.057	0.057/0.071	0.054/0.070	0.051/0.059
ρ M-N	0.081	0.084	0.091	0.091	0.091	0.094	0.095	0.092
ρ M-O_4	0.037	None	None	None	None	0.041	0.039	0.039
∇^2ρ Ac-O_1	0.395	0.383	0.400	0.397	0.415	0.431	0.452	0.482
∇^2ρ Ac-O_2	0.351	0.316	0.409	0.410	0.418	0.492	0.505	0.522
∇^2ρ Ac-O_3	None	0.109	0.155	0.151	0.161	0.188	0.187	0.181
∇^2ρ M-O_2	0.593	0.662	0.541	0.566	0.542	0.354	0.335	0.371
∇^2ρ Ac-N	0.085/0.116	0.092/0.124	0.112/0.142	0.113/0.144	0.120/0.146	0.136/0.163	0.143/0.170	0.142/0.163
∇^2ρ M-N	0.334	0.331	0.373	0.381	0.370	0.392	0.400	0.388
∇^2ρ M-O_4	0.154	None	None	None	None	0.160	0.154	0.153
H Ac-O_1	-0.101	-0.098	-0.159	-0.164	-0.165	-0.204	-0.205	-0.194
H Ac-O_2	-0.044	-0.032	-0.078	-0.077	-0.079	-0.145	-0.148	-0.134
H Ac-O_3	None	0.001	0	0	0	-0.003	-0.002	-0.001
H M-O_2	-0.026	-0.031	-0.020	-0.022	-0.020	-0.010	-0.009	-0.011
H Ac-N	0/-0.004	0/-0.004	-0.004/0.009	-0.004/-0.009	-0.003/-0.008	-0.009/-0.013	-0.008/-0.013	-0.006/-0.009
H M-N	-0.017	-0.018	-0.021	-0.021	-0.021	-0.027	-0.023	-0.022
H M-O_4	-0.003	None	None	None	None	-0.004	-0.003	0.003
ε Ac-O_1	0.001	0.007	0.004	0.006	0.003	0.003	0.006	0.003
ε Ac-O_2	0.040	0.054	0.040	0.045	0.052	0.027	0.031	0.035
ε Ac-O_3	None	0.051	0.022	0.019	0.170	0.027	0.097	0.089
ε M-O_2	0	0.009	0.010	0.012	0.011	0.002	0.010	0.004
ε Ac-N	0.110/0.230	0.152/0.213	0.189/0.234	0.197/0.240	0.320/0.182	0.240/0.280	0.329/0.237	0.248/0.181
ε M-N	0.054	0.052	0.0643	0.057	0.063	0.053	0.056	0.052
ε M-O_4	0.070	None	None	None	None	0.069	0.083	0.070
DI Ac-O_1	2.638	2.600	2.829	2.830	2.848	2.890	2.895	2.895
DI Ac-O_2	1.948	1.790	2.190	2.190	2.209	2.530	2.552	2.503
DI Ac-O_3	None	0.727	0.890	0.890	0.891	1.000	0.980	0.955
DI M-O_2	1.120	1.266	1.00	1.000	0.986	0.689	0.671	0.720
DI Ac-N	0.735/0.909	0.759/0.928	0.441/0.515	0.880/1.030	0.881/1.025	1.010/1.130	1.002/1.130	0.992/1.048
DI M-N	0.892	0.921	0.490	0.970	0.977	0.960	0.949	0.212/0.955
DI M-O_4	0.549	None	None	None	None	0.600	0.578	0.589

Table4.9: QTAIM Topological analysis showing the calculated electron density ρ, ∇^2ρ, H, ε, and DI at the BCPs of various bonds of interest in the cobalt containing actinide complexes $[AcO_2(Co)L]^n$ Where n=0,-1,-2 All the values are in a.u.

Figure 4.3 represents the variation of the electron density at the BCP of the Ac-O_1 bond with the actinide as well as with the transition metal. It shows an abrupt increase in its value in going from thorium to protactinium complexes. Furthermore, its value does not show much variation up to U(IV) complexes but again it shows a sudden rise for U(VI) complexes. The electron density at the BCP of the Ac-O_1 among all the complexes shows maxima for the U(VI) complexes and thereafter for neptunium and plutonium complexes either it stays constant or shows a decline.

Like $[AnO_2(1)\ L]^{-n}$ complexes, where n=0,1,2 (Table 4.6), in case of other transition metal containing complexes of the actinides, there is an accumulation of the electron density at the BCPs of the Ac-O_1 bond with the increase of the oxidation state of the actinide as well as with the increase of the atomic number of the actinide, indicating more shared interactions in these cases.

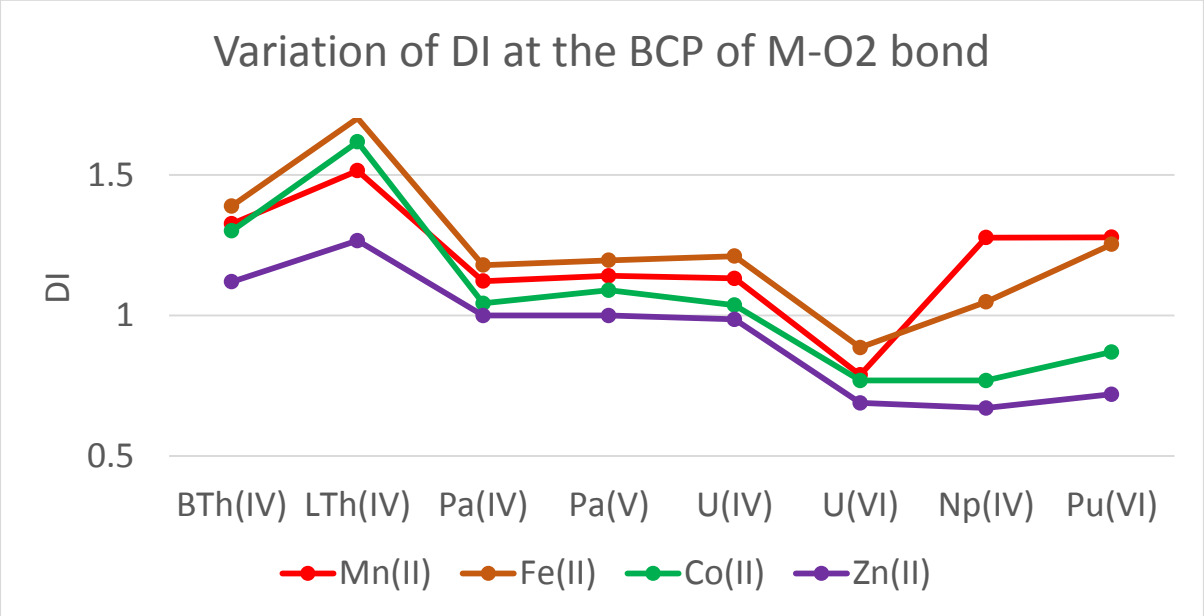

Figure4.4: Variation of the delocalization index (DI) at the BCP of the M-O_2 bond.

In most of the complexes, the transition metal does not sit in the cavity plane and is pulled out towards the endo oxygen and thus have considerable interactions with it. The plot in Figure 4.4 depicts the variation of delocalization index at the BCP of the M-O_2 bond with the change in the transition metal as well as with the actinide. This plot correlates very well with our plot for the variation of the bond length of M-O_2 in Figure 4.2. From the analysis of both plots, we can conclude that in case of thorium complexes, all the transition metals (Mn, Fe, Co and Zn) form a strong bond to O_2, with iron forming the strongest, whereas in case of U(VI) complexes, all these metals lie very much on the pyrrolic plane in the lower cavity and show very weak interactions with the endo oxygen.

Among various transition metals considered in our study, zinc forms the weakest whereas iron forms the strongest interactions with the actinyl endo oxygen O_2 giving rise to very important cation-cation interactions in these complexes.

4.4 Conclusion

Many heterobimetallic complexes of the macrocyclic ligand were studied using density functional theory followed by QTAIM analysis. The upper cavity contains actinyl cations $Th^{IV}O_2$, $Pa^{IV}O_2$, $Pa^{V}O_2^{1+}$, $U^{IV}O_2$, $U^{VI}O_2^{2+}$, $Np^{VI}O_2^{2+}$ and $Pu^{VI}O_2^{2+}$ and the lower cavity contains Mn^{II}, Fe^{II}, Co^{II} and Zn^{II}. Two different geometries for the thorium complexes namely $^{B}[Th^{IV}O_2(4)\ L]^{2-}$ and $^{L}[ThIVO_2(4)\ L]^{2-}$ were studied and the former was found to be more stable than the latter by an amount of 24.88 Kcal/mol. However, $^{L}[Th^{IV}O_2(4)\ L]^{2-}$ was found to have strong interactions of the 3d metal with the actinyl endo oxygen. We encountered three different coordination environments, viz. trigonal, tetrahedral and pentagonal, around the transition metal in the lower pocket whereas the actinide is either 6 or 7 coordinated. In $^{B}[Th^{IV}O_2(4)\ L]^{2-}$ complex, thorium is 6 coordinated whereas in all other complexes the actinide in the upper cavity has nearly pentagonal bipyramidal geometry.

The effect of the actinide contraction is clearly seen in the bond length of Ac-O/Ac-N as we proceed from thorium to plutonium. Among various actinides from thorium to plutonium in different oxidation states in the Pacman heterobimetallic complexes containing 3d transition metal in the lower pocket, uranium in the U(VI) complex is found to form very strong U-O/U-N bonds whereas thorium forms comparatively weak bonds. As the actinyl endo oxygen in case of U(VI) complexes is strongly bonded to the uranium so it has weak interactions with the transition metal irrespective of the transition metal. Mayer and NBO bond order were calculated but NBO were found to be underestimating the bond strength in each case. Furthermore, all these observations are well supported by the QTAIM data analysis. Based on the QTAIM analysis, we found that the uranium in the U(VI) complex forms the strongest bond to the uranyl oxygen in each of the complexes having different TM in one of the cavities of the Pacman ligand.

All these complexes fall in the category of the cation-cation interactions as they all exhibit strong interactions of the actinyl endo oxygen to the transition metal. These interactions lead to the desymmetrization of the actinyl oxo group. Among these four different transition metals, we found that iron forms strong interactions whereas zinc and manganese complexes have the least interactions with O2 and this is supported by bond length, bond order as well as QTAIM data. Moreover, these findings agrees well with the previous studies on the analogues complexes[56].

Chapter 5

Summary and Future Studies

5.1 Summary

In this thesis, we report the comparative computational studies on the bonding analysis of the complexes of early actinides with the octadentate, tetraanionic polypyrrolic ligand H_4L (Figure 1.1). All the studied complexes adopt the well-known Pacman shape.

A total of 29 complexes involving both mononuclear as well as binuclear complexes of the first three actinides with the Schiff-base polypyrrolic ligand were studied using density functional theory. The actinides considered in our case study involves Th(IV), Pa(IV), Pa(V), U(IV) and U(VI). Both DFT and QTAIM studies were done to analyse the bonding patterns of the actinyls in the N_4 donor compartments of the ligand in comparision to the U(VI) analogues. In case of mononuclear complexes of ThO_2 with the ligand, Th-O bonds were so long that the actinyl endo oxygen abstracts the two protons from the vacant pocket and it behaves as a water molecule and this behavior was different from all other actinyl considered in our work.

In case of binuclear complexes, in addition to the earlier known butterfly structures, we explored two more unusual structures namely Diamond D and Zigzag Z, named after the shape of the Ac-O skeleton. The diamond structure is considered as an isomer of the well-known butterfly B structure as both have the same formula. These shapes were found to be adopted by Th (IV), Pa (IV), Pa (V) and U (IV) complexes. In case of the diamond structures, the actinide in the lower cavity does not sit in the polypyrrolic plane. However, the butterfly structure was found to be more stable than its analogous diamond structure. Likewise, among Tri and Z isomers, in case of Pa(V) complexes, the Tri isomer was found to be more stable.

In case of all the binuclear complexes of the early actinides, we found that there is an appreciable interaction of the actinyl endo oxygen of one compartment with the actinide sitting in the other cavity. Moreover, in all cases of these complexes we found that the Ac-O_{endo} is comparatively longer than their respective Ac-O_{exo} bond indicating clearly cation-cation interactions.

DFT studies as well as QTAIM analysis both predicted the largest amount of covalency in case of U(VI) complexes. Moreover, QTAIM analysis data suggest that both U−O and Pa−O are more covalent than the Th analogues and the Ac-O_{exo} bond is stronger than the Ac-O_{endo} bond and these conclusions agreed with our findings on the basis of geometrical analysis.

In the other case study, we studied 32 heterobinuclear complexes of the early actinides with the Schiff-base pypyrrolic ligand using density functional approach. In this binucleating ligand, we placed actinyls, namely $Th^{IV}O_2$, $Pa^{IV}O_2$, $Pa^{V}O_2^{1+}$, $U^{IV}O_2$, $U^{VI}O_2^{2+}$, $Np^{VI}O_2^{2+}$ and $Pu^{VI}O_2^{2+}$, in one of the N4 compartments whereas a 3d transition metal (Mn^{II}, Fe^{II}, Co^{II} and Zn^{II}) was placed in the other cavity. In case of thorium complexes, we found two geometries $^{B}[Th^{IV}O_2(1\text{-}4)\ L]^{2-}$ and $^{L}[Th^{IV}O_2(1\text{-}4)\ L]^{2-}$ with the former found to be more stable than the latter. In case of the $^{B}[Th^{IV}O_2(1\text{-}4)\ L]^{2-}$ complex, the O1-Th-O2 bond angle was found to be 125.9^{0} while in case of $^{L}[Th^{IV}O_2(1\text{-}4)\ L]^{2-}$ it is 157^{0} . In case of the $^{L}[Th^{IV}O_2(4)\ L]^{2-}$ complex, there are strong interactions of the 3d metal with the actinyl endo oxygen. Three different cases of the coordination environment around the transition metal were found namely trigonal, tetrahedral and pentagonal in these complexes whereas the actinide was found to be either 6 or 7 coordinated.

The effect of actinide contraction is clearly seen in the bond length of Ac-O/Ac-N as we move from thorium to plutonium along the actinide series. Among all the heterobimetallic

complexes, uranium in case of U(VI) complexes is found to form very strong bonds to the uranyl oxygens whereas thorium forms comparatively weak bonding to the oxygens. Moreover, the uranium forms weak interactions with the transition metal irrespective of the type of the transition metal sitting in the other pocket. Among various transition metals placed in the lower pocket, iron found to form strong interactions with the actinyl endo oxygen while zinc forming the weakest among others which was supported by bond length, bond order as well as QTAIM data. These complexes also fall in the category of cation-cation interactions as they all show strong interactions of the actinyl endo oxygen to the transition metal. Formal bond order evidence has been found for the transition metal to actinyl endo oxygen partial bond formation for all the complexes.

QTAIM analysis was applied to all the complexes studied in this project. This approach was used to study the electronic structure of the heterobimetallic complexes and it focuses on the properties of the molecular electron density and not on the orbital structure. We analyzed the electron density, Laplacian of the electron density, energy density, ellipticity and delocalization index at the bond critical point of the various bonds of interest in these complexes. Based on the analysis done by using QTAIM, we could access the relative extend of covalency in the metal-ligand bonding. The BCPs data suggests that there is marginally more covalency in case of U-O/U-N than rest of its counterparts. Moreover, in all the complexes, Ac-O1 bond is found to be shorter and hence stronger than the corresponding Ac-O2 bond.

Overall, the investigation into the comparative studies of the bonding behavior of the actinide complexes would lead to add to our existing knowledge of the polypyrrolic macrocycle, periodic trends across the actinide series, cation-cation interactions and binuclear metal complexes.

5.2 Future studies related to our work in this thesis

Various possible ways by which we would like to continue our research related to our present work are as follows:

1. In case of mononuclear as well as binuclear complexes of early actinides, we would like to study the Pacman complexes with the rest of the actinyls as that would allow us to analyze the bonding patterns of these complexes in a broader way. This study would be helpful in examining the behavior of the later actinides which usually behave as lanthanides. Moreover, we would be interested in studying the complexes of these actinyls with other Schiff-base polypyrrolic ligands such as L^2 and L^3 and see how these would be different from the ones with L^1 ligand.
2. The addition of spin-orbit and multiplicity effects is found to play significant role for many properties as well as for the studies on low oxidation state or open shell complexes. As most of our complexes have unpaired electrons so the inclusion of the spin-orbit and multiplet effects within DFT may improve the accuracy of our results.
3. In case of heterobinuclear complexes in our 2^{nd} case study, we can further extend our series to other actinides and look for the trends in the bonding behavior along the whole series.
4. In both the case studies, we can further extend our work on the comparative studies among the complexes of actinides and lanthanides with the Schiff-base polypyrrolic ligand and it would be interesting to see how these two f-block elements differ in their bonding pattern with the macrocyclic ligand. The actinides should have more covalency than the lanthanides.
5. As in our work, we did only the gas phase calculations for both of the case studies and we would like to include solvation effects in our work and see how solvation effects

would affect our results. Although in both case studies, we included THF molecules to account for explicit solvation but we would like to go for implicit solvation as well.

6. Another potential study could include the analysis of the periodic trends in the bonding behavior of the actinides with some other similar macrocyclic ligands.

Appendix

Table S1: The table showing the optimized bond lengths for the protonated butterfly structures. All the BLs are in a. u. B-H stands for the single protonation and B-2H for the double protonation

BL's [BO]	Th(IV)-B		Pa(IV)-B		Pa(V)-B		U(IV)-B		U(VI)-B	
	B-H	B-2H	B-H	B-2H	B-H	B-2H	B-H	B-2H	B-H	B-2H
Ac-O_{exo}	1.97 (2.35,)	1.94 (2.34)	1.88 (2.42)	1.87 (2.42)	1.86 (2.43)	1.85 (2.43)	1.86 (2.43)	1.86 (2.43)	1.80 (2.47)	1.80 (2.48)
Ac_1-O_{endo}	2.19 (1.14) 2.49 (0.60)	2.17 (1.14) 3.08 (0.15)	2.13 (1.17) 2.38 (0.64)	2.14 (1.12) 2.78 (0.27)	2.12 (1.17) 2.34 (0.65)	2.04 (1.36) 4.26 (0)	2.10 (1.19) 2.35 (0.62)	2.10 (1.19) 2.68 (0.68)	2.06 (1.16) 2.30 (0.68)	2.06 (1.16) 2.69 (0.27)
Ac_2-O_{endo}	2.19 (1.14) 2.49 (0.60)	2.17 (1.14) 3.07 (0.15)	2.13 (1.17) 2.38 (0.64)	2.10 (1.22) 2.93 (0.20)	2.12 (1.17) 2.34 (0.65)	2.15 (0.97) 2.60 (0.43)	2.12 (1.14) 2.32 (0.66)	2.10 (1.14) 2.68 (0.66)	2.06 (1.16) 2.31 (0.68)	2.06 (1.16) 2.69 (0.27)
Ac_1-Ac_2	3.75 (0.17)	3.95 (0.15)	3.66 (0.20)	3.89 (0.19)	3.64 (0.21)	4.17 (0.14)	3.55 (0.54)	3.67	3.51 (0.22)	3.69 (0.19)
O_{endo}-H	0.97 (1.05)	0.99 (0.95) 0.99 (0.95)	0.97 (1.01)	0.99 (0.92) 0.99 (0.92)	0.97 (1.00)	0.98 (0.93) 0.98 (0.95)	1.00 (1.00)	0.98 0.98	0.97 (0.97)	0.99 (0.90) 0.99 (0.90)

Table S2: The bite angle (α) between the two N_4 donor planes of the polypyrrolic ligand in case of M and B structures.

Bite angle(º)	Th-4	Pa-4	Pa-5	U-4	U-6
Mononuclear	69.36	64.73	60.88	65.57	61.99
Butterfly	87.99	84.60	80.03	83.13	72.22

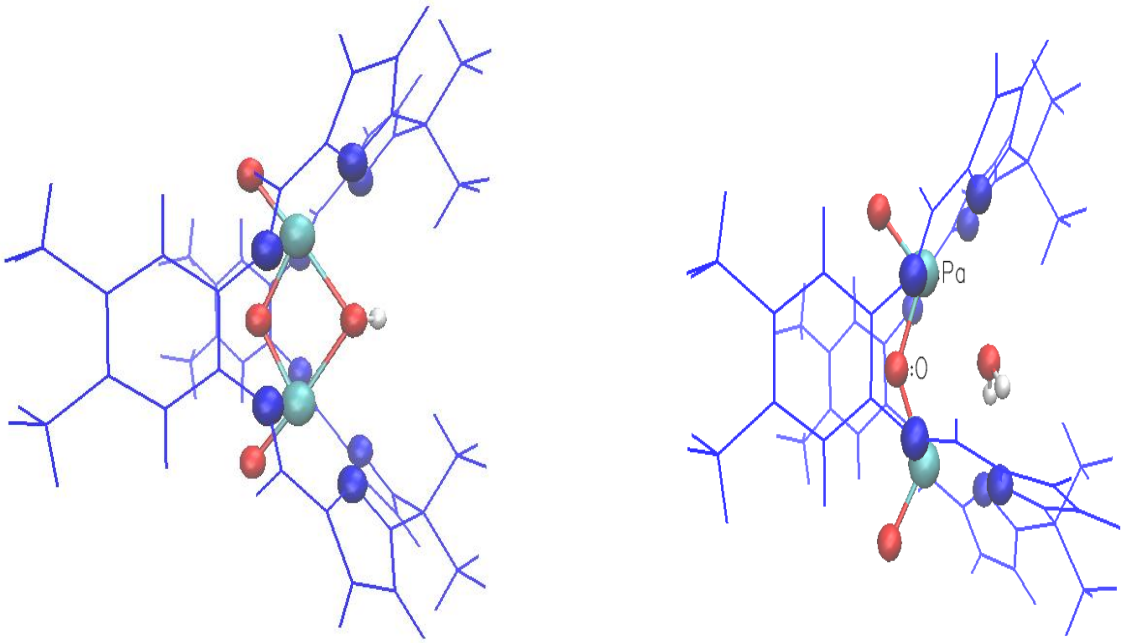

Figure S 1: The optimized geometries for the singly and doubly protonated versions for the B structure for the Pa(IV)-B.

Table S3: Mayer bond order and NBOs of the specified bonds in the Butterfly and Diamond structures of Th, Pa and U.

Bond orders	Th(IV)-B		Th(IV)-D		Pa(IV)-B		Pa(IV)-D		[Pa(V)]-B		Pa(V)-D		[U(IV)]-B		[U(VI)]-B	
	Mayer	NBO	Mayer	NBO	Mayer	NBO	Mayer	NBO	Mayer	NBO	Mayer	NBO	Mayer	NBO	Mayer	NBO
Ac_1-O_{exo}	2.30	1.42	2.28	1.41	2.42	1.92	2.39	1.92	2.41	1.94	2.40	1.93	2.43	2.01	2.44	2.18
Ac_1-O_{endo}	1.12 1.14	0.76 0.77	1.01 1.20	0.70 0.81	1.17 1.17	0.97 0.97	0.63 1.66	1.38 0.51	1.17 1.17	0.98	0.72 1.56	1.22 0.49	1.17 1.19	1.00 1.03	1.02 1.15	1.06 1.11
Ac2-Oendo	1.12 1.14	0.76 0.77	1.26 1.04	0.70 0.81	1.17 1.18	0.97 0.97	0.66 1.73	1.43 0.52	1.17 1.17	0.98	0.77 1.62	1.42 0.65	1.17 1.19	1.00 1.03	1.02 1.15	1.06 1.11
Ac2-Oexo	2.30	1.42	2.18	1.36	2.42	1.92	2.35	1.87	2.41	1.94	2.35	1.97	2.43	2.01	2.44	2.18
Ac1-N	0.19 0.28	0.17 0.22	0.19 0.30	0.18 0.23	0.15 0.21	0.29 0.34	0.18 0.23	0.25 0.35	0.29 0.41	0.29 0.35	0.30 0.41	0.28 0.36	0.17 0.22	0.34 0.38	0.45 0.56	0.49 0.56
Ac2-N	0.19 0.28	0.17 0.22	0.06 0.21 0.33	0.00 0.03 0.14 0.21	0.30 0.42	0.29 0.34	0.38 0.46	0.01 0.31 0.29 0.35	0.29 0.41	0.29 0.35	0.19 0.33 0.42 0.44	0.12 0.26 0.32 0.33	0.33 0.43	0.34 0.38	0.45 0.56	0.49 0.56

Table S4: Charges on the various atoms of interest in the butterfly and diamond complexes of Th, Pa and U.

Atoms	Th(IV)		Pa(IV)		Pa(V)		B4 [U(IV)]	B5 [U(VI)]
	B	D	B	D	B	D		
Ac_1	0.24	0.28	0.47	0.50	0.48	0.49	0.40	0.58
Ac_2	0.24	0.37	0.47	0.51	0.48	0.59	0.40	0.58
$O_{exo}(Ac_1)$	-0.58	-0.57	-0.45	-0.43	-0.43	-0.42	-0.40	-0.28
O_{endo}	-0.45 -0.46	-0.46 -0.43	-0.36 -0.38	-0.36 -0.35	-0.35 -0.38	-0.37 -0.35	-0.33 -0.35	-0.26 -0.28
$O_{exo}(Ac_2)$	-0.58	-0.53	-0.45	-0.42	-0.43	-0.38	-0.40	-0.28

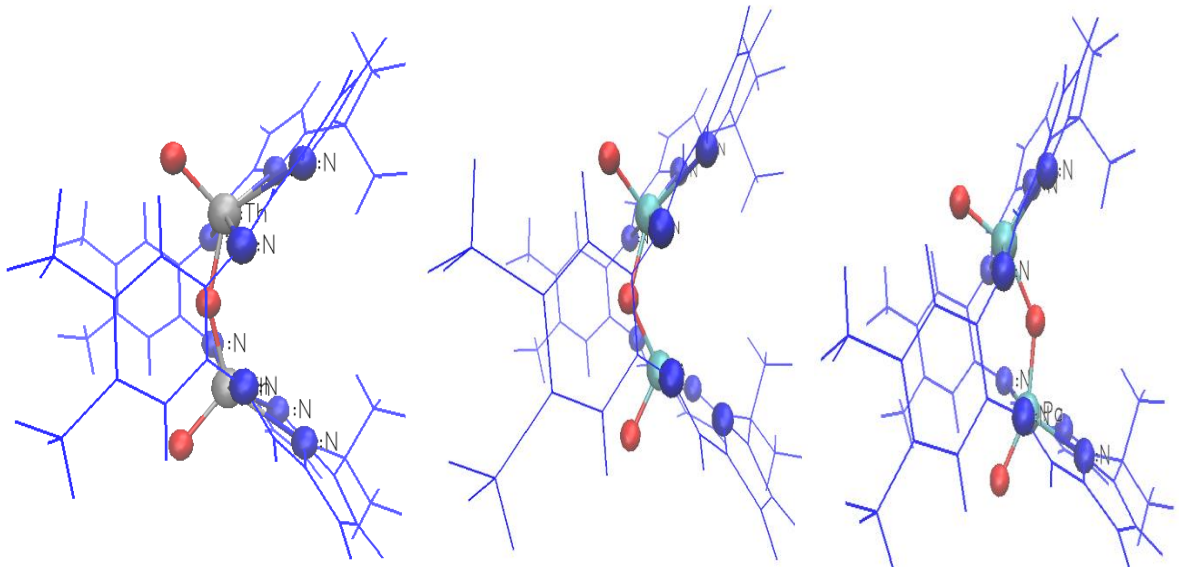

(a) (b) (c)

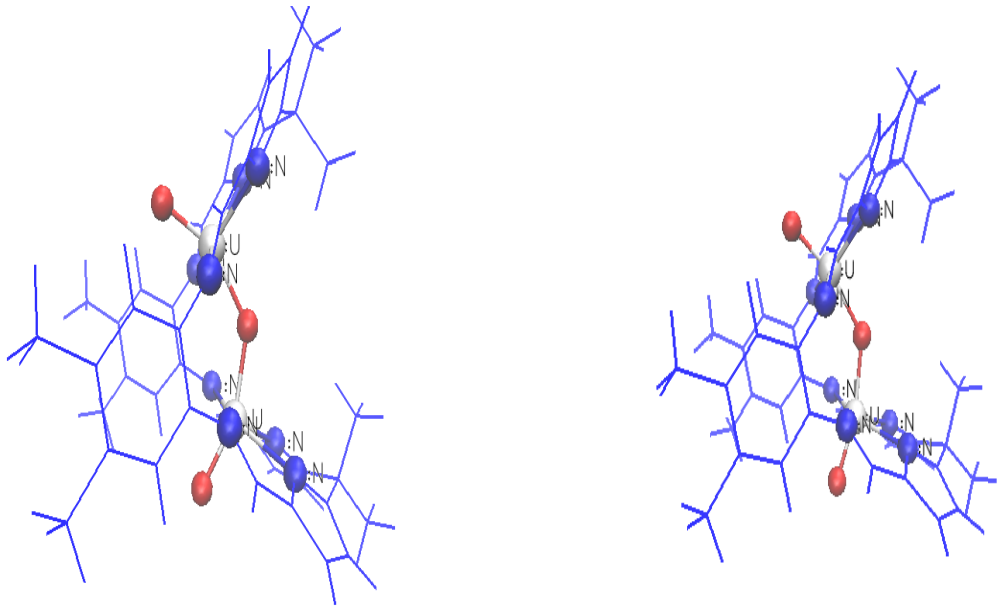

(d) (e)

Figure S 2: The optimised geometries for (a) Th(IV)-Z (b) Pa(IV)-Z (c) Pa(V)-Tri (d) U(IV)-Tri and (e) U(VI)-Tri complexes.

Table S5: Optimized gas phase bond lengths(Å), Bond order in parentheses, Bond angles (in degrees) and Mulliken's charges for the complexes Th(IV)-Z, Pa(IV)-Z, Pa(V)-Tri, U(IV)-Tri,

Bond length [BO]	Th(IV)-Z	Pa(IV)-Z	Pa(V)-Tri	U(IV)-Tri	U(VI)-Tri
Ac-O_{exo}	1.95 [2.34, *1.52*]	1.88 [2.41, *1.83*]	1.85 [2.44, *2.03*]	1.86 [2.42, *1.96*]	1.80 [2.47, *2.22*]
Ac-O_{endo}	2.16 [1.14, *0.75*]	2.12 [1.17, *0.93*]	2.10 [1.16, *0.96*]	2.10 [1.16, *0.97*]	2.06 [1.15, *1.04*]
Ac-N	2.65/2.76 [0.28/0.41, *0.21/0.27*]	2.54/2.60 [0.38/0.49 *0.32/0.37*]	2.41/2.55 [0.41/0.59, *0.36/0.51*]	2.45/2.59 [0.40/0.53, *0.36/0.46*]	2.33/2.41 [0.57/0.70, *0.59/0.70*]
Bond angle(^{0})					
O_{exo}-Ac1-O_{endo}	117.47	110.39	152.41	153.8	164.13
O_{exo}-Ac2-O_{endo}	117.66	110.39	152.26	153.79	164.17
Charges					
Ac1	0.50	0.50	0.66	0.47	0.47
O_{exo}(Ac1)	-0.53	-0.43	-0.37	-0.41	-0.41
O_{endo}	-0.44	-0.37	-0.34	-0.34	-0.34
Ac2	0.50	0.50	0.66	0.47	0.47
O_{exo}(Ac2)	-0.53	-0.43	-0.37	-0.41	-0.41

Table S6: Topological analysis to calculate electron densities at the Ac-O_{exo}/Ac-O_{endo} BCPs for the Mononuclear complexes. ρ = magnitude of electron density at BCPs, $\nabla^2\rho$= laplacian of ρ at BCPs, H = energy density at the BCPs, ε= ellipticity of the bond. All the values are given in a.u.

The Nitrogen at position 4 and 15 have the same values of the parameters whereas the N at 6 and 14 positions have the same values.

Parameters	Th(IV)-M	Pa(IV)-M	Pa(V)-M	U(IV)-M	U(VI)-M
ρ Ac-O_{exo}	0.20	0.23	0.24	0.24	0.28
ρ Ac-O_{endo}	0.06	0.20	0.19	0.22	0.25
ρ O_{endo}-H	0.26				
ρ Ac-N4,15	0.034	0.037	0.037	0.038	0.050
ρ Ac-N6,14	0.048	0.052	0.054	0.054	0.068
∇^2ρ Ac-O_{exo}	0.40	0.41	0.41	0.43	0.44
∇^2ρ Ac-O_{endo}	0.18	0.39	0.38	0.43	0.45
∇^2ρ O_{endo}-H	-0.12				
∇^2ρ Ac-N4,15	0.093	0.100	0.101	0.111	0.121
∇^2ρ Ac-N6,14	0.120	0.134	0.135	0.154	0.157
H Ac-O_{exo}	-0.11	-0.15	-0.16	-0.16	-0.20
H Ac-O_{endo}	-0.007	-0.11	-0.10	-0.13	-0.17
H O_{endo}-H	-0.38				
H Ac-N4,15	-0.001	-0.002	-0.002	-0.002	-0.006
H Ac-N6,14	-0.005	-0.007	-0.007	-0.007	-0.012
ε Ac-O_{exo}	0	0	0	0	0
ε Ac-O_{endo}	0.14	0	0	0	0
ε O_{endo}-H	0.01				
ε Ac-N4,15	0.15	0.19	0.20	0.13	0.23
ε Ac-N6,14	0.19	0.22	0.22	0.06	0.27
DI Ac-O_{exo}	2.68	2.81	2.81	2.84	2.89
DI Ac-O_{endo}	1.18	2.51	2.51	2.72	2.76
DI O_{endo}-H	0.60				
DI Ac-N4,15	0.80	0.81	0.81	0.92	0.95
DI Ac-N6,14	0.95	0.98	0.99	1.10	1.12

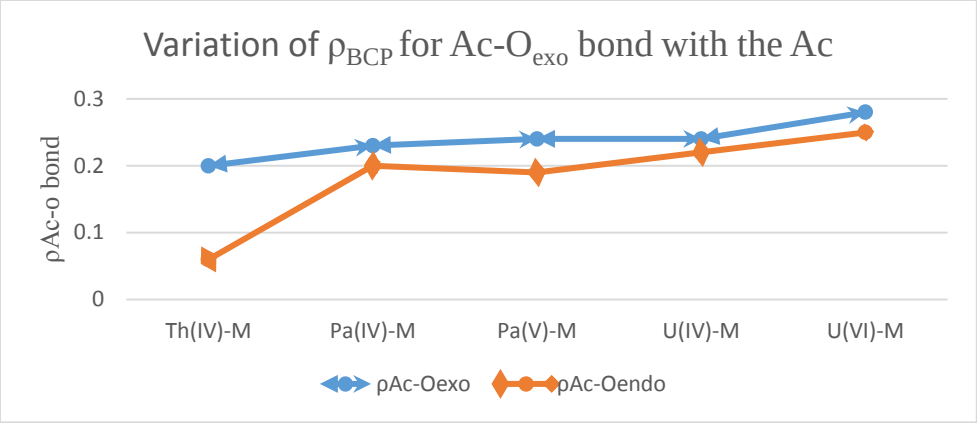

Figure S 3: The variation of electron density at the BCP with the function of actinide for the Ac-O_{exo} and Ac-O_{endo} bonds in various mononuclear complexes.

Table S7: Topological analysis of calculate electron densities at the Ac-O_{exo}/Ac-O_{endo} BCPs in various Butterfly complexes. ρ = magnitude of electron density at BCp, $\nabla^2\rho$= laplacian of ρ at BCPs, H = energy density at the BCPs, ε= ellipticity of the bond. All the values are given in a.u.

Parameters	Th(IV)-B	Pa(IV)-B	Pa(V)-B	U(IV)-B	U(VI)-B
ρ Ac1-O_{exo}	0.16	0.22	0.22	0.23	0.27
ρ Ac1-O_{endo}	0.10	0.12	0.12	0.12	0.13
	0.09	0.12	0.12	0.12	0.14
ρ Ac1-$N_{4,15}$	0.025	0.040	0.042	0.043	0.061
ρ Ac1-$N_{6,14}$	0.033	0.048	0.048	0.049	0.070
$\nabla^2\rho$ Ac1-O_{exo}	0.37	0.41	0.41	0.44	0.45
$\nabla^2\rho$ Ac1-O_{endo}	0.29	0.34	0.34	0.37	0.38

	0.26	0.30	0.30	0.32	0.34
$\nabla^2\rho$ Ac1-N4,15	0.079	0.105	0.114	0.116	0.141
$\nabla^2\rho$ Ac1-N6,14	0.096	0.121	0.129	0.130	0.160
H Ac1-O_{exo}	-0.03	-0.14	-0.14	-0.15	-0.19
H Ac1-O_{endo}	-0.02	-0.04	-0.04	-0.41	-0.45
	-0.03	-0.04	-0.04	-0.43	-0.52
H Ac1-N4,15	0	-0.003	-0.003	-0.004	-0.010
H Ac1-N6,14	-0.001	-0.005	-0.006	-0.006	-0.013
ε Ac1-O_{exo}	0.017	0.016	0.016	0.017	0.015
ε Ac1-O_{endo}	0.02	0.01	0.005	0.011	0.015
	0.03	0.038	0.035	0.043	0.053
ε Ac1-N4,15	0.12	0.15	0.16	0.23	0.22
ε Ac1-N6,14	0.14	0.19	0.19	0.28	0.26
DI Ac1-O_{exo}	2.53	2.79	2.81	2.83	2.91
DI Ac1-O_{endo}	1.53	1.59	1.59	1.61	1.63
	1.49	1.59	1.59	1.60	1.61
DI Ac1-N4,15	0.68	0.84	0.84	1.00	1.03
DI Ac1-N6,14	0.79	0.95	095	1.12	1.14

Table S6: Topological analysis of calculate electron densities at the Ac-O_{exo}/Ac-O_{endo} BCPs in various Zigzag and triangle shaped complexes. ρ = magnitude of electron density at BCp, $\nabla^2\rho$= laplacian of ρ at BCPs, H = energy density at the BCPs, ε= ellipticity of the bond. All the values are given in a.u.

Parameters	Th(IV)-Z	Pa(IV)-Z	Pa(V)-Tri	U(IV)-Tri	U(VI)-Tri
ρ Ac-O_{exo}	0.19	0.23	0.24	0.23	0.27
ρ Ac-O_{endo}	0.11	0.12	0.12	0.12	0.13
ρ Ac1-N4,15	0.035	0.049	0.057	0.049	0.078
ρ Ac1-N6,14	0.045	0.057	0.076	0.066	0.090
$\nabla^2\rho$ Ac-O_{exo}	0.40	0.45	0.41	0.44	0.43
$\nabla^2\rho$ Ac-O_{endo}	0.32	0.36	0.34	0.35	0.37
$\nabla^2\rho$ Ac1-N4,15	0.096	0.123	0.131	0.135	0.163
$\nabla^2\rho$ Ac1-N6,14	0.118	0.139	0.171	0.174	0.198
H Ac-O_{exo}	-0.10	-0.15	-0.17	-0.14	-0.20
H Ac-O_{endo}	-0.36	-0.44	-0.45	-0.41	-0.51
H Ac1-N4,15	-0.002	-0.006	-0.009	-0.006	-0.017
H Ac1-N6,14	-0.005	-0.009	-0.016	-0.012	-0.023
ε Ac-O_{exo}	0.017	0.011	0.003	0.013	0.005
ε Ac-O_{endo}	0.051	0.008	0.029	0.09	0
ε Ac1-N4,15	0.10	0.13	0.18	0.18	0.28
ε Ac1-N6,14	0.19	0.16	0.31	0.24	0.34
DI Ac-O_{exo}	2.69	2.81	2.82	2.85	2.95
DI Ac-O_{endo}	1.63	1.65	1.66	1.66	1.67
DI Ac1-N4,15	0.78	0.94	0.98	1.15	1.17
DI Ac1-N6,14	0.92	1.15	1.17	1.28	1.30

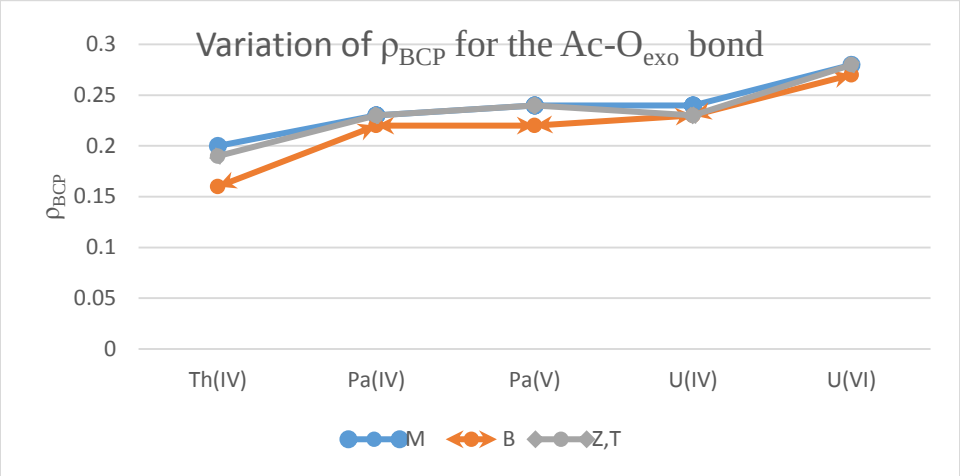

Figure S 4: The variation of electron density at the BCP for the Ac-Oexo bond in M, B, Zigzag as well as Triangle shaped complexes.

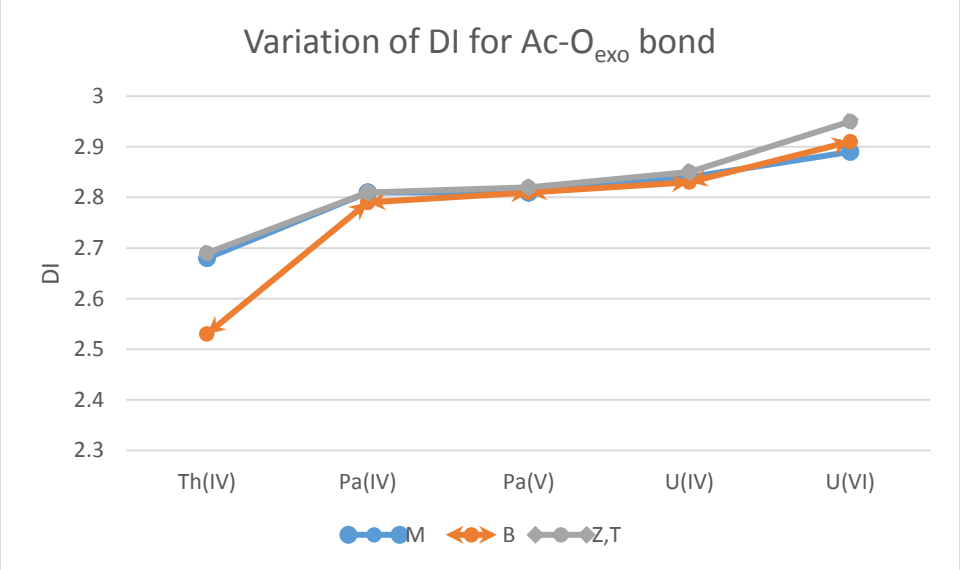

Figure S 5: The variation of the delocalization index value at the BCP for the Ac-O_{exo} bond in the Mononuclear, Binuclear, Zigzag and Triangle shaped complexes.

Bibliography

1. Wang D, van Gunsteren WF, Chai Z. Recent Advances in Computational Actinoid Chemistry. *Chem Soc Rev*. 2012;41(17):5836. doi:10.1039/c2cs15354h

2. Schreckenbach G, Shamov GA. Theoretical Actinide Molecular Science. *Acc Chem Res*. 2010;43(1):19-29. doi:10.1021/ar800271r

3. Andrea T, Eisen MS. Recent Advances in Organothorium and Organouranium Catalysis. *Chem Soc Rev*. 2008;37(3):550-567. doi:10.1039/B614969N

4. Renshaw JC, Handley-Sidhu S, Brookshaw DR. Pathways of Radioactive Substances in the Environment. In: ; :152-176. doi:10.1039/9781849732888-00152

5. Wang PW, Hirsch RF. Nuclear Waste Management: Accomplishments of the Environmental Management Science Program. In: ; 2006:2-10. doi:10.1021/bk-2006-0943.ch001

6. Choppin GR. Actinide Speciation in the Environment. *J Radioanal Nucl Chem*. 2007;273(3):695-703. doi:10.1007/s10967-007-0933-3

7. David L. Clark, Siegfried S. Hecker, Gordon D. Jarvinen and MPN. *The Chemistry of the Actinide and Transactinide Elements*. 2nd ed. springer; 2006.

8. (http://www.hanford.gov/).

9. Pepper M, Bursten BE. The Electronic Structure of Actinide-Containing Molecules: A Challenge to Applied Quantum Chemistry. *Chem Rev*. 1991;91(5):719-741. doi:10.1021/cr00005a005

10. Schreckenbach G, Hay PJ, Martin RL. Density Functional Calculations on Actinide Compounds: Survey of Recent Progress and Application to [UO2X4]2− (X=F, Cl, OH) and AnF6 (An=U, Np, Pu). *J Comput Chem*. 1999;20(1):70-90. doi:10.1002/(SICI)1096-987X(19990115)20:1<70::AID-JCC9>3.0.CO;2-F

11. Gregory R. Choppin. *Separation of F-Elements By Solvent Extraction*. New York: Springer; 1995.

12. Minasian SG, Keith JM, Batista ER, et al. Determining Relative f and d Orbital Contributions to M–Cl Covalency in MCl 6 2– (M = Ti, Zr, Hf, U) and UOCl 5 – Using Cl K-Edge X-ray Absorption Spectroscopy and Time-Dependent Density Functional Theory. *J Am Chem Soc*. 2012;134(12):5586-5597. doi:10.1021/ja2105015

13. Kaltsoyannis N. Does Covalency Increase or Decrease across the Actinide Series? Implications for Minor Actinide Partitioning. *Inorg Chem*. 2013;52(7):3407-3413. doi:10.1021/ic3006025

14. L. R. JM, N. M. E, Fuger. *The Chemistry of Actinides and Transuranic Elements*. 3rd ed. The Netherland: Springer; 2006.

15. Arnold PL, Potter (née Jones) NA, Magnani N, et al. Synthesis of Bimetallic Uranium and Neptunium Complexes of a Binucleating Macrocycle and Determination of the Solid-State Structure by Magnetic Analysis. *Inorg Chem*. 2010;49(12):5341-5343.

doi:10.1021/ic100374j

16. Arnold PL, Patel D, Blake AJ, Wilson C, Love JB. Selective Oxo Functionalization of the Uranyl Ion with 3d Metal Cations. *J Am Chem Soc*. 2006;128(30):9610-9611. doi:10.1021/ja0634167

17. Arnold PL, Dutkiewicz MS, Zegke M, et al. Subtle Interactions and Electron Transfer between U^{III}, Np^{III}, or Pu^{III} and Uranyl Mediated by the Oxo Group. *Angew Chemie*. 2016;128(41):12989-12993. doi:10.1002/ange.201607022

18. Pan Q-J, Odoh SO, Schreckenbach G, Arnold PL, Love JB. Theoretical Exploration of Uranyl Complexes of a Designed Polypyrrolic Macrocycle: Structure/Property Effects of Hinge Size on Pacman-Shaped Complexes. *Dalt Trans*. 2012;41(29):8878. doi:10.1039/c2dt31055d

19. Ward AL, Buckley HL, Lukens WW, Arnold J. Synthesis and Characterization of Thorium(IV) and Uranium(IV) Corrole Complexes. *J Am Chem Soc*. 2013;135(37):13965-13971. doi:10.1021/ja407203s

20. Arnold PL, Jones GM, Pan Q-J, Schreckenbach G, Love JB. Co-linear, Double-Uranyl Coordination by an Expanded Schiff-Base Polypyrrole Macrocycle. *Dalt Trans*. 2012;41(22):6595. doi:10.1039/c2dt30658a

21. Arnold PL, Blake AJ, Wilson C, Love JB. Uranyl Complexation by a Schiff-Base, Polypyrrolic Macrocycle. *Inorg Chem*. 2004;43(26):8206-8208. doi:10.1021/ic0487070

22. Arnold PL, Blake AJ, Wilson C, Love JB. Uranyl Complexation by a Schiff-Base, Polypyrrolic Macrocycle. *Inorg Chem*. 2004;43(26):8206-8208. doi:10.1021/ic0487070

23. F A Cotton and G. Wilkinson. *Advanced Inorganic Chemistry*. New York: John Wiley and sons; 1988.

24. https://en.wikipedia.org/wiki/Actinide.

25. http://periodic.lanl.gov/elements/93.html.

26. Norman N Greenwood AE. *Chemistry of the Elements*. 2nd ed.; 1997.

27. Clain, A. F.; de Aquino, J. O.; Domingues, M. D. F. No Title. *Quim Nov*. 1999;22(5):677-678.

28. Betti M. Civil use of depleted uranium. *J Environ Radioact*. 2003;64(2-3):113-119. doi:10.1016/S0265-931X(02)00042-5

29. Nikolas Kaltsoyannis and Peter Scott. *The F-Elements*.; 1999.

30. Steele H, Taylor RJ. A Theoretical Study of the Inner-Sphere Disproportionation Reaction Mechanism of the Pentavalent Actinyl Ions. *Inorg Chem*. 2007;46(16):6311-6318. doi:10.1021/ic070235c

31. Runde W. The Chemical Interactions of Actinides in the Enviornment. *Los Alamos Sci*. 2000.

32. Pyykkö P. Recent Developments in the Theory of f-Element Molecules. *Inorganica Chim*

Acta. 1987;139(1-2):243-245. doi:10.1016/S0020-1693(00)84086-4

33. CHOPPIN GR. Solution Chemistry of the Actinides. *Radiochim Acta*. 1983;32(1-3):43-53. doi:10.1524/ract.1983.32.13.43

34. *https://repositories.lib.utexas.edu/handle/2152/10998?show=full*.

35. Leverd PC, Nierlich M, Dumazet-Bonnamour I, Lamartine R. Using a Large Calixarene as a Polyalkoxide Ligand: Tert-butylcalix[12]arene and its Complex with the Uranyl Cation. *Chem Commun*. 2000;(6):493-494. doi:10.1039/b000909l

36. Mohapatra PK, Sengupta A, Iqbal M, Huskens J, Godbole S V., Verboom W. Remarkable Acidity Independent Actinide Extraction with a Both-side Diglycolamide-Functionalized Calix[4]arene. *Dalt Trans*. 2013;42(24):8558. doi:10.1039/c3dt50557j

37. De Ramírez FM, Varbanov S, Padilla J, Bünzli JCG. Physicochemical Properties and Theoretical Modeling of Actinide Complexes with a Para-Terf-Butylcalix[6]arene Bearing Phosphinoyl Pendants. Extraction Capability of the Calixarene toward f elements. *J Phys Chem B*. 2008;112(35):10976-10988. doi:10.1021/jp710848m

38. Mokhtari B, Pourabdollah K, Dallali N. A Review of Calixarene Applications in Nuclear Industries. *J Radioanal Nucl Chem*. 2011;287(3):921-934. doi:10.1007/s10967-010-0881-1

39. Kiegiel K, Steczek L, Zakrzewska-trznadel G. Application of Calixarenes as Macrocyclic Ligands for Uranium (VI): A Review. *J Chem*. 2013;2013(Vi):1-16. doi:10.1155/2013/762819

40. Bombieri G, De Paoli G, Immirzi A. Crown Ether Complexes of Actinide Elements an X-ray Study of the Conformational Change of the Crown Ether Within the $UO_2(NO_3)_2(H_2O)_2$(18-crown-6) molecule. *J Inorg Nucl Chem*. 1978;40(5):799-802. doi:10.1016/0022-1902(78)80154-7

41. Shamov GA, Schreckenbach G, Martin RL, Hay PJ. Crown Ether Inclusion Complexes of the Early Actinide Elements, $[AnO_2(18\text{-crown-}6)]^{n+}$, An = U, Np, Pu and n= 1, 2: A Relativistic Density Functional Study. *Inorg Chem*. 2008;47(5):1465-1475. doi:10.1021/ic701192t.

42. Arliguie T, Belkhiri L, Bouaoud S-E, et al. Lanthanide(III) and Actinide(III) Complexes $[M(BH_4)_2(THF)_5][BPh_4]$ and $[M(BH_4)_2$(18-crown-6)$][BPh_4]$ (M = Nd, Ce, U): Synthesis, Crystal Structure, and Density Functional Theory Inv. *Inorg Chem*. 2009;48(Copyright (C) 2014 American Chemical Society (ACS). All Rights Reserved.):221-230. doi:10.1021/ic801685v

43. Gong Y, Gibson JK. Crown Ether Complexes of Uranyl, Neptunyl, and Plutonyl: Hydration Differentiates Inclusion Versus Outer Coordination. *Inorg Chem*. 2014;53(11):5839-5844. doi:10.1021/ic500724q

44. Burrell AK, Hemmi G, Lynch V, Sessler JL. Uranylpentaphyrin: An Actinide Complex of an Expanded Porphyrin. *J Am Chem Soc*. 1991;113(12):4690-4692. doi:10.1021/ja00012a053

45. Sessler, J. L.; Vivian, A. E.; Seidel, D.; Burrell, A. K.; Hoehner, M.; Mody, T. D.; Gebauer, A.; Weghorn, S. J.; Lynch V. Actinide Expanded Porphyrin Complexes. 2001:411-434.

46. Sessler, J. L.; Seidel, D.; Vivian, A. E.; Lynch, V.; Scott, B. L.; Keogh DW. Hexaphyrin(1.0.1.0.0.0): An Expanded Porphyrin Ligand for the Actinide Cations Uranyl (UO_2^{2+})and Neptunyl (NpO_2^{+1}). *Angew Chem, Int Ed Engl*. 2001;3.

47. Zhang Z, Lim JM, Ishida M, et al. Cyclo[m]pyridine[n]pyrroles: Hybrid Macrocycles That Display Expanded π-Conjugation upon Protonation. *J Am Chem Soc*. 2012;134(9):4076-4079. doi:10.1021/ja211985k

48. Ho I-T, Zhang Z, Ishida M, et al. A Hybrid Macrocycle with a Pyridine Subunit Displays Aromatic Character upon Uranyl Cation Complexation. *J Am Chem Soc*. 2014;136(11):4281-4286. doi:10.1021/ja412520g

49. Sessler, J. L.; Gorden, A. E. V.; Seidel, D.; Hannah, S.; Lynch, V.; Gordon, P. L.; Donohoe, R. J.; Tait, C. D.; Keogh DW. Characterization of the Interactions Between Neptunyl and Plutonyl Cations and Expanded Porphyrins. *Inorg Chem acta*. 2002;341:54-70.

50. Barnea E, Andrea T, Kapon M, Eisen MS. Formation of Inclusion Organoactinide Complexes with Boron-Containing Macrocycles. *J Am Chem Soc*. 2004;126(16):5066-5067. doi:10.1021/ja0498843

51. J. L. Sessler SJW. *Expanded, Contracted and Isomeric Porphyrins, Vol. 15*. Ist. elsevier; 1997.

52. Sessler JL, Weghorn SJ, Hiseada Y, Lynch V. Hexaalkyl Terpyrrole: A New Building Block for the Preparation of Expanded Porphyrins. *Chem – A Eur J*. 1995;1(1):56-67. doi:10.1002/chem.19950010110

53. Sessler, J. L.; Gebauer, A.; Hoehner, M. C.; Lynch V. Synthesis and Characterization of an Oxasapphyrin-Uranyl Complex. *Chem Commun*. 1992;31:1835-1836. doi:10.1039/A803975E

54. Melfi PJ, Kim SK, Lee JT, et al. Redox Behavior of Cyclo[6]pyrrole in the Formation of a Uranyl Complex. *Inorg Chem*. 2007;46(13):5143-5145. doi:10.1021/ic700781t

55. Shamov GA, Schreckenbach G. Relativistic Density Functional Theory Study of Dioxoactinide(VI) and -(V) Complexation with Alaskaphyrin and Related Schiff-Base Macrocyclic Ligands. *J Phys Chem A*. 2006;110(30):9486-9499. doi:10.1021/jp063060l

56. Berard JJ, Schreckenbach G, Arnold PL, Patel D, Love JB. Computational Density Functional Study of Polypyrrolic Macrocycles: Analysis of Actinyl-Oxo to 3d Transition Metal Bonding. *Inorg Chem*. 2008;47(24):11583-11592. doi:10.1021/ic8010772

57. Pan Q-J, Shamov GA, Schreckenbach G. Binuclear Uranium(VI) Complexes with a "Pacman" Expanded Porphyrin: Computational Evidence for Highly Unusual Bis-Actinyl Structures. *Chem - A Eur J*. 2010;16(7):2282-2290. doi:10.1002/chem.200902014

58. Pan Q-J, Schreckenbach G. Binuclear Hexa- and Pentavalent Uranium Complexes with a

Polypyrrolic Ligand: A Density Functional Study of Water- and Hydronium-Induced Reactions. *Inorg Chem*. 2010;49(14):6509-6517. doi:10.1021/ic100245a

59. Pan Q-J, Schreckenbach G, Arnold PL, Love JB. Theoretical Predictions of Cofacial Bis(actinyl) Complexes of a Stretched Schiff-Base Calixpyrrole Ligand. *Chem Commun*. 2011;47(20):5720. doi:10.1039/c1cc10979k

60. Yao J, Zheng X-J, Pan Q-J, Schreckenbach G. Highly Valence-Diversified Binuclear Uranium Complexes of a Schiff-Base Polypyrrolic Macrocycle: Prediction of Unusual Structures, Electronic Properties, and Formation Reactions. *Inorg Chem*. 2015;54(11):5438-5449. doi:10.1021/acs.inorgchem.5b00483

61. Su D-M, Zheng X-J, Schreckenbach G, Pan Q-J. Highly Diverse Bonding between Two U 3+ Ions When Ligated by a Flexible Polypyrrolic Macrocycle. *Organometallics*. 2015;34(21):5225-5232. doi:10.1021/acs.organomet.5b00649

62. Liao M-S, Kar T, Scheiner S. Actinyls in Expanded Porphyrin: A Relativistic Density-Functional Study †. *J Phys Chem A*. 2004;108(15):3056-3063. doi:10.1021/jp036927d

63. Sundararajan M, Sinha V, Bandyopadhyay T, Ghosh SK. Can Functionalized Cucurbituril Bind Actinyl Cations Efficiently? A Density Functional Theory Based Investigation. *J Phys Chem A*. 2012;116(17):4388-4395. doi:10.1021/jp3015194

64. Chen F, Qu N, Wu Q, Zhang H, Shi W, Pan Q. Structures and Uranium-Uranium Multiple Bond of Binuclear Divalent Uranium Complex of Pyrrolic Schiff-base Macrocycle: a Relativistic DFT Probe. *Acta Chim Sin*. 2017;75(5):457. doi:10.6023/A17010008

65. Zheng X-J, Qu N, Xuan L-C, Pan Q-J. Infrared Vibrational Spectra, Electronic Structures, and Formation Reactions of Polypyrrolic Mono - and Bis -actinyl Complexes: A Relativistic DFT Study. *Int J Quantum Chem*. 2017;117(13):e25378. doi:10.1002/qua.25378

66. Arnold PL, Dutkiewicz MS, Zegke M, et al. Subtle Interactions and Electron Transfer between U III , Np III , or Pu III and Uranyl Mediated by the Oxo Group. *Angew Chemie Int Ed*. 2016;55(41):12797-12801. doi:10.1002/anie.201607022

67. Lan J-H, Wang C-Z, Wu Q-Y, et al. A Quasi-relativistic Density Functional Theory Study of the Actinyl(VI, V) (An = U, Np, Pu) Complexes with a Six-Membered Macrocycle Containing Pyrrole, Pyridine, and Furan Subunits. *J Phys Chem A*. 2015;119(34):9178-9188. doi:10.1021/acs.jpca.5b06370

68. O'Brien KTP, Kaltsoyannis N. Computational Study of An-X Bonding (An = Th{,} U; X = p-block-based ligands) In Pyrrolic Macrocycle-Supported Complexes From The Quantum Theory Of Atoms In Molecules And Bond Energy Decomposition Analysis. *Dalt Trans*. 2017;46(3):760-769. doi:10.1039/C6DT04340B

69. Givaja G, Blake AJ, Wilson C, Schröder M, Love JB. Macrocyclic Diiminodipyrromethane Complexes: Structural Analogues of Pac-Man Porphyrins. *Chem Commun*. 2003;(19):2508-2509. doi:10.1039/B308443D

70. Sessler JL, Cho W-S, Dudek SP, Hicks L, Lynch VM, Huggins MT. Synthesis and Study of a Calixpyrrole-texaphyrin chimera: A New Oligopyrrolic Chloride Anion Receptor. *J*

Porphyr Phthalocyanines. 2003;7(2):97-104. doi:10.1142/S1088424603000136

71. Arnold PL, Patel D, Blake AJ, Wilson C, Love JB. Selective Oxo Functionalization of the Uranyl Ion with 3d Metal Cations. *J Am Chem Soc*. 2006;128(30):9610-9611. doi:10.1021/ja0634167

72. Arnold PL, Patel D, Wilson C, Love JB. Reduction and Selective Oxo Group Silylation of the Uranyl Dication. *Nature*. 2008;451(7176):315-317. doi:10.1038/nature06467

73. Arnold PL, Love JB, Patel D. Pentavalent Uranyl Complexes. *Coord Chem Rev*. 2009;253(15-16):1973-1978. doi:10.1016/j.ccr.2009.03.014

74. Arnold PL, Pécharman A-F, Hollis E, et al. Uranyl Oxo Activation and Functionalization by Metal Cation Coordination. *Nat Chem*. 2010;2(12):1056-1061. doi:10.1038/nchem.904

75. Arnold PL, Hollis E, White FJ, Magnani N, Caciuffo R, Love JB. Single-Electron Uranyl Reduction by a Rare-Earth Cation. *Angew Chemie Int Ed*. 2011;50(4):887-890. doi:10.1002/anie.201005511

76. Arnold PL, Pécharman A-F, Love JB. Oxo Group Protonation and Silylation of Pentavalent Uranyl Pacman Complexes. *Angew Chemie Int Ed*. 2011;50(40):9456-9458. doi:10.1002/anie.201104359

77. Arnold PL, Jones GM, Odoh SO, Schreckenbach G, Magnani N, Love JB. Strongly Coupled Binuclear Uranium–Oxo Complexes from Uranyl Oxo Rearrangement and Reductive Silylation. *Nat Chem*. 2012;4(3):221-227. doi:10.1038/nchem.1270

78. Jones GM, Arnold PL, Love JB. Controlled Deprotection and Reorganization of Uranyl Oxo Groups in a Binuclear Macrocyclic Environment. *Angew Chemie Int Ed*. 2012;51(50):12584-12587. doi:10.1002/anie.201207609

79. Arnold PL, Hollis E, Nichol GS, et al. Oxo-Functionalization and Reduction of the Uranyl Ion through Lanthanide-Element Bond Homolysis: Synthetic, Structural, and Bonding Analysis of a Series of Singly Reduced Uranyl–Rare Earth $5f^1$ -$4f^n$ Complexes. *J Am Chem Soc*. 2013;135(10):3841-3854. doi:10.1021/ja308993g

80. Collman JP, Wagenknecht PS, Hutchison JE. Molecular Catalysts for Multielectron Redox Reactions of Small Molecules: The"Cofacial Metallodiporphyrin" Approach. *Angew Chemie Int Ed English*. 1994;33(1516):1537-1554. doi:10.1002/anie.199415371

81. Pistorio BJ, Chang CJ, Nocera DG. A Phototriggered Molecular Spring for Aerobic Catalytic Oxidation Reactions. *J Am Chem Soc*. 2002;124(27):7884-7885. doi:10.1021/ja026017u

82. Chang CJ, Baker EA, Pistorio BJ, et al. Structural, Spectroscopic, and Reactivity Comparison of Xanthene- and Dibenzofuran-Bridged Cofacial Bisporphyrins. *Inorg Chem*. 2002;41(12):3102-3109. doi:10.1021/ic0111029

83. Ren W, Zi G, Fang D-C, Walter MD. Thorium Oxo and Sulfido Metallocenes: Synthesis, Structure, Reactivity, and Computational Studies. *J Am Chem Soc*. 2011;133(33):13183-13196. doi:10.1021/ja205280k

84. Seaman LA, Pedrick EA, Tsuchiya T, Wu G, Jakubikova E, Hayton TW. Comparison of the Reactivity of 2-Li-C $_6$ H $_4$ CH $_2$ NMe $_2$ with MCl $_4$ (M=Th, U): Isolation of a Thorium Aryl Complex or a Uranium Benzyne Complex. *Angew Chemie Int Ed*. 2013;52(40):10589-10592. doi:10.1002/anie.201303992

85. Hohloch S, Garner ME, Parker BF, Arnold J. New Supporting Ligands in Actinide Chemistry: Tetramethyltetraazaannulene Complexes with Thorium and Uranium. *Dalt Trans*. 2017;46(40):13768-13782. doi:10.1039/C7DT02682J

86. Marks TJ. Actinide Organometallic Chemistry. *Science (80-).* 1982;217(4564):989-997. doi:10.1126/science.217.4564.989

87. Gregson M, Lu E, Tuna F, et al. Emergence of Comparable Covalency in Isostructural Cerium (iv)– and Uranium (iv)–Carbon Multiple Bonds. *Chem Sci*. 2016;7(5):3286-3297. doi:10.1039/C6SC00278A

88. Evans WJ. The Importance of Questioning Scientific Assumptions: Some Lessons from f Element Chemistry †. *Inorg Chem*. 2007;46(9):3435-3449. doi:10.1021/ic062011k

89. Lukens WW, Edelstein NM, Magnani N, Hayton TW, Fortier S, Seaman LA. Quantifying the σ and π Interactions Between U(V) f Orbitals and Halide, Alkyl, Alkoxide, Amide and Ketimide Ligands. *J Am Chem Soc*. 2013;135(29):10742-10754. doi:10.1021/ja403815h

90. Duignan TJ, Autschbach J. Impact of the Kohn–Sham Delocalization Error on the 4f Shell Localization and Population in Lanthanide Complexes. *J Chem Theory Comput*. 2016;12(7):3109-3121. doi:10.1021/acs.jctc.6b00238

91. Sullivan JC, Hindman JC, Zielen AJ. Specific Interaction between Np(V) and U(VI) in Aqueous Perchloric Acid Media1. *J Am Chem Soc*. 1961;83(16):3373-3378. doi:10.1021/ja01477a004

92. Burns PC. U6+ Minerals and Inorganic Compounds: Insights into an Expanded Structural Hierarchy of Crystal Structures. *Can Mineral*. 2005;43(6):1839-1894. doi:10.2113/gscanmin.43.6.1839

93. Forbes TZ, Burns PC. The Role of Cation–Cation Interactions in a Neptunyl Chloride Hydrate and Topological Aspects of Neptunyl Structural Units. *J Solid State Chem*. 2007;180(1):106-112. doi:10.1016/j.jssc.2006.09.026

94. Forbes TZ, Burns PC, Soderholm L, Skanthakumar S. Crystal Structures and Magnetic Properties of $NaK_3(NpO_2)_4(SO_4)_4(H_2O)_2$ and $NaNpO_2SO_4H_2O$: Cation−Cation Interactions in a Neptunyl Sulfate Frame. *Chem Mater*. 2006;18(6):1643-1649. doi:10.1021/cm0523687

95. Forbes TZ, Wallace C, Burns PC. Neptunyl Compounds: Polyhedron Geometries, Bond-Valence Parameters, and Structural Hierarchy. *Can Mineral*. 2008;46(6):1623-1645. doi:10.3749/canmin.46.6.1623

96. N. N. Krot MSG. Cation—Cation Interaction in Crystalline Actinide Compounds. *Usp Khim*. 2004;73(1):89-100.

97. Fortier S, Hayton TW. Oxo Ligand Functionalization in the Uranyl ion (UO_2^{2+}). *Coord*

Chem Rev. 2010;254(3-4):197-214. doi:10.1016/j.ccr.2009.06.003

98. Mougel V, Horeglad P, Nocton G, Pécaut J, Mazzanti M. Inside Cover: Stable Pentavalent Uranyl Species and Selective Assembly of a Polymetallic Mixed-Valent Uranyl Complex by Cation-Cation Interactions (Angew. Chem. Int. Ed. 45/2009). *Angew Chemie Int Ed*. 2009;48(45):8382-8382. doi:10.1002/anie.200905187

99. Nocton G, Horeglad P, Pécaut J, Mazzanti M. Polynuclear Cation−Cation Complexes of Pentavalent Uranyl: Relating Stability and Magnetic Properties to Structure. *J Am Chem Soc*. 2008;130(49):16633-16645. doi:10.1021/ja804766r

100. Sullivan JC, Hindman JC, Zielen AJ. Specific Interaction between Np(V) and U(VI) in Aqueous Perchloric Acid Media 1. *J Am Chem Soc*. 1961;83(16):3373-3378. doi:10.1021/ja01477a004

101. Nagasaki S, Kinoshita K, Enokida Y, Suzuki A. Solvent Extraction of Np (V) with CMPO from Nitric Acid Solutions Containing U (VI). *J Nucl Sci Technol*. 1992;29(11):1100-1107. doi:10.1080/18811248.1992.9731641

102. Grigoriev MS, Krot NN, Bessonov AA, Suponitsky KY. Dimeric Dioxocations, $(NpO^{2+})_2$, in the Structure of bis(μ-2-fluorobenzoato-κ 2 O : O ′)di-μ-oxo-bis[(2,2′-bipyridine-κ 2 N , N ′)oxoneptunium(V)]. *Acta Crystallogr Sect E Struct Reports Online*. 2007;63(2):m561-m562. doi:10.1107/S1600536807002164

103. Cousson A, Dabos S, Abazli H, Nectoux F, Pagès M, Choppin G. Crystal Structure of a Neptunyl Cation-Cation Complex (NpO_2^{+1}) with Mellitic Acid: $Na_4(NpO_2)_2Cl_{12}O_{12}\cdot 8H_2O$. *J Less Common Met*. 1984;99(2):233-240. doi:10.1016/0022-5088(84)90220-0

104. John GH, May I, Sarsfield MJ, et al. The Structural and Spectroscopic Characterisation of Three Actinyl Complexes with Coordinated and Uncoordinated Perrhenate: $[UO_2 (ReO_4)_2 (TPPO)_3]$, $[\{(UO_2)(TPPO)_3 \}_2 (\mu_2 -O_2$. *Dalt Trans*. 2004;(5):734-740. doi:10.1039/B313045B

105. Albrecht-Schmitt TE, Almond PM, Sykora RE. Cation−Cation Interactions in Neptunyl(V) Compounds: Hydrothermal Preparation and Structural Characterization of $NpO_2(IO_3)$ and α- and β-$AgNpO_2$ (SeO_3). *Inorg Chem*. 2003;42(12):3788-3795. doi:10.1021/ic034124z

106. Burdet F, Pécaut J, Mazzanti M. Isolation of a Tetrameric Cation−Cation Complex of Pentavalent Uranyl. *J Am Chem Soc*. 2006;128(51):16512-16513. doi:10.1021/ja067445t

107. Wilkerson MP, Burns CJ, Dewey HJ, et al. Basicity of Uranyl Oxo Ligands upon Coordination of Alkoxides. *Inorg Chem*. 2000;39(23):5277-5285. doi:10.1021/ic000142u

108. Natrajan L, Burdet F, Pécaut J, Mazzanti M. Synthesis and Structure of a Stable Pentavalent-Uranyl Coordination Polymer. *J Am Chem Soc*. 2006;128(22):7152-7153. doi:10.1021/ja0609809

109. Alekseev E V., Krivovichev S V., Malcherek T, Depmeier W. One-Dimensional Array of Two- and Three-Center Cation−Cation Bonds in the Structure of Li_4 $[(UO_2)_{10} O_{10} (Mo_2O_8)]$. *Inorg Chem*. 2007;46(21):8442-8444. doi:10.1021/ic7009385

110. Alekseev E V., Krivovichev S V., Depmeier W, et al. One-Dimensional Chains in Uranyl Tungstates: Syntheses and Structures of $A_8[(UO_2)_4(WO_4)_4(WO_5)_2]$ (A=Rb, Cs) and $Rb_6[(UO_2)_2O(WO_4)$. *J Solid State Chem*. 2006;179(10):2977-2987. doi:10.1016/j.jssc.2006.05.015

111. Sullens TA, Jensen RA, Shvareva TY, Albrecht-Schmitt TE. Cation−Cation Interactions between Uranyl Cations in a Polar Open-Framework Uranyl Periodate. *J Am Chem Soc*. 2004;126(9):2676-2677. doi:10.1021/ja031695h

112. Alekseev E V., Krivovichev S V., Depmeier W, et al. $Na_2Li_8[(UO_2)_{11}O_{12}(WO_5)_2]$: Three Different Uranyl-Ion Coordination Geometries and Cation–Cation Interactions. *Angew Chemie Int Ed*. 2006;45(43):7233-7235. doi:10.1002/anie.200601207

113. Kubatko K-A, Burns PC. Cation−Cation Interactions in Sr_5 $(UO_2)_20$ $(UO_6)_2O_{16}(OH)_6$ $(H_2O)_6$ and $Cs(UO_2)_9U_3O_{16}$ $(OH)_5$. *Inorg Chem*. 2006;45(25):10277-10281. doi:10.1021/ic0609453

114. Forbes TZ, Burns PC, Soderholm L, Skanthakumar S. Crystal Structures and Magnetic Properties of NaK_3 $(NpO_2)_4(SO_4)_4(H_2O)_2$ and $NaNpO_2$ SO_4 H_2O: Cation−Cation Interactions in a Neptunyl Sulfate Frame. *Chem Mater*. 2006;18(6):1643-1649. doi:10.1021/cm0523687

115. Almond PM, Skanthakumar S, Soderholm L, Burns PC. Cation−Cation Interactions and Antiferromagnetism in $Na[Np(V)O_2$ $(OH)_2$]: Synthesis, Structure, and Magnetic Properties. *Chem Mater*. 2007;19(2):280-285. doi:10.1021/cm0621040

116. Forbes TZ, Burns PC. Synthesis, Structure Determination, and Infrared Spectroscopy of (NpO2)2(SO4)(H2O)4: Prevalence of Cation–Cation Interactions and Cationic Nets in Neptunyl Sulfate Compounds. *J Solid State Chem*. 2009;182(1):43-48. doi:10.1016/j.jssc.2008.08.032

117. Cramer CJ. *Essentials of Computational Chemistry*. 2nd ed. USA: John Wiley and Sons; 2004.

118. Jensen MP, Choppin GR. Complexation of Uranyl(VI) by Aqueous Orthosilicic Acid. *Radiochim Acta*. 1998;82(s1). doi:10.1524/ract.1998.82.special-issue.83

119. Träber SC, Höllriegl V, Li WB, et al. Estimating the Absorption of Soil-Derived Uranium in Humans. *Environ Sci Technol*. 2014;48(24):14721-14727. doi:10.1021/es504171r

120. Pyykkö P. Relativistic Effects in Structural Chemistry. *Chem Rev*. 1988;88(3):563-594. doi:10.1021/cr00085a006

121. Schrödinger E. Quantisierung als Eigenwertproblem. *Ann Phys*. 1926;385(13):437-490. doi:10.1002/andp.19263851302

122. Born M, Oppenheimer R. Zur Quantentheorie der Molekeln. *Ann Phys*. 1927;389(20):457-484. doi:10.1002/andp.19273892002

123. D LL, Lifshitz EM. *Quantum Mechanics*. 3rd ed.; 1977.

124. Gordon A, Avron JE. Born-Oppenheimer Approximation near Level Crossing. *Phys Rev*

Lett. 2000;85(1):34-37. doi:10.1103/PhysRevLett.85.34

125. Waschewsky, G. C. G.; Kash, P. W.; Myers, T. L.; Kitchen, D. C.; Butler L. Front cover. *J Chem Soc Faraday Trans*. 1994;90(12):X045. doi:10.1039/ft99490fx045

126. Roothaan CCJ. New Developments in Molecular Orbital Theory. *Rev Mod Phys*. 1951;23(2):69-89. doi:10.1103/RevModPhys.23.69

127. C. J. Cramer. *Essentials of Computational Chemistry*. John Wiley and Sons; 2004.

128. P.J. Hay R. L. Martin. Computational Studies of Actinide Chemistry. *Los Alamos Sci*. 2000:382-391.

129. Hohenberg P, Kohn W. Inhomogeneous Electron Gas. *Phys Rev*. 1964;136(3B):B864-B871. doi:10.1103/PhysRev.136.B864

130. Kohn W, Sham LJ. Self-Consistent Equations Including Exchange and Correlation Effects. *Phys Rev*. 1965;140(4A):A1133-A1138. doi:10.1103/PhysRev.140.A1133

131. Cramer CJ, Truhlar DG. Density Functional Theory for Transition Metals and Transition Metal Chemistry. *Phys Chem Chem Phys*. 2009;11(46):10757. doi:10.1039/b907148b

132. Cohen AJ, Mori-Sánchez P, Yang W. Challenges for Density Functional Theory. *Chem Rev*. 2012;112(1):289-320. doi:10.1021/cr200107z

133. Grimme S, Antony J, Ehrlich S, Krieg H. A Consistent and Accurate ab initio Parametrization of Density Functional Dispersion Correction (DFT-D) For the 94 Elements H-Pu. *J Chem Phys*. 2010;132(15):154104. doi:10.1063/1.3382344

134. Kozuch S, Gruzman D, Martin JML. DSD-BLYP: A General Purpose Double Hybrid Density Functional Including Spin Component Scaling and Dispersion Correction †. *J Phys Chem C*. 2010;114(48):20801-20808. doi:10.1021/jp1070852

135. Zhao Y, Truhlar DG. Applications and Validations of the Minnesota Density Functionals. *Chem Phys Lett*. 2011;502(1-3):1-13. doi:10.1016/j.cplett.2010.11.060

136. Perdew JP, Ruzsinszky A, Tao J, Staroverov VN, Scuseria GE, Csonka GI. Prescription for the Design and Selection of Density Functional Approximations: More Constraint Satisfaction with Fewer Fits. *J Chem Phys*. 2005;123(6):62201. doi:10.1063/1.1904565

137. Leeuwen R Van, Baerends EJ. An Analysis of Nonlocal Density Functionals in Chemical Bonding. *Int J Quantum Chem*. 1994;52(4):711-730. doi:10.1002/qua.560520405

138. Gugelchuk MM, Cui Y. Performance of Pure and Hybrid DFT Methods in Calculations of Ethylene Iodonium and Methyl Iodide. *J Mol Struct Theochem*. 1996;365(2-3):111-117. doi:10.1016/0166-1280(96)04484-3

139. Perdew JP, Burke K, Ernzerhof M. Generalized Gradient Approximation Made Simple. *Phys Rev Lett*. 1996;77(18):3865-3868. doi:10.1103/PhysRevLett.77.3865

140. Tao J, Perdew JP, Staroverov VN, Scuseria GE. Climbing the Density Functional Ladder: Nonempirical Meta–Generalized Gradient Approximation Designed for Molecules and Solids. *Phys Rev Lett*. 2003;91(14):146401. doi:10.1103/PhysRevLett.91.146401

141. Becke AD. A New Mixing of Hartree–Fock and Local Density-Functional Theories. *J Chem Phys*. 1993;98(2):1372-1377. doi:10.1063/1.464304

142. Pyykkö P, Desclaux JP. Relativity and The Periodic System of Elements. *Acc Chem Res*. 1979;12(8):276-281. doi:10.1021/ar50140a002

143. Pyykkö P, Li J, Runeberg N. Quasirelativistic Pseudopotential Study of Species Isoelectronic to Uranyl and the Equatorial Coordination of Uranyl. *J Phys Chem*. 1994;98(18):4809-4813. doi:10.1021/j100069a007

144. Dirac PAM. Quantum Mechanics of Many-Electron Systems. *Proc R Soc A Math Phys Eng Sci*. 1929;123(792):714-733. doi:10.1098/rspa.1929.0094

145. van Lenthe E, Ehlers A, Baerends E-J. Geometry Optimizations in the Zero Order Regular Approximation for Relativistic Effects. *J Chem Phys*. 1999;110(18):8943-8953. doi:10.1063/1.478813

146. Dyall KG, van Lenthe E. Relativistic Regular Approximations Revisited: An Infinite-Order Relativistic Approximation. *J Chem Phys*. 1999;111(4):1366-1372. doi:10.1063/1.479395

147. Reiher M. Relativistic Douglas-Kroll-Hess theory. *Wiley Interdiscip Rev Comput Mol Sci*. 2012;2(1):139-149. doi:10.1002/wcms.67

148. Laikov DN. A New Class of Atomic Basis Functions For Accurate Electronic Structure Calculations Of Molecules. *Chem Phys Lett*. 2005;416(1-3):116-120. doi:10.1016/j.cplett.2005.09.046

149. Dyall KG. An Exact Separation Of The Spin-Free And Spin-Dependent Terms Of The Dirac–Coulomb–Breit Hamiltonian. *J Chem Phys*. 1994;100(3):2118-2127. doi:10.1063/1.466508

150. Laikov DN. Fast Evaluation of Density Functional Exchange-Correlation Terms Using The Expansion Of the Electron Density in Auxiliary Basis Sets. *Chem Phys Lett*. 1997;281(1-3):151-156. doi:10.1016/S0009-2614(97)01206-2

151. D. N. Laikov. An Implementation Of The Relativistic Density Functioscalarnal Theory For Molecular Calculations With Gaussian Basis Sets.2000.

152. Laikov DN, Ustynyuk YA. PRIRODA-04: A Quantum-Chemical Program Suite. New Possibilities in The Study of Molecular Systems With the Application of Parallel Computing. *Russ Chem Bull*. 2005;54(3):820-826. doi:10.1007/s11172-005-0329-x

153. R.F.W. Bader. *Atoms in Molecules, A Quantum Thoery*. Oxford: Oxford University Press; 1990.

154. te Velde G, Bickelhaupt FM, Baerends EJ, et al. Chemistry with ADF. *J Comput Chem*. 2001;22(9):931-967. doi:10.1002/jcc.1056

155. Glendening ED, Landis CR, Weinhold F. Natural Bond Orbital Methods. *Wiley Interdiscip Rev Comput Mol Sci*. 2012;2(1):1-42. doi:10.1002/wcms.51

156. Hirshfeld FL. Bonded-Atom Fragments For Describing Molecular Charge Densities.

Theor Chim Acta. 1977;44(2):129-138. doi:10.1007/BF00549096

157. Mulliken RS. Electronic Population Analysis on LCAO–MO Molecular Wave Functions. I. *J Chem Phys*. 1955;23(10):1833-1840. doi:10.1063/1.1740588

158. Wang C-Z, Gibson JK, Lan J-H, et al. Actinide (An = Th-Pu) Dimetallocenes: Promising Candidates For Metal-Metal Multiple Bonds. *Dalt Trans*. 2015;44(39):17045-17053. doi:10.1039/C5DT02811F

159. Fryer-Kanssen I, Austin J, Kerridge A. Topological Study of Bonding in Aquo and Bis(triazinyl)pyridine Complexes of Trivalent Lanthanides and Actinides: Does Covalency Imply Stability? *Inorg Chem*. 2016;55(20):10034-10042. doi:10.1021/acs.inorgchem.6b00968

160. Kerridge A. f-Orbital Covalency In The Actinocenes (An = Th-Cm): Multiconfigurational Studies And Topological Analysis. *RSC Adv*. 2014;4(24):12078-12086. doi:10.1039/C3RA47088A

161. Zaiter A, Amine B, Bouzidi Y, Belkhiri L, Boucekkine A, Ephritikhine M. Selectivity of Azine Ligands Toward Lanthanide(III)/Actinide(III) Differentiation: A Relativistic DFT Based Rationalization. *Inorg Chem*. 2014;53(9):4687-4697. doi:10.1021/ic500361b

162. Di Pietro P, Kerridge A. Assessing Covalency in Equatorial U-N bonds: Density Based Measures Of Bonding in BTP and Isoamethyrin Complexes of Uranyl. *Phys Chem Chem Phys*. 2016;18(25):16830-16839. doi:10.1039/C6CP01273F

163. Kaltsoyannis N. Seventeen-Coordinate Actinide Helium Complexes. *Angew Chemie Int Ed*. 2017;56(25):7066-7069. doi:10.1002/anie.201700245

164. Lu T, Chen F. Multiwfn: A Multifunctional Wavefunction Analyzer. *J Comput Chem*. 2012;33(5):580-592. doi:10.1002/jcc.22885

165. Reed AE, Curtiss LA, Weinhold F. Intermolecular Interactions From a Natural Bond Orbital, Donor-Acceptor Viewpoint. *Chem Rev*. 1988;88(6):899-926. doi:10.1021/cr00088a005

166. Kaltsoyannis N. Does Covalency Increase or Decrease across the Actinide Series? Implications for Minor Actinide Partitioning. *Inorg Chem*. 2013;52(7):3407-3413. doi:10.1021/ic3006025

167. Neidig ML, Clark DL, Martin RL. Covalency in f-Element Complexes. *Coord Chem Rev*. 2013;257(2):394-406. doi:10.1016/j.ccr.2012.04.029

168. Kozimor SA, Yang P, Batista ER, et al. Trends in Covalency for d- and f-Element Metallocene Dichlorides Identified Using Chlorine K-Edge X-ray Absorption Spectroscopy and Time-Dependent Density Functional Theory. *J Am Chem Soc*. 2009;131(34):12125-12136. doi:10.1021/ja9015759

169. Dutkiewicz MS, Farnaby JH, Apostolidis C, et al. Organometallic neptunium(III) complexes. *Nat Chem*. 2016;8(8):797-802. doi:10.1038/nchem.2520

170. Minasian SG, Keith JM, Batista ER, et al. New Evidence for 5f Covalency in Actinocenes

Determined from Carbon K-edge XAS and Electronic Structure Theory. *Chem Sci*. 2014;5(1):351-359. doi:10.1039/C3SC52030G

171. Formanuik A, Ariciu A-M, Ortu F, et al. Actinide Covalency Measured by Pulsed Electron Paramagnetic Resonance Spectroscopy. *Nat Chem*. 2016;9(6):578-583. doi:10.1038/nchem.2692

172. Polinski MJ, Grant DJ, Wang S, et al. Differentiating between Trivalent Lanthanides and Actinides. *J Am Chem Soc*. 2012;134(25):10682-10692. doi:10.1021/ja303804r

173. De Jong, W. A.; Visscher, L.; Nieuwpoort WC. On the Bonding and the Electric Field Gradient of the Uranyl Ion. *J Mol Struct THEOCHEM*. 1998;458(1-2):41-52. doi:10.1016/S0166-1280(98)00347-9

174. Denning RG. Electronic Structure and Bonding in Actinyl Ions and their Analogs. *J Phys Chem A*. 2007;111(20):4125-4143. doi:10.1021/jp071061n

175. Wadt WR. Why Uranyl ion(2+) is Linear and Isoelectronic Thorium Dioxide is Bent. *J Am Chem Soc*. 1981;103(20):6053-6057. doi:10.1021/ja00410a011

176. Tatsumi K, Hoffmann R. Bent cis d0 MoO_2^{2+} vs. linear trans d0f0 UO_2^{2+}: a significant role for nonvalence 6p orbitals in uranyl. *Inorg Chem*. 1980;19(9):2656-2658. doi:10.1021/ic50211a035

177. Givaja G, Volpe M, Leeland JW, et al. Design and Synthesis of Binucleating Macrocyclic Clefts Derived from Schiff-Base Calixpyrroles. *Chem – A Eur J*. 2007;13(13):3707-3723. doi:10.1002/chem.200600989

178. Leeland JW, White FJ, Love JB. Encapsulation of a Magnesium Hydroxide Cubane by a Bowl-Shaped Polypyrrolic Schiff Base Macrocycle. *J Am Chem Soc*. 2011;133(19):7320-7323. doi:10.1021/ja201630b

179. Arnold PL, Stevens CJ, Farnaby JH, Gardiner MG, Nichol GS, Love JB. New Chemistry from an Old Reagent: Mono- and Dinuclear Macrocyclic Uranium(III) Complexes from $[U(BH_4)_3(THF)_2]$. *J Am Chem Soc*. 2014;136(29):10218-10221. doi:10.1021/ja504835a

180. Laikov DN. *An Implementation of the Scalar Relativistic Density Functional Theory for Molecular Calculations with Guassian Basis Sets*.

181. Laikov DN. Ph.D. (Phys. Math.)Thesis. 2000.

182. Laikov DN. A New Class Of Atomic Basis Functions For Accurate Electronic Structure Calculations Of Molecules. *Chem Phys Lett*. 2005;416(1-3):116-120. doi:10.1016/j.cplett.2005.09.046

183. Ustynyuk DNLA. PRIRODA-04: A Quantum-Chemical Program Suite. New Possibilities in The Study of Molecular Systems With the Application of Parallel Computing. 2005;54(3):820-826.

184. Mayer Istvan. *Simple Theorem, Proof and Derivative in Quantum Chemistry*.

185. Hirshfeld FL. Bonded-Atom Fragments For Describing Molecular Charge Densities. *Theor Chim Acta*. 1977;44(2):129-138. doi:10.1007/BF00549096

186. Shamov GA, Schreckenbach G, Vo TN. A Comparative Relativistic DFT and Ab Initio Study on the Structure and Thermodynamics of the Oxofluorides of Uranium(IV), (V) and (VI). *Chem - A Eur J*. 2007;13(17):4932-4947. doi:10.1002/chem.200601244

187. Shamov GA, Schreckenbach G. Density Functional Studies of Actinyl Aquo Complexes Studied Using Small-Core Effective Core Potentials and a Scalar Four-Component Relativistic Method. *J Phys Chem A*. 2005;109(48):10961-10974. doi:10.1021/jp053522f

188. Shamov GA, Schreckenbach G. Density Functional Studies of Actinyl Aquo Complexes Studied Using Small-Core Effective Core Potentials and a Scalar Four-Component Relativistic Method. *J Phys Chem A*. 2006;110(43):12072-12072. doi:10.1021/jp0662855

189. Berard JJ, Shamov GA, Schreckenbach G. A Density Functional Study of the Various Forms of UN_4O_{12} Containing Uranyl Nitrate. *J Phys Chem A*. 2007;111(42):10789-10803. doi:10.1021/jp073688b

190. Bomble YJ. Amsterdam Density Functional 2005 Scientific Computing and Modelling NV, Vrije Universiteit, Theoretical Chemistry, De Boelelaan 1083, 1081 HV Amsterdam, the Netherlands. http://www.scm.com. See Web site for pricing information. *J Am Chem Soc*. 2006;128(9):3103. doi:10.1021/ja0598311

191. van Lenthe, E.; Ehlers, A.; Baerends EJ. Geometry Optimizations in the Zero Order Regular Approximation for Relativistic Effects. *J chem phys*. 1999:8943-8953. doi:10.1063/1.478813

192. Lenthe E van, Baerends EJ, Snijders JG. Relativistic Regular Two-Component Hamiltonians. *J Chem Phys*. 1993;99(6):4597-4610. doi:10.1063/1.466059

193. van Lenthe E, Baerends EJ, Snijders JG. Relativistic Total Energy Using Regular Approximations. *J Chem Phys*. 1994;101(11):9783-9792. doi:10.1063/1.467943

194. Richard F. W. Bader. *Atoms in Molecule-A Quantum Theory*. Oxford, UK: Oxford University Press,; 2000.

195. Hay PJ, Martin RL, Schreckenbach G. Theoretical Studies of the Properties and Solution Chemistry of AnO_2^{2+} and AnO_2 Aquo Complexes for An = U, Np, and Pu. *J Phys Chem A*. 2000;104(26):6259-6270. doi:10.1021/jp000519h

196. Berthet J-C, Nierlich M, Ephritikhine M. Isolation of a Uranyl $[UO_2]$ Species: Crystallographic Comparison of the Dioxouranium(V) and (VI) Compounds $[UO_2(OPPh_3)_4](OTf)_n$ (n=1, 2). *Angew Chemie Int Ed*. 2003;42(17):1952-1954. doi:10.1002/anie.200250506

197. Nocton G, Horeglad P, Vetere V, et al. Synthesis, Structure, and Bonding of Stable Complexes of Pentavalent Uranyl. *J Am Chem Soc*. 2010;132(2):495-508. doi:10.1021/ja9037164

198. Brown JL, Wu G, Hayton TW. Oxo Ligand Silylation in a Uranyl β-Ketoiminate Complex. *J Am Chem Soc*. 2010;132(21):7248-7249. doi:10.1021/ja1013739

199. Shamov GA, Schreckenbach G, Martin RL, Hay PJ. Crown Ether Inclusion Complexes of the Early Actinide Elements, $[AnO_2(18\text{-crown-}6)]^{n+}$, An = U, Np, Pu and n= 1, 2: A

Relativistic Density Functional Study. *Inorg Chem*. 2008;47(5):1465-1475. doi:10.1021/ic7015403

200. John K. Gibson WA de J. *Experimental and Theoretical Approaches to Actinide Chemistry*. John Wiley & Sons; 2018.

201. Clark, D. L.; Palmer, P. D.; Tait, C. D.; Keogh DW. Actinide Research Quarterly, 2004, First Quarter.

202. Volpe M, Reid SD, Blake AJ, Wilson C, Love JB. Early Transition Metal Complexes of Dinucleating Pacman Ligands: X-ray Crystal Structures of Mixed-Valence VIII/VIV Complexes. *Inorganica Chim Acta*. 2007;360(1):273-280. doi:10.1016/j.ica.2006.07.058

203. Veauthier JM, Cho W-S, Lynch VM, Sessler JL. Calix[4]pyrrole Schiff Base Macrocycles. Novel Binucleating Ligands for μ-Oxo Iron Complexes. *Inorg Chem*. 2004;43(4):1220-1228. doi:10.1021/ic0352001

204. Tassell MJ, Kaltsoyannis N. Covalency in AnCp4 (An = Th-Cm): A Comparison of Molecular Orbital{,} Natural Population and Atoms-in-Molecules Analyses. *Dalt Trans*. 2010;39(29):6719-6725. doi:10.1039/C000704H

205. Kirker I, Kaltsoyannis N. Does Covalency Really Increase Across the 5f Series? A Comparison of Molecular Orbital{,} Natural Population{,} Spin and Electron Density Analyses of $AnCp_3$ (An = Th-Cm; Cp = [small eta]5-C5H5). *Dalt Trans*. 2011;40(1):124-131. doi:10.1039/C0DT01018A

206. Jones MB, Gaunt AJ, Gordon JC, Kaltsoyannis N, Neu MP, Scott BL. Uncovering f-Element Bonding Differences and Electronic Structure in a Series of 1 : 3 and 1 : 4 Complexes with a Diselenophosphinate Ligand. *Chem Sci*. 2013;4(3):1189-1203. doi:10.1039/C2SC21806B

207. Arnold PL, Turner ZR, Kaltsoyannis N, Pelekanaki P, Bellabarba RM, Tooze RP. Covalency in Ce(IV) and U(IV) Halide and N-Heterocyclic Carbene Bonds. *Chem - A Eur J*. 2010;16(31):9623-9629. doi:10.1002/chem.201001471

208. Blake MP, Kaltsoyannis N, Mountford P. Heterobimetallic Complexes Containing Ca–Fe or Yb–Fe Bonds: Synthesis and Molecular and Electronic Structures of $[M\{CpFe(CO)_2\}_2(THF)_3]_2$ (M = Ca or Yb). *J Am Chem Soc*. 2011;133(39):15358-15361. doi:10.1021/ja207487j

209. Saleh LMA, Birjkumar KH, Protchenko A V, et al. Group 3 and Lanthanide Boryl Compounds: Syntheses, Structures, and Bonding Analyses of Sc−B, Y−B, and Lu−B σ-Coordinated NHC Analogues. *J Am Chem Soc*. 2011;133(11):3836-3839. doi:10.1021/ja2007092

210. Schnaars DD, Gaunt AJ, Hayton TW, et al. Bonding Trends Traversing the Tetravalent Actinide Series: Synthesis, Structural, and Computational Analysis of An IV (Ar acnac)$_4$ Complexes (An = Th, U, Np, Pu; Ar acnac = Ar N C(Ph)CHC(Ph) O ; Ar = 3,5- t Bu 2 C 6 H 3). *Inorg Chem*. 2012;51(15):8557-8566. doi:10.1021/ic301109f

211. Mansell SM, Kaltsoyannis N, Arnold PL. Small Molecule Activation by Uranium Tris(aryloxides): Experimental and Computational Studies of Binding of N_2, Coupling of

CO, and Deoxygenation Insertion of CO_2 under Ambient Conditions. *J Am Chem Soc*. 2011;133(23):9036-9051. doi:10.1021/ja2019492

212. Kaltsoyannis N. Covalency Hinders AnO_2 (H_2O) + → AnO(OH) $^{+2}$Isomerisation (An = Pa–Pu). *Dalt Trans*. 2016;45(7):3158-3162. doi:10.1039/C5DT04317D

213. Mountain ARE, Kaltsoyannis N. Do QTAIM Metrics Correlate with the Strength of Heavy Element–Ligand Bonds? *Dalt Trans*. 2013;42(37):13477. doi:10.1039/c3dt51337h

214. C. F. Matta RJ, Boyd. *The Quantum Theory of Atoms in Molecules*. WILEY-VCH Verlag; 2007.

215. Stalke D. Meaningful Structural Descriptors from Charge Density. *Chem - A Eur J*. 2011;17(34):9264-9278. doi:10.1002/chem.201100615

216. Cremer D, Kraka E. Chemical Bonds without Bonding Electron Density ? Does the Difference Electron-Density Analysis Suffice for a Description of the Chemical Bond? *Angew Chemie Int Ed English*. 1984;23(8):627-628. doi:10.1002/anie.198406271

217. Hlina JA, Pankhurst JR, Kaltsoyannis N, Arnold PL. Metal–Metal Bonding in Uranium–Group 10 Complexes. *J Am Chem Soc*. 2016;138(10):3333-3345. doi:10.1021/jacs.5b10698

218. Vallet V, Wahlgren U, Grenthe I. Probing the Nature of Chemical Bonding in Uranyl(VI) Complexes with Quantum Chemical Methods. *J Phys Chem A*. 2012;116(50):12373-12380. doi:10.1021/jp3091123

219. Michelini M del C, Russo N, Sicilia E. Gas-Phase Chemistry of Actinides Ions: New Insights into the Reaction of UO^+ and UO^{2+} with Water. *J Am Chem Soc*. 2007;129(14):4229-4239. doi:10.1021/ja065683i

220. Arnold PL, Pécharman AF, Love JB. Oxo Group Protonation and Silylation of Pentavalent Uranyl Pacman Complexes. *Angew Chemie - Int Ed*. 2011;50(40):9456-9458. doi:10.1002/anie.201104359

221. Sessler, J. L.; Seidel, D.; Vivian, A. E.; Lynch, V.; Scott, B. L.; Keogh DW. Hexaphyrin(1.0.1.0.0.0): An Expanded Porphyrin Ligand for the Actinide Cations Uranyl (UO_2^{2+})and Neptunyl (NpO_2^{+1}). *Angew Chem, Int Ed Engl*. 40:591.

222. Love JB. A Macrocyclic Approach to Transition Metal and Uranyl Pacman Complexes. *Chem Commun*. 2009;(22):3154. doi:10.1039/b904189c

223. Arnold PL, Potter (née Jones) NA, Carmichael CD, Slawin AMZ, Roussel P, Love JB. Constructing Cerium Supramolecular Wheels and Encapsulating Uranium with a Schiff-Base Calixpyrrole Ligand. *Chem Commun*. 2010;46(11):1833. doi:10.1039/b921132b

224. Lee C, Yang W, Parr RG. Development of the Colle-Salvetti Correlation-Energy Formula into a Functional of the Electron Density. *Phys Rev B*. 1988;37(2):785-789. doi:10.1103/PhysRevB.37.785

225. Stephens PJ, Devlin FJ, Chabalowski CF, Frisch MJ. Ab Initio Calculation of Vibrational Absorption and Circular Dichroism Spectra Using Density Functional Force Fields. *J Phys*

Chem. 1994;98(45):11623-11627. doi:10.1021/j100096a001